สหสัมพันธ์ระหว่างขนาดอนุภาคและความเสถียรทางความร้อนเมื่อมีความชื้นอยู่ของวายซีโอไลต์

นายสมยศ สมบัติชัยศักดิ์

วิทยานิพนธ์นี้เป็นส่วนหนึ่งของการศึกษาตามหลักสูตรปริญญาวิศวกรรมศาสตรมหาบัณฑิต
สาขาวิชาวิศวกรรมเคมี ภาควิชาวิศวกรรมเคมี
คณะวิศวกรรมศาสตร์ จุฬาลงกรณ์มหาวิทยาลัย
ปีการศึกษา 2546

ISBN 974-17-3815-3

CORRELATION BETWEEN PARTICLE SIZE AND HYDROTHERMAL STABILITY OF Y ZEOLITE

Mr. Somyod Sombatchaisak

A Thesis Submitted in Partial Fulfillment of the Requirements
for the Degree of Master of Engineering in Chemical Engineering
Department of Chemical Engineering
Faculty of Engineering
Chulalongkorn University
Academic Year 2003
ISBN 974-17-3815-3

Thesis Title	CORRELATION BETWEEN PARTICLE SIZE AND HYDROTHERMAL STABILITY OF Y ZEOLITE
By	Mr Somyod Sombatchaisak
Field of Study	Chemical Engineering
Thesis Advisor	Professor Piyasan Praserthdam, Dr.Ing.

Accepted by the Faculty of Engineering, Chulalongkorn University in Partial Fulfillment of the Requirements for the Master's Degree

……Dean of the Faculty of Engineering
(Professor Direk Lawansiri, Ph.D.)

THESIS COMMITTEE

…… Chairman
(Montree Wongsri, D.Sc.)

……. Thesis Advisor
(Professor Piyasan Praserthdam, Dr.Ing.)

…….. Member
(Suphot Phatanasri, D.Eng.)

…….. Member
(Bongkot Ngamsom, D.Eng.)

สมยศ สมบัติชัยศักดิ์: สหสัมพันธ์ระหว่างขนาดอนุภาคและความเสถียรทางความร้อนเมื่อมีความชื้นอยู่ของซีโอไลต์วาย (CORRELATION BETWEEN PARTICLE SIZE AND HYDROTHERMAL STABILITY OF Y ZEOLITE) อ. ที่ปรึกษา : ศ.ดร.ปิยะสาร ประเสริฐธรรม, 119 หน้า. ISBN 974-17-4162-6

ทำการทดสอบผลของขนาดอนุภาคในช่วง 0.16 ถึง 2.01 ไมโครเมตรต่อค่าความเสถียรทางความร้อนและความชื้นของวายซีโอไลต์ภายใต้สภาวะฟลูอิดคาตาไลติกแครกกิ้ง ขนาดอนุภาคเฉลี่ยที่เหมาะสมซึ่งให้ค่าความเสถียรทางความร้อนและความชื้นสูงที่สุดคือขนาด 0.45 ไมโครเมตร โดยทำการทดสอบการเสื่อมสภาพทางโครงสร้าง เป็นสาเหตุจากการเกิดการหลุดออกของอลูมิเนียม (dealumination) โดยผลของอลูมิเนียมนิวเคลียร์แมคเนติกเรโซแนน (Al^{27}MAS-NMR) จากสหสัมพันธ์ใหม่ที่สร้างขึ้นโดยความสัมพันธ์ของค่าความเป็นผลึก (crystallinity) ที่สภาวะหลังการทดสอบต่อสภาวะก่อนการทดสอบ (C/C_o) เท่ากับเศษหนึ่งส่วนรากที่สองของขนาดผลึกเริ่มต้น (d_0) ของวายซีโอไลต์ สหสัมพันธ์นี้สามารถทำนายค่าความเสถียรทางความร้อนและความชื้นของวายซีโอไลต์ ได้ในช่วงผลึกขนาดเล็กถึงขนาดกลางในสภาวะอุณหภูมิที่ทำการทดสอบ สำหรับผลึกขนาดใหญ่กว่า 0.45 ไมโครเมตรน่าจะเกิดการเปลี่ยนแปลงทางโครงสร้าง (Structural defect) ของซีโอไลต์มากกว่า เนื่องจากมีค่าอัตราส่วนระหว่างกรดบรอนสเตดต่อลิวอีสมากกว่า ทำให้ไม่สามารถใช้สหสัมพันธ์นี้ในช่วงผลึกขนาดใหญ่ได้ ซึ่งคุณสมบัติความเป็นกรดนี้ถูกทดสอบโดยการเทคนิคไล่ออกของแอมโมเนีย (NH_3 TPD) และการดูดซับของไพริดีน (pyridine adsorption)

ภาควิชา……..วิศวกรรมเคมี……..… ลายมือชื่อนิสิต…….

สาขาวิชา……วิศวกรรมเคมี……. ลายมือชื่ออาจารย์ที่ปรึกษา……..

ปีการศึกษา…….2546……..

##4570580721: MAJOR CHEMICAL ENGINEERING
KEY WORD: PARTICEL SIZE / Y ZEOLITE / HYDROTHERMAL STABILITY

SOMYOD SOMBATCHAISAK: CORRELATION BETWEEN PARTICLE SIZE AND HYDROTHERMAL STABILITY OF Y ZEOLITE. THESIS ADVISOR: PROFESSOR PIYASAN PRASERTHDAM, Dr.Ing. 119 pp. ISBN 974-17-4162-6

Abstract

The effect of particle size in the range of 0.16-2.01 μm on the hydrothermal stability of Y zeolite under simulated FCC condition was investigated. The average particle size of 0.45 μm was found to be the optimum particle size of Y zeolite to retain high %crystallinity upon hydrothermal treatment as structural destruction caused likely dealumination was confirmed Al^{27}MAS-NMR results. The new correlation was developed by plotting the relative crystallinity (C/C_o) against one per the square root of the particle size (d_0) of Y zeolite. The correlation accurately predicts the hydrothermal stability of Y zeolite in small to medium particle sizes for a given temperature. For the larger particle sizes of Y zeolite (> 0.45 μm), due probably to the presence of more structural defects in the zeolite as shown by higher Brø nsted/Lewis acid ratios, no exact correlation between particle size and hydrothermal stability was found by investigation from NH_3 TPD and pyridine adsorption, respectively.

Department……Chemical Engineering… Student's signature…….
Field of study…Chemical Engineering… Advisor's signature…….
Academic year…..2003……

ACKNOWLEDGEMENTS

The author would like to express his greatest gratitude to his advisor, Professor Piyasan Praserthdam for his invaluable guidance throughout this study. In addition, he is also grateful to Dr Montree Wongsri, as the chairman and, Dr Suphot Phatanasri and Dr Bongkot Ngamsom as the member of the thesis committee.

The author would like to acknowledge with appreciation to Dr Joongjai Panpranot, Dr Chuwong Chaisuk, and Dr Okorn Mekasuwandumrong for enormous number of suggestions and assistance.

Special thank to petrochemical laboratory member who has encouragement and guided him over the year of this study

Finally he would also like to manifest his greatest gratitude to his parent and his family for their support and encouragement.

CONTENTS

CONTENTS (Cont.)

CONTENTS (Cont.)

LIST OF TABLES

LIST OF FIGURES

LIST OF FIGURES (Cont.)

CHAPTER I

INTRODUCTION

Fluid catalytic cracking (FCC) produces approximately one-third of the world's gasoline supply with faujasite-type zeolites. The commercial FCC catalysts are consisted of 1-2 μm Y zeolite embedded in the matrix of 40-80 μm spherical amorphous aluminosilicate particles. While circulating in an FCC unit, zeolites encounter severe hydrothermal conditions resulting in physical and chemical changes that affect surface area, pore volume, and catalytic cracking performance of zeolites. Several factors influencing the hydrothermal stability of Y zeolite have been reported including Si/Al ratio [1-2], dealumination procedure [3-7], and hydrothermal aging conditions [8-9]. Higher hydrothermal stability of zeolites was obtained by preparing zeolites with higher Si/Al ratio or by incorporating rare earth or noble metals into the zeolite framework to help preventing dealumination upon hydrothermal treatment [10-13].

Particle size of zeolites has been found to affect the performances of zeolites for many catalytic reactions. For example, Rajagopalan et al. [14] studied the effect of particle size of NaY zeolite in the range of 0.06-0.65 μm on the activity and selectivity in FCC reaction. It was found that the catalysts containing smaller-particle zeolites showed higher activity in the cracking of gasoil and higher selectivity to gasoline and light cycle oil than the ones containing larger-particle zeolites. Gianetto et al. [15] showed similar results for the ultra stable submicron Y (USSY) zeolites. The changes of zeolite particle size significantly affected the amount of total aromatics, benzene, C_4 olefins, and coke during FCC. Al Khattaf and de Lasa [16] reported that the cracking conversion of 1,3,5-tri-*iso*-propyl-benzene using 0.4 μm Y zeolite was higher than that using 0.9 μm zeolite due to the constrained diffusional transport in the larger Y-zeolite particles. However, smaller-particle zeolites were often found to be less stable than larger particle ones. The optimum size of zeolite crystal is, therefore, required in order to achieve the desired performance [17-18]. In a

previous study reported from our laboratory, Praserthdam et al. [19] investigated the effect of particle size on the durability of Co/HZSM-5 in selective reduction of NO. The smaller particle size Co/HZSM-5 showed the greater durability. The critical diameter of the particle size of Co/HZSM-5 for such reaction was determined to be 2 μm.

In this study, a new correlation between particle size and hydrothermal stability of Y zeolite was developed. The effects of particle size and pretreatment conditions simulated those in FCC reaction on the structural changes of Y zeolite were investigated by means of X-ray diffraction (XRD), nuclear magnetic resonance (NMR), scanning electron microscopy (SEM), BET surface area (BET), temperature-programmed desorption (TPD) of NH_3, and Fourier transform infrared (FTIR) spectroscopy of adsorbed pyridine.

1.1 Thesis Objective

To find correlation between particle size and hydrothermal stability of Y zeolite

1.2 Thesis Scope

1.2.1 Preparation Y zeolites (Si/Al = 4.5) using hydrothermal method at Si/Al is equal to 4.5 in order to varying particle size.

1.2.2 Treatment of the assyn-Y zeolite under hydrothermal treatment condition as follows:

1.2.2.1 Temperature 873, 973, 1073, 1173 and 1273 K

1.2.2.2 Steam partial pressure 5, 10, 20, 50, and 100 mole percent of water

1.2.2.3 Time 0.5, 1, 2, 3, 5 h

1.2.3 Characterization of Y zeolite samples by the following methods

(a) Structure and crystallinity of samples by X-ray diffractrometer (XRD).

(b) Morphology of sample by Scanning Electron Microscopy (SEM).

(c) Specific surface area by N_2 adsorption based on BET method (BET).

(d) Determination of chemical composition of catalysts by X-ray Fluorscence (XRF).

(e) Quantitative analysis of tetrahedral aluminium in samples by ^{27}Al nuclear magnetic resonance (^{27}Al NMR).

(f) Acid Contents and strength of acid sites in samples by temperature programmed desorption of ammonia (NH_3TPD).

(g) Types and strength of acid sites in samples by pyridine adsorption.

1.2.4 To find the optimum correlation between particle size and hydrothermal stability of Y zeolite at various treated conditions.

The present thesis is arranged as follows:

Chapter II presents the literature reviews of synthesis, hydrothermal stability, dealumination, acid sites, and particle size of Y zeolite.

Chapter III presents the theoretical consideration on Y zeolite.

Chapter IV presents the experimental systems and operation procedures. The experimental results obtained from the laboratory scale and standard measurements are reported and discussed in chapter V.

The last chapter gives overall conclusion emerged from this work. Finally the calculation of percent crystallinity and data experiments are included in appendices at the end of this thesis.

CHAPTER II

LITERATURE REVIEWS

In this chapter, literature reviews have been made for 2.1) Synthetic of Y zeolite, 2.2) Hydrothermal treatment, 2.3) Acid sites, and 2.4) Particle size of zeolite

2.1 Synthetic of Y zeolite

Barrer's in the mid late 1940's inspired of the Linde Division of Union Carbine Corporation to initiate studies in zeolite synthesis in search of new approaches for separation and purification of air. Between 1949 and 1954 R.M. Milton and coworker D.W. Breck discovered a number of commercially significant zeolites, type A, X, and Y. In 1954 Union Carbide commercialized synthetic zeolites as a new class of industrial materials for separation and purification. The earliest applications were the drying of refrigerant gas and nature gas. In 1955 T.B. Reed and D.W. Breck reported the structure of synthesis zeolite A. In 1959 Union Carbide marketed the "ISOSIV" process for normal-isoparaffin separation, representing the first major bulk separation process using true molecular sieving selectivity. Also in 1959 a Y zeolite zeolite catalyst was marketed by Carbide as an isomerization catalyst.

Zeolites are aluminosilicate-based microporous material containing well-defined pore and channel system with molecular dimensions. In the pore system of Y zeolite, the three-dimensional channel system (7.8Å in diameter) links three kinds of cages, α, β and 6-ring prism [20]. Only the α-cage is accessible to N_2 and bigger molecules; it accounts for a pore volume of 0.35 ml/g in a perfectly crystallized Y

zeolite [21]. It has been observed that there are about 20% less pore volume measured by n-hexane than that by N_2 [22].

Bauer and coworkers in the early 1960s developed the use of reaction mixtures containing quaternary ammonium ions or other cations to direct the crystallization process. In their work and succeeding studies, a primary motivation was to attempt to synthesize zeolites with large apertures than X and Y. This did not occur, but instead organic species were found to modify the synthesis process in a variety of ways that led to the discovery of many new zeolites, and new methods of synthesizing zeolite with structures similar to previously known zeolite.

In 1962 Mobil Oil introduced the use of synthetic of zeolite X as a cracking catalyst. In 1969 Grace described the first modification chemistry based on steaming Y zeolite to form an “ultrastable” Y. In 1967-1969 Mobil Oil reported the synthesis of the high silica zeolites beta and ZSM-5. In 1974 Henkel introduced zeolite A in detergents as a replacement for the environmentally suspect phosphates. By 1977 industry-wide 22,000 tons of Y zeolite was in use in catalytic cracking. In 1977 Union Carbide introduced zeolite for ion-exchange separation.

Exactly, zeolites are generally synthesized by a hydrothermal process from a source of alumina (e.g., sodium aluminate or aluminium sulfate) and of silica (e.g., a silica sol, fumed silica, or sodium water glass) and an alkali such as NaOH, and/or a quaternary ammonium compound. An inhomogeneous gel is produced which gradually crystallizes, in some cases forming more than one type of zeolite in succession. Nucleation effects can be important, and an initial induction period at near ambient temperature may be followed by crystallization temperature that may range up to 473 K or higher. The pressure is equal to the saturated vapor pressure of the water present.

After synthesis the zeolite are washed, dried, heated to remove water of crystallization, and calcined in air, e.g., at about 823 K. Organic species are also thus removed. For most catalytic purpose, the zeolite is converted into acidic form. For some zeolites this can be achieved by treatment with aqueous HCl without

significantly altering the framework structure. For other zeolites Na^+ is replaced with NH_4^+ via an ammonium compound such as NH_4OH, NH_4Cl or NH_4NO_3.Upon heating NH_3 is driven off, leaving the zeolite in the acid form. For some reaction a hydrogenation component such as platinum or nickel is introduced by impregnation or ion exchange [23].

The final product depends on a complex interplay between many variables including SiO_2/Al_2O_3 ratio in the starting medium, nucleating agents, temperature, pH, water content, aging, stirring, and the presence of various inorganic and organic cations. Much remains to be learned about how the initial reaction mixture forms the precursor species and how these arrange into the final crystalline products. A key concept is that the cations present give rise to a templating action, but clearly the process is more complex.

The mechanism of action of the organic species is still controversial. It was originally thought to be primarily a templating effect, but later it was found that at least some of zeolites could be synthesized without an organic template. Further, organic species other than quaternary ammonium compounds had directing effects not readily ascribed to their size or shape. However, an important result was the zeolites of higher SiO_2/Al_2O_3 ratio than before could be synthesized. Previously, only structures with SiO_2/Al_2O_3 ratios of about 10 or less could be directly forms, but with organic additives, zeolites with ratio of 20 to 100 or more can be directly prepared.

Recently, Y zeolite has been found to exhibit a good catalytic performance for catalytic process because of its unique properties, for instance the main pore structure is uniform three-dimension with widely pore opening enough to admit the large molecules, excellent flexibility structure to control Al content of the structure for possible to optimize active catalyst, high thermal and hydrothermal stability in order to withstand regenerate conditions.

However, the synthesis of Y zeolite is a complex process, due to the complexly growth of pure crystal of Y zeolite is very sensitive to preparation

condition. Furthermore the poor crystal has negative effect to the performance of Y zeolite catalyst.

The synthesis of Y zeolite is a typical inorganic reaction procedure, the properties of the product being affected by temperature, stirring, mixing method, concentration, and time of aging. While effective, seeding necessitates the preparation of two separate gels and is quite sensitive to changes in procedure, the reserve time and temperature effects. Since synthesis based on colloidal silica involves a single gel, such systems are better for investigating the effects of gel aging and easier to prepare under industrial conditions [24-25].

Iso Miyanohara and coworker [26] presented the process for prepareing Y zeolite had a SiO_2/Al_2O_3 ratio of at least about 4. The process was comprise of two step, in the first step an aqueous alkali silicate solution and aqueous alkali aluminate solution were mixed together in order to form gel in the mix solution. In the second step, the separated gel is incorporated in an aqueous alkaline mixed solution to obtain slurry and, then a Y zeolite crystal is formed in the slurry.

Furthermore, the effect of aging on synthesis has been investigated and described for some zeolites, especially for A zeolite [27-28]. Aging is generally considered to play a significant role in the synthesis of Y zeolite, especially to suppress phases other than faujasite. Some studies have already been carried out to determine how aging influences the synthesis of Y zeolite and smaller Y zeolite crystals have been obtained by using different methods in which aging is a noteworthy tool [29].

Köroğlu et al [24] studied the effects of low-temperature gel aging on the synthesis of Y zeolite. It was determined that both the particle sizes and the span of the size distribution may be decreased further by aging the aging temperature below room temperature. The alkalinity of the gel composition seemed to play a significant role in determining the magnitude of the effects of lowering the aging temperature on particle size and the size distributions of the aged zeolite sample. The Si/Al ratio of Y

zeolite was enhanced when the lower aging temperature and less alkaline gel composition were used.

2.2 Hydrothermal treatment

The hydrothermal treatment is a useful technique to examine zeolite structural changes when exposed to hydrothermal conditions with the assumption of no other influences such as contaminants metals levels, catalyst addition rate, etc. Structural changes of the catalyst caused by steam treatment include reducing surface area, microporosity, and crystallinity which attributed to decreasing cracking activity and changing selectivity of the cracking catalyst [30].

Hydrothermal treatment (deep- or shallow-bed calcination in the presence or absence of water vapor) involves aluminum extraction and dehydroxylation [31]. It may result in two major modifications to the zeolite catalysts: (1) structure modifications in which the framework Si/Al is changed, resulting in a change in the number and eventually the strength of the Brönsted acid sites as well as in the number and strength of the Lewis acid sites present on the NFAl species; (2) porosity modifications which may change the initial pore diameter and thus the availability of the acid sites.

Besides, hydrothermal stability is an important requirement to be fulfilled by the zeolite component of an FCC catalyst since it influences both the activity level of the equilibrium catalyst and the amount of fresh catalyst addition need. It is therefore necessary to get acquainted with the nature of deactivation process. [32]. Hydrothermal treatments at different temperatures and for different times have been used long in order to break down the extreme high initial activity of fresh cracking catalyst, to make them suitable for determining and comparing their catalytic properties by means of standard activity tests.

Treatment conditions are important of parameters which affect on steam treatment, many previous researchers studied about that, McElhiney [33] proposed a single specific condition for steam aging cracking catalyst at 1088 K with 100% steam and ambient pressure for 5 h. This method had the purpose to reduce the structural and catalytic properties of certain fresh commercial catalysts to equilibrium levels in a short period of time for further evaluation using microactivity test [34]. This sample steam aging procedure has been found capable of reducing the acidity of fresh FCC under study to those that same FCC exit after being used in an actual FCCU. However, this method provides insufficient data to describe hydrothermal stability of a cracking catalyst.

According to an evaluation of fluid cracking catalysts, made by Mcclean and Moorehead in 1989 [35], it has been stated that a number of laboratories used a fixed time and temperature ranges from 1033-1088 K to achieve a range of deactivated samples. The aged samples obtained were evaluated in a microactivity test (MAT) unit. Zeolite surface area and unit cell size as functions of were shown in plots. Also in Mclean and Moorehead study [35], the temperature was fixed and the time was varied from 5-60 h with a preferred time of 4-24 h. Hydrothermal stability curves were constructed.

Gardner et al [36] reported to irreversible deactivation kinetics of H-USY and H-ZSM-5 zeolites with a steam aging technique. The effects of steam partial pressure, temperature and time on zeolite hydrothermal stability have been investigated. Catalyst performance was described in a form of kinetic model of zeolite surface area reduction as a function of aforementioned three variables.

In addition to the various steam treatment methods discussed, two techniques for introducing catalysts into laboratory reactors have been used. Gas-solid contacting schemes had also been taken into account for steam treatment procedures. The type of gas-solid contacting used produced differing steam aged catalyst properties [37]. The work done by Kerr [38] reported two methods to fill a ceramic “boat” with catalyst sample. These two methods had also been reported by Basacek and Patzelova [39].

The first method described steam treatment under “deep bed” conditions [38]. An aged distribution within the sample was formed due to the variation in gas-solid contacting along the depth of the bed. With water or ammonia molecules liberated during this treatment, self-steaming of the lower layers of the zeolite sample occur.

The second method described steam treatment under “shadow bed” conditions [38]. A thin layer of zeolite catalyst sample was filled in the ceramic “boat”. Shallow-bed steam treatment provided good gas-solid contacting and perhaps results in more homogeneously deactivated sample. This sample was found to be especially useful with extremely fine zeolite particles when the fluidized bed method was unsuitable.

On the other hand, metal loading also may improve hydrothermal stability of zeolite. Dangsawai et al [12] found that Pd-modification of Cu/H-ZSM-5 improved its stability for NO removal under hydrothermal conditions. Pd/Cu/H-ZSM-5 showed higher activity for NO conversion than Cu/H-ZSM-5, although there was a decrease in the activity of the Pd/Cu/H-ZSM-5 after pretreatment. The conversion of NO to N_2 on the pretreated Pd/Cu/H-ZSM-5 was twice that on the pretreated Cu/H-ZSM-5 at a reaction temperature above 773 K. Destruction of the zeolite framework was not a significant factor in deactivation of the catalyst.

Praserthdam et al [11] reported that the MFI framework stability of Cu/H-MFI was maintained after pretreatment at 1073 K in a He stream with 10 mol% H_2O by the presence of Pd. The dealumination of tetrahedral Al in MFI framework was completely prevented when the amount of Pd loading was 0.3wt% or higher. The stabilization effects of Pd are due to the prevention of dealumination and the ability to maintain the active Cu^{2+} species. The presence of an optimum amount of Pd in Pd/Cu/H-MFI, approximately 0.2-0.3 wt% loading, improved the catalysts stability for NO removal under hydrothermal treatment conditions. Further loading of Pd higher than 0.3 wt% may cause some changes in Pd and Cu on H-MFI.

Indeed, the hydrothermal treatment is found to cause dealumination of the zeolite lattice and formation of extralattice aluminium species of low symmetry,

which remain within the pores of zeolite [40-41]. The effect of hydrothermal treatment on the structure and properties of zeolite with a range of aluminium contents has been investigated. Characterization of the treated zeolite was undertaken with solid-state NMR (^{27}Al and ^{29}Si), Infrared water adsorption, X-ray diffraction [40], and chemical analysis [36].

Generally, Dealumination decreased the amount of extraframework Al species and, hence, the difference between the amounts of Al and Brönsted sites. Dealumination also decreased the number of Lewis acid sites [42]. IR studies of pyridine desorption evidenced that, as well as strong Brönsted sites (Si-OH-Al), there were also weak Brönsted sites, not Si-OH-Al; their nature is not clear. The contribution of such weak Brönsted sites decreased with the extent of dealumination. Dealumination removed the less acidic hydroxy groups first.

Many authors have investigated the chemistry of dealumination of the zeolite lattice, making the details of the process of both processes quite clear. The essence of the process is that the presence of both water vapor and multivalent cations contributes to the stabilization of the dealuminated sites. All reaction schemes agree in pointing out that as a result of any hydrothermal effect the Si/Al ratio can only increase, and that re-entering of aluminum into the tetrahedral positions of the lattice is impossible.

Tang Yi and coworker [43] studied the effect of dealumination defect on the properties of Y zeolite. The unit cell size and IR asymmetric stretch frequency of dealuminated zeolite were defected by the defect structure, because the hydroxyl nest was larger than the SiO_4 tetrahedron but smaller than AlO_4 tetrahedron and the presence of hydroxyl group in the nest weakened the Si-O bounds in the framework. In consequence, the thermal and hydrothermal stabilities of zeolite were lowered due to the presence of defect structure. The defect structure also influenced the acid distribution. For sample with high defect concentration the strong acidity was reduced and medium acidity was increased significantly because of the composition of zeolite during heat treatment.

Klinowski, Thomas, Fyfe and Gobbi [44] dealuminated NaY zeolite samples using various methods including steaming and acid leaching. High resolution magic-angle-spinning solid-state ^{29}Si and ^{27}Al NMR spectroscopy was used to monitor structural changes within the zeolite framework. The results showed that the empty aluminum atom vacancies were partially reoccupied by silicon atoms which not only came from noncrystallization fractions of zeolite but also from the local recrystallization of the framework silicon atoms.

The recent studies demonstrated that part of aluminium atom disconnected from the framework during calcination or steaming could reinsert by post-synthesis hydrothermal treatments [45-46]. The state of the aluminium atoms in actual catalysts would then strongly depend on the nature and severity of the activation treatments as well as on the composition and structure of parent solid. Careful characterization of the local environment of the aluminium atom was therefore essential for the understanding of the catalytic properties of zeolite.

Besides, the extent of dealumination decreased in the same order as the number of T-sites in four-ring: Beta > Mordinite > ZSM-5 > terricirite. Factors such as the zeolite structure type, the Si/Al ratio of the framework, the particle size, and the number of Brönsted acid sites interacting with the framework or the number of defect sites influenced the dealumination behavior of an individual zeolite sample. Zeolite beta can be very easily dealuminated. After the deep bed calcination, only about one-fourth of the alumination atoms remained in the lattice and a large amount of EFAI was present. The XRD powder patterns and the surface areas showed that the crystallinity of the sample was retained after treatment [47].

On the other hand, dealumination was used to increase the Si/Al ratio of the zeolitic framework, while increase the thermal stability but also because the amount of acidity [40,48]. Dealumination was performed various treatment by various thermal or hydrothermal treatments complexation by oxalic acid, direct replacement of aluminium by silicon with gaseous silicon tetrachloride [41], HCl treatment [49] and dicarboxylic acid treatment [42].

Guo Xing et al [4] prepared siliceous Y zeolite (SiO_2/Al_2O_3 >150) through repeated dealumination with $SiCl_4$ and steam, displays high thermal and hydrothermal stability. After aged at 1473 K for 4 h, siliceous Y zeolite show specific surface area as high as 510 m^2/g. Even steamed at 1273 K for 4 h, it skill keeps its framework perfectly. When palladium is supported on SY-A carrier, in which 12.3% alumina has been loaded on siliceous Y zeolite, the catalyst shows higher oxidation activity than $Pd/La\text{-}Al_2O_3$ even heated or steamed at 1273 K for 4 h. Its excellent resistances to heat and steam make it a promising catalyst for high-temperature catalytic combustion.

Kerr [50] treated NaY zeolite with an acidic solution of ethylenediamine tetraacetic acid (EDTA) to obtain a homogeneously dealuminated zeolite sample. His proposed dealumination mechanism was that each missing aluminum atom was replaced by four hydrogen bonding to the oxygen atoms of the vacated tetrahedron. The four hydroxyl products each bonded to silicon were believed to condense to yield water and form Si-O-Si bonds upon heating. The new Si-O-Si bond has been found to improve the framework thermal stability. The optimum removal of aluminum for thermal stability was in the range of 25-50%.

Gallezot, Beaumont and Barthomeuf [51] followed the same procedure as in Kerr's work by using EDTA to remove aluminum atoms of NaY zeolite and derived a homogeneously dealuminated zeolite sample. The results obtained from x-ray powder diffraction showed no significant change of the occupancy factor of the zeolite framework atoms. This was interpreted as the vacancies in the framework left by homogeneously removed aluminum atoms were refilled through a local crystallization process so the overall structure was preserved. The process was found to involve the formation of new SiO_4 tetrahedral. Two possible sources of silicon atoms were either from siliceous impurities, which are often present in synthesis zeolites or from the zeolite framework itself.

Sulikowski, Karge and Mishin [52] proposed an improved method for dealumination of faujasite-type zeolites with silicon tetrahedral treatment. With this method, in contrast to hydrothermal treatment or acid leaching, the direct substitution

of the framework aluminum by silicon atoms was reported. However, the reaction has a limited temperature up to about 773 K. Beyond this point, higher of dealumination cannot be obtained due to the deposition of the reaction product $NaAlCl_4$ in the pore system. The presence of aluminum extra-framework species was revealed by ^{27}Al MAS NMR spectroscopy.

2.3. Acid sites

The total acidity of zeolite catalysts may be considered to be a contribution of both an extensive factor representative of the number of acid sites and an intensive factor representative of the strength of the individual sites [53-54]. For structurally pure hydrogen-zeolites, the nature of acid sites is conceptually well defined. In that case Brønsted acid is associated with the labile protons in the neighborhood of tetrahedrally coordinated lattice aluminum sites. Thus, the extensive factor of acidity is simply the number of protons held by the lattice aluminum per unit volume. Already in 1965 it was recongnized [55] that the intensive factor could be greatly enhanced by the simple process of partial dehydroxylation that reduces the extensive factor.

There are many factors which may affect the intensive factor of the acidity in zeolites. For example, it has been well documented that an optimum aluminum concentration exists in zeolites which corresponds to maximum acidity. Although further increasing the lattice aluminum concentration results in an increase in the extensive factor, the intensive factor is reduced due to delocalization of the negative charge density in the lattice.

The charge density increase with increasing of Si/Al ratio based on electrostatic consideration. It was conceived that these phenomena are related to reduction of electrostatic interaction between framework sites, and possibly to difference in the order of aluminum in zeolite crystal-the location of Al in crystal structure [56].

The interactions between adsorbed molecules and the framework and cations in the channels of zeolites have been investigated by a wide range of experimental and theoretical techniques. Such information is useful in investigating the catalytic properties of zeolite. For example, to investigate the acid sites in zeolite, a basic probe molecule such as ammonia or pyridine may be introduced, and changes in the vibrational of the guest give information about the nature of the site where the molecule is adsorbed. Hence, infrared studies of pyridine adsorbed in hydrogen-Y zeolite reveal the formation of a pyridinium ion in the latter, indicating that adsorption is at Brønsted and Lewis acid.

Classical Brønsted and Lewis acid models of acidity have used to classify the active sites on zeolites. Brønsted acidity is proton donor acidity; a tridiagonally coordinated alumina atom is an electron deficient and can accept an electron pair, therefore behaves as a Lewis acid [57].

Protonic acid centers of zeolite are generated in various ways. Figure 2.1 depicts the thermal decomposition of ammonium-exchanged zeolite yielding the hydrogen form [23].

The Brønsted acidity due to water ionization on polyvalent cations, described below, is depicted in Figure 2.2 [58].

$$M^{n+} + xH_2O \text{ ----------> } M(OH)_x^{(n-x)} + xH^+ \qquad (2.1)$$

The exchange of monovalent ions by polyvalent cations could improve the catalytic property. Those highly charged cations create very centers by hydrolysis phenomena. Brønsted acid sites are also generated by the reduction of transition metal

cations. The concentration of OH groups of zeolite containing transition metals was note to increase by hydrogen at 298-723 K to increase with the rise of the reduction temperature [59].

$$Cu^{2+} + H_2 \text{ ----------> } Co^{o} + 2H^{+} \quad (2.2)$$

$$Ag^{+} + 1/2H_2\text{----------->}Ag^{o} + H \quad (2.3)$$

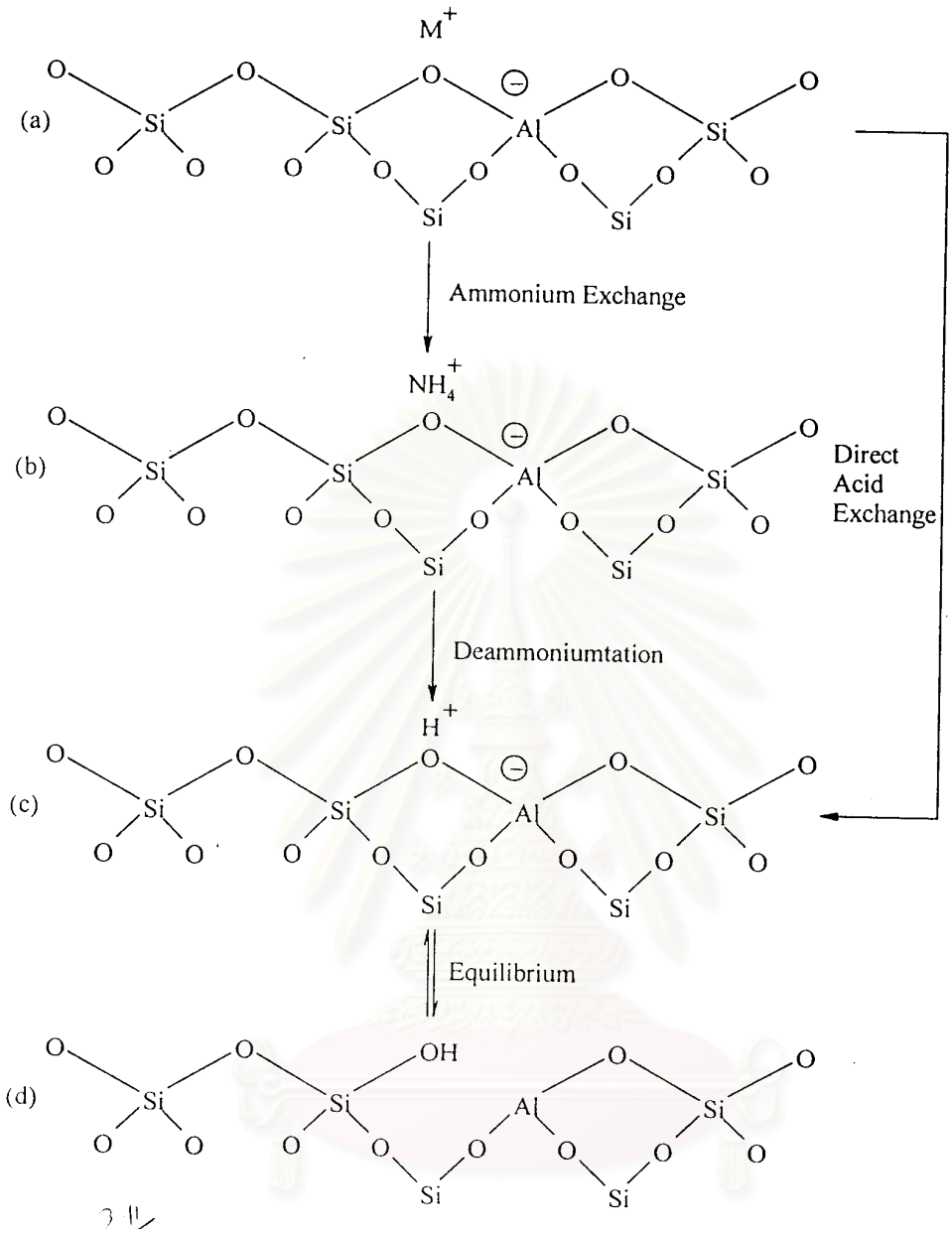

Figure 2.1 Diagram of the surface of a zeolite framework [23].

a) In the as-synthesis form M^+ either an organic cation or an alkali metal cation.

b) Ammonium in exchange produces the NH^+ exchanged form.

c) Thermal treatment is used to remove ammonia, producing the H^+, acid form.

d) The acid form in (c) is in equilibrium with the shown in (d), where is a silanol group adjacent to tricoordinate aluminium.

The formation of Lewis acidity from Brønsted acid sites is depicted in Figure 2.3 [23]. The dehydration reaction decreases the number of protons and increases that of Lewis sites. Brønsted (OH) and Lewis (-Al-) sites can be present simultaneously in the structure of zeolite at high temperature. Dehydroxylation is thought to occur in ZSM-5 zeolite above at 773 K and calcination at 1073 K to 1173 K produces irreversible dehydroxylation, which causes defection in crystal structure of zeolite.

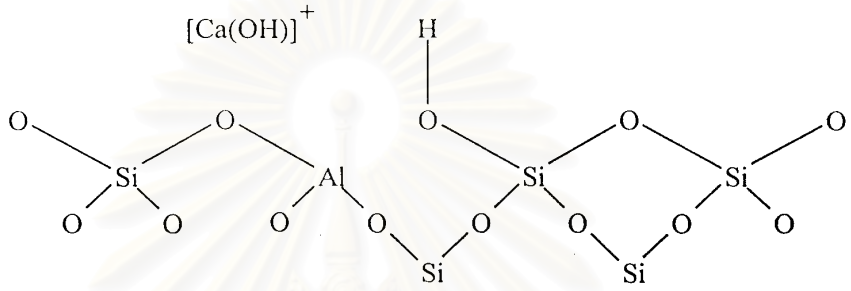

Figure 2.2 Water molecules coordinated to polyvalent cation is dissociated by heat treatment yielding Brønsted acidity [23].

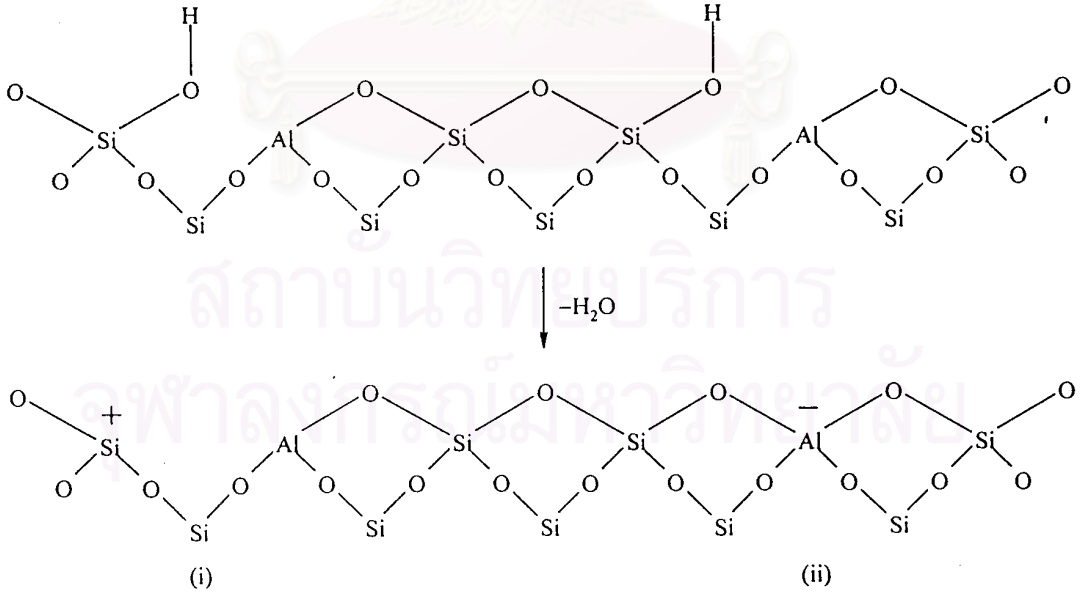

Figure 2.3 Lewis acid sites developed by dehydroxylation of Brønsted acid site [23].

Dealumination is believed to occur during dehydroxylation, which may result from the steam generation within the sample. The dealumination is indicated by an increase in the surface concentration of aluminum on the crystal. The dealumination process is expressed in Figure 2.4 [23]. The extent of dealumination monotonously increases with the partial pressure of steam.

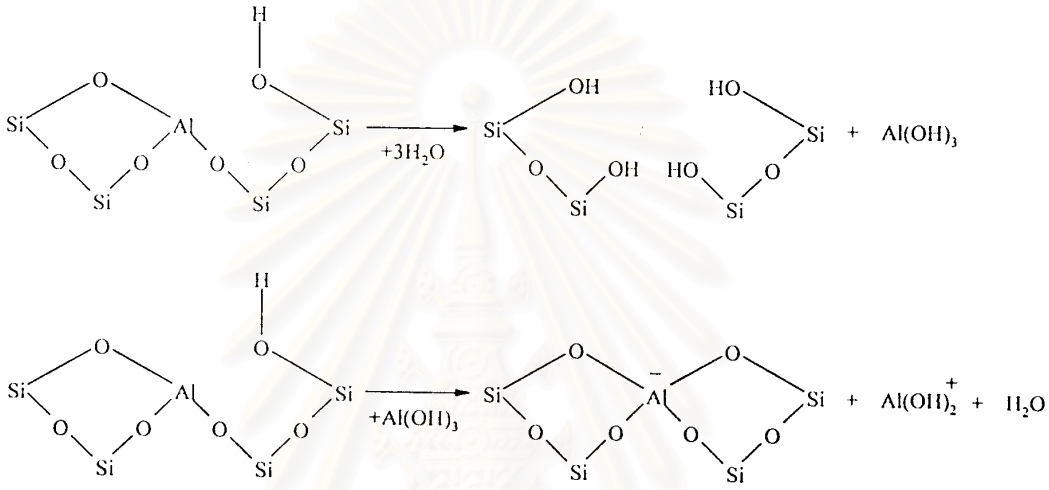

Figure 2.4 Steam dealumination process in zeolite [23]

In general, the increase in Si/Al ratio will increase acidic strength and thermal stability of zeolite [61]. Since the numbers of acidic OH groups depend on the number of aluminium in zeolites framework, decrease in Al content is expected to reduce catalytic activity of zeolite. If the effect of increase in the acidic centers, increase in Al content, shall result in enhancement of catalytic activity.

An improvement in thermal or hydrothermal stability has been ascribed to the lower density of hydroxyl groups, which id parallel to that of Al content [23]. A longer distance between hydroxyl groups decreases the probability of dehydroxylation that generates defects on structure of zeolites.

Boréave et al [60] studied about nature and strength of acid sites in HY zeolites, has allowed a detailed study of the acidity of commercial HY faujasites, both non-dealumanated and dealuminated by hydrothermal treatment. These techniques have been used with different basic probe molecules such as ammonia, pyridine and 2,6-lutidine. They have demonstrated the existence of three different regions of acid strength.

Temperature programmed desorption of bases can very easily show differences in the acidity between catalysts. Nevertheless, some difficulties are encountered when trying to quantify these differences because the peaks due to desorption from acid sites with different strength overlap extensively, leading to complex thermograms. The classical usage of TPD involves a success of experiments that are lengthy to carry out and give only a rather limited amount of information regarding the acid strength of the solid [61-62]. However, several methods have been proposed to allow the use of a single TPD experiment to obtain more detailed information concerning the acid strength distribution of a zeolite [63]. In order to investigate the effect of pre-treatments on the zeolitic structure further, ammonia-TPD experiments were carried out to follow the changes in the acidity of the Y-zeolite supports when subjected to different treatments. The highest amount of desorbed NH_3 was detected from the original Y-zeolite. Pre-calcination and hydrothermal aging of the parent zeolite resulted in considerably decreased acidity as the hydrothermally treated Y-zeolite, though keeping the same desorption pattern, exhibited ca. 50 times decreased ammonia adsorption.

Abello et al [64] was determined TPD of NH_3 which has been used to obtain information about the strength of the interactions between ammonia ad a Na-Y zeolite. Monte Carlo simulation was employed to interpret the TPD spectra taking into account a distance a discrete inhomogeneity of the zeolite structure. Zeolite showed a significant amount of adsorption sites (80%) distributed in the adsorptive potential range between 22 and 33 kcal/mol. The heat of adsorption decreased with increasing ammonia coverage from 30 to 19.4 kcal/mol, and these values were in agreement with microcalorimetric measurements.

2.4. Particle size

Over the past decade, processing heavy oil in fluid catalytic cracking (FCC) units has become more prevalent due to the declining availability and higher price of light crudes. These market trends have made resid upgrading economically more attractive. However, processing heavy feedstocks containing bulky molecules offer new challenges to FCC given the possible hindered transport of hydrocarbon species inside the zeolite structure.

Y-zeolites have been used extensively in FCC since the 1960s. The commercial FCC catalysts are manufactured with 1–2 μm zeolites dispersed in an amorphous silica–alumina matrix forming the 60 μm particles [65]. In these catalysts, most of the active sites are located within the zeolite pore structure. In order for the reaction to proceed, molecules have to evolve through the large matrix pores into the zeolite crystals. As a result only certain hydrocarbon species with a molecular size smaller than a given dimension can penetrate the zeolite pore structure [66]. For the larger hydrocarbon molecules, only the active sites situated on the external surface area of the zeolites, representing about 3% of the total surface area, are available [67].

While diffusion in the catalyst matrix belongs to the well-known Knudsen regime, diffusion in zeolites falls into the configurational regime [68]. This kind of diffusion is a process with activation energy substantially larger than the ones for other types of diffusion. Since the size of the molecule in the pore is nearly the size of the passageway, the diffusion of molecules in zeolites is governed by a continuous interaction between the zeolite crystal and diffusing molecules.

The particle size of catalysts for cracking hydrocarbons in fluidized beds reactors (FCC process), which are basically composed of a zeolite component (Y zeolite) in matrix and various additives, are subjected to severe, changing environments in the cyclic operation of commercial units. This is due to the circulation between the reducing atmosphere of the reactor at about 773 K and the oxidizing atmosphere of the regenerator at about 1023 K, where coke is burnt off in air in the presence of steam [69]. A strong dealumination process is induced on the

zeolite, as well as profound changes in both the chemical and physical properties of the fresh compound catalyst. It is well known that the loss of aluminum from the zeolite crystal structure translates into unit cell size shrinking concomitantly with the appearance of extra-framework aluminum species; finally, this ends up with the so-called “equilibrium” catalyst (E-CAT). The very different properties of the E-CATs as compared with fresh samples have repercussions on the catalytic performance, stressing the need for proper evaluation procedures [70].

2.4.1 Scope of zeolite crystal-size control

The sensitivity of zeolite catalysts to crystal-size effects derives from the same properties that account for their selectivity. Slow configurational diffusion in molecular-size micropores justifies the preferential adsorption of small reagents and the selective desorption of small products, but this property can also severely impair the effectiveness of the catalyst. Shape-selective catalytic reactions on zeolites and diffusion in zeolites have been the object of recent reviews. In any case, shape selectivity is higher for larger crystals. The optimum particle size for shape-selective catalysis is the result of a compromise between selectivity and effectiveness.

Several parameters influence the choice of the optimum size of zeolite crystals: (a) shape-selective catalysis requires larger crystals; (b) catalyst effectiveness is larger for smaller crystals; (c) in bifunctional catalysts, particle size can influence the average distance between acidic and metallic sites, and modify the product distribution; (d) coke deactivation can be more severe for larger crystals; (e) diffusion of matrix components is easier in the case of smaller crystals; (f) template extraction, cation exchange, even distribution of metal functions are more easily performed for smaller crystals; (g) diffusion of water and extra-framework species as a function of particle size affect the hydrothermal stability in activation conditions; (h) regeneration of used catalysts can be more difficult for larger crystals; (i) filtration and recovery of very small crystals is a technological challenge.

Particle size is ultimately imposed by the catalytic reaction: TS-1 crystals larger than a fraction of μm are considered unfitted as phenol hydroxylation catalysts,

due to the slow diffusion at the low temperature of reaction. In other cases, the optimum particle size should take into account both reactivity and zeolite activation, as in the case of zeolite beta as cracking catalyst.

2.4.2. Parameters affecting zeolite particle size

How to control the size of zeolite crystals? Zeolites follow the usual laws of crystal growth, available in recently re-edited textbooks. In batch crystallization, particle size is a function of the ratio between rate of nucleation and rate of growth. Both rates increase with supersaturation, but the exponential law of the nucleation rate rises more sharply than the low-order power law of the growth rate. As a consequence, smaller crystals and rapid syntheses are observed at high supersaturation. Unfortunately, supersaturation can hardly be considered as an independent variable in zeolite synthesis, concentrations being often controlled by the solubility of ill-characterized amorphous precursors. Several parameters (alkalinity, ionic strength, dilution, and temperature) influence silicate solubility and modify the concentration levels in the synthesis system. The presence of an amorphous "gel" also affects diffusion processes in the mother solution, and stirring effectively modifies crystallization kinetics. Nucleation can be affected by other procedures, like aging of the synthesis medium, seeding, and selective crystallization poisoning. The application of classical laws of crystal growth to zeolite synthesis has been thoroughly checked by modeling of zeolite crystallization with population balance models.

The formation of unwanted competing phases is especially easy in zeolite crystallization. The preparation of each phase has to be independently optimized, and classical reviews are available on zeolite synthesis. Notwithstanding the differences among procedures for the formation of diverse phases, several parameters affect in a similar way all zeolite crystallizations. We can classify these parameters as:

- Crystallization conditions: temperature, stirring, seeding, gel aging;
- Composition-dependent parameters: alkalinity, dilution, ratio between Si and other tetrahedron-forming elements, template concentration, ionic strength, presence of crystallization poisons.

The particle size of zeolites is a significant parameter that effect the performance in several application related to catalysis, diffusion, adsorption, ion exchange, etc. Although the filtration and recovery of small zeolite crystals may be desired for obtaining higher catalytic effectiveness, lower coke formation, faster diffusion and higher external surface area as well as for easier cation exchange and template extraction [71]. Thin zeolites film to be utilized in potential applications, such as those related to the membrane separations [72] can also is prepared by using the synthesis conditions that allow the formation of small crystals.

The synthesis of microsized of Y zeolite has received much attention owing to its special properties, such as possession of a highly catalytic center, high surface atom ratio, large surface area, high surface energy [73-74]. FCC catalysts prepared from microsized Y zeolite with Si/Al ratio posses high catalytic activity and can be used in the refining of residual and heavy oils. It is also reported that use of microsized NaY zeolite can improve catalytic selectivity, reduce coke formation, increase the yield of diesel oil and promote gasoline quality; it can also be used in the fine chemical industry [75-76].

Acid zeolites as catalyst condensation of acetophenone with benzene derivatives was studied by Cilment et al [77]. Influence of zeolite crystalline structure and catalyst particle size on the course of the reaction reveals that a severe diffusion restriction is controlling the conversion and the selectivity of this process. In the case of tridirectional Y zeolites, we have seen that some kind of diffusion control does also exist. Indeed the conversion obtained on the HY with average particle size of 0.8 μm,

was lower than that obtained on a HY zeolite with similar framework Si/Al but with an average crystalline of 0.3 μm.

Alkylation of biphenyl with propylene was carried out over HY zeolites in the literature [78]. The influence of framework Si/Al ratio and particle size for the Y zeolite has been studied and it has been observed that, under the reaction condition used here, the process is not diffusion controlled. The high IPBP selectivity as well as the differences observed between the two zeolite samples have been explained on the based of differences in particle size and assuming that on this zeolite structure the reaction only takes place on the external surface.

Reaction testing involved different reaction times and temperatures, using Y zeolite of different particle size (0.4 and 0.9 μm) was reported by Al-Khattaf et al [16]. It was shown that 1,3,5-TIPB cracking using the 0.4 μm Y zeolite, higher 1,3,5-TIPB conversion were obtained. It is postulated that the 1,3,5-TIPB conversion differences are caused by constrained diffusional transport in the Y zeolite crystals and that the increase of temperature changes the catalytic cracking of 1,3,5-TIPB from diffusionally controlled regime to the kinetically controlled regime.

Aguiar et al [79] studied about the cracking of 1,3,5-TIPB carried out over two Y zeolite of 63 and 193 nm average particle sizes, revealed that much higher rates of reaction are obtained with the smaller crystallite sample. Nevertheless, when the rates of disappearance, which were at first expressed per g of zeolitic, were divided by the number of aluminum atoms on the external zeolitic surface, equal values were obtained for both zeolites. These results confirm the assumption that the reaction is taking place on just the external surface of the crystals.

Maselli and Peters [80] reported that small Y-zeolites were both more active and produced more liquid products than the large zeolites. Rajagopalan et al. [14] cracked gas oil using small and large Y-zeolites. These authors observed that the small size zeolites produced more gasoline and LCO and less coke and light gases than the large ones. Gianetto et al. [15] reported that the smaller Y-zeolite crystals

produced more olefins, *iso*-paraffins, less aromatics and less coke than the bigger crystals.

Besides, the importance of the lattice stability for the formation of Brönsted acid sites was further stressed by the influence of particle size on the catalytic activity. The preparation of small grain zeolite beta has been also considered as a desirable target in order to increase the effectiveness of the catalyst [81].

In the other hand, the utilization of larger crystal, on the other hand, may be favorable for other purposes. The determination of crystalochemical parameters, the generation of intrinsic crystal diffusion and adsorption data and obtaining higher selectivity in shape-selective catalysis requires the employment of larger crystals [82]. In some applications, especially those related to adsorption and catalysis, the utilization of an optimum size of zeolite crystals may be required for achieving the desired performance [17].

The development of method for producing zeolites with controllable macroshape and particle size is of great technological importance. Spherical form is often preferable e.g. for catalytic applications due to limit attrition and easy handing [83]. Further, the size and the arrangement of the particles building up a catalyst have a crucial role for its performance.

Recently, the relationship between hydrothermal stability and particle size of zeolite was studied; Frederic et al [84] studied the influence of composition and size of the parent crystals of zeolite beta on its acidity, stability and catalytic activity. The optimum in catalytic activity of zeolite beta was strongly influenced by dealumination during the activation process. Dealumination was generally favored in the case of aluminium-rich zeolites and, within an isostructural series, the stability of tetrahedral aluminium decreased as the aluminium molar ratio increased. Smaller crystals with higher aluminium contents were formed under synthesis condition that generated tetrahedra distortions and silanol defects, with a significant decrease of the thermal stability.

Bonetto et al [85] studied the optimum of zeolite beta in cracking catalyst. The zeolite betas with different particle sized have been used as catalysts for gas-oil cracking. An optimum compromise between stability, activity and selectivity has been found for a sample with an average particle size of 0.4 μm. This sample, before and after steaming, gived a slightly lower selectivity for gasoline and coke than a high and a low unit cell size USY zeolite, respectively. The optimized zeolite beta produced more liquefied petroleum gas alkens and a relatively high iso-butane yield that were useful for methyl tert butyl ether and alkylation gasoline production. Zeolite beta with the same silica-to-alumina ratio, but with particle size in a narrow distribution countered at ca. 0.17, 0.40 and 0.70 μm, was used to study the stability. The percentage of crystallinity retention during steaming was reported. The stability increased with increasing particle size but this increase was not very high.

Zhang et al. [41] studied the thermal and hydrothermal stability of nanosized and microsized HZSM-5 zeolite. The samples were treated at varies temperature as 400-700^{o}C and under 100% water vapor for 2 h. Both nanosizes and microsizes were slightly decreased as the hydrothermal temperature increased. The hydrothermal treatment of nanosizes and microsizes also caused the zeolite framework to dealuminate. The peak intensity of the framework Al at 52 ppm in the ^{27}Al MAS NMR spectra of the nanosizes decreased more readily than that of microsizes and the line width of the ^{27}Al MAS NMR spectra also broadened slightly after the hydrothermal treatment. The result from XRD measurement relative crystallinity of nanosizes was because more decreases slowly than that of the microsizes. By nuclear solid-state NMR combine with BET surface and XRD investigations the hydrothermal stability of the nanosizes was almost the same that of the microsizes. In addition, with low aluminaium contact it was found to be more resistant to dealumination was calcination and hydrothermal treatment and degree of dealumination was greater when steam was present in the treatment [37].

Next, the effect of particle size on the durability of Co/HZSM-5 in the selective catalytic reduction (SCR) of NO with methane was studied by Praserthdam et al [11]. The durability of the catalysts subjected to hydrothermal treatment with a He stream containing 10% steam at 873 K for 24 h. was investigated. After hydrothermal treatment, the decrease of catalytic activity for small particle sizes of

Co/HZSM-5 (1.0 and 1.8 μm) was less than for large particle sizes of Co/HZSM-5(5.6 and 7.6 μm). This infers that the durability of Co/HZSM-5 increased with a decrease in particle size. Small particle size catalyst showed a slight decrease in crystallinity and tetrahedral aluminum while the large particle size catalyst lost crystallinity and tetrahedral aluminum. This indicated that the occurrence of framework dealumination was higher in the large particle size catalyst.

In another zeolite, Toophorm et al [86] synthesized polycrystalline zeolite beta using hydrothermal method at various conditions. The particle sizes in the range of 0.2 to 0.9 μm were obtained. The samples were treated at 1073 K with 10 mole percent of water for 30 min. The changes of each size of zeolite beta before and after treatment were observed by ^{27}Al MAS NMR spectrometer, BET surface area measurement and X-ray diffraction. It was found that hydrothermal treatment caused dealumination. The relative area of tetrahedral ^{27}Al MAS NMR decreased similarly in accordance with the BET surface area while the crystallinity obtained from XRD was slightly changed for all sizes. It was found that change of the small particle size was easily occurred than that of the large one. However, the silicon to aluminium ratio in the zeolite framework of the sample after treatment decreased to constant values. The fresh catalysts for small particle size showed higher activity than that for large one but a significant change of activity with time on stream was pronounced. However, the similar activity for both sizes after hydrothermal treatment was observed. In addition, it was also observed that for the same particle size sample, extent of dealumination of the high Si/Al ratio is lower than that of the low one.

From the above literature reviews, particle size of Y zeolite is an important parameter used in various catalytic reactions. However, the effect of particle size on the hydrothermal stability of Y zeolite has not been fully studied. Thus, the correlation between effect of particle size and hydrothermal stability was studied in order to obtain the optimum formula of Y zeolite with high crystallinity, In addition, the correlated equation was used with determining stability at different size and treated parameters.

CHAPTER III

THEORY

3.1 Structure of Zeolite

Zeolite are highly crystalline, hydrated aluminosilicates that upon dehydration develop in the ideal crystal a uniform pore structure having minimum channel diameters(aperture) of from about 0.3 to 1.0 nm. The size depends primarily on the type of zeolites and secondarily on the cations present and the nature of treatments such as calcination, leaching, and various chemical treatments. Zeolites have been of intense interest as catalysts for some three decades because of the high activity and unusual selectivity they provide, mostly in a variety of acid– catalyzed reaction. In many cases, but not all, the unusual selectivity is associated with the extremely fine pore structure, which permits only certain molecules to penetrate into the interior of the catalyst particles, or only certain products to escape from the interior. In some cases unusual selectivity seems to stem instead from constrains that the pore structure sets on allowable transition states, sometimes termed spacio – selectivity.

The structure of the zeolite consists of a three–dimensional framework of the $SiO_4$and AlO_4 tetrahedra as presented in Figure 3.1 [87], each of which contains a silicon or aluminum atom in the center. In 1982, Barrer defined zeolites as the porous tectosilicates [88], that is, three – dimensional networks built up of TO_4- tetrahedra where T is silicon or aluminum. The oxygen atoms are sheared between adjoining tetrahedral, which can be present in various ratios and arrange in a variety of ways. The framework thus obtained pores, channels, and cages, or interconnected voids.

A secondary building unit (SBU) consists of selected geometric groupings of those tetrahedral. There are sixteen such building units, which can be used to describe all of known zeolite structures; for example, 4 (S4R), 6 (S6R), and 8 (S8R) – member single ring, 4-4 (D6R), 8-8 (D8R)-member double rings. The topologies of these units are shown in Figure 3.2 [89]. Also listed are the symbols used to describe them. Most zeolite framework can be generated from several different SBU's. Descriptions of known zeolite structures based on their SBU's are listed in Table 3.1 [90]. Both zeolite ZSM-5 and Ferrierite are described by their 5-1 building units. Offertile, Zeolite L, Cancrinite, and Erionite are generated using only single 6-member rings. Some zeolite structures can be described by several buildings. The sodalite framework can be built from either the single 6-member ring or the single 4-member ring. Faujasite (type X or type Y) and zeolite be constructed using 4 ring or 6 ring building units. Zeolite a can also be formed using double 4 ring building units, whereas Faujasite cannot.

Zolites may be represented by the empirical formula:

$$M_{2/n}\, Al_2O_3 x SiO_2 y H_2O$$

or by a structural formula:

$$M_{x/n}\, [(Al_2O_3)_x\, (SiO_2)_y]\, wH_2O$$

where the bracketed term is the crystallographic unit cell. The metal cation (of valence n) is present it produces electrical neutrality science for each aluminum tetrahedron in the lattice there is an overall charge of – 1. Access to the channels is limited by aperture consisting of a ring of oxygen atoms of connected tetrahedra. There may be 4, 5, 6, 8, 10, or 12 oxygen atoms in the ring. In some cases an interior cavity exists of larger diameter in the aperture; in others, the channel is of uniform diameter like a tube [23].

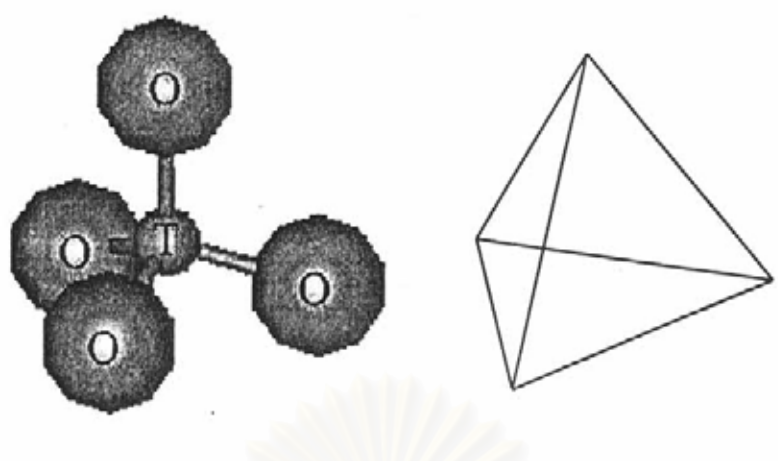

Figure 3.1 TO_4 tetrahedra (T=Si or Al) [87]

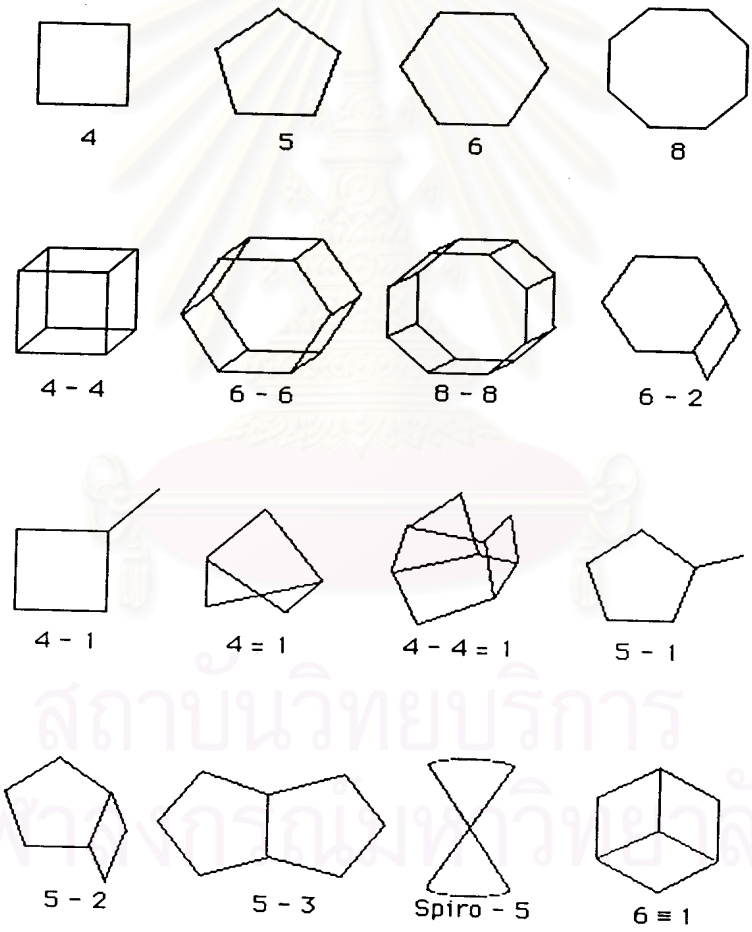

Figure 3.2 Secondary building units (SBU's) found in zeolite structures [87]

Table 3.1 Zeolites and their secondary building units. The nomenclature used is consistent with that presented in Figure 3.4 [90]

ZEOLITE	SECONDARY BUILDING UNITS							
	6	4	4-4	6-6	8-8	4-1	5-1	4-4=1
Bikilaite							X	
Li-A (BW)	X	X	X					
Analcime	X	X						
Yagawaralite	X		X					
Episibite							***X***	
ZSM-5							X	
ZSM-11							X	
Ferrierite							X	
Cachiardite							X	
Brewsterite	X							
Laumonite		X						
Modenite							X	
Sodalite	X	X						
Henulandite								X
Stibite								X
Natrolite						X		
Thomdonite						X		
Edingtonite						X		
Cancrinite		X						
Zeolite L		X						
Mazzite	X							
Merlinoite	X		X		X			
Philipsite	X		X					
Zeolite Losod		X						
Erionite	X	X						
Paulingite	X							
Offeretite		X						
TMA-E(AB)	X	X						
Gismondine	X		X					
Levyne		X						
ZK-5	X	X	X		X			
Chabazite	X	X			X			
Gmelinite	X	X	X		X			
Rho	X	X	X			X		
Type A	X	X	X	X				
Faujasite	X	X			X			

3.2 Category of Zeolite

There are over 40 known natural zeolites and more than 150 synthetic zeolites have been reported [91]. The number of synthetic zeolites with new structure morphologies grows rapidly with time. Based on size of their pore opening, zeolites can be roughly divided into five major categories, namely 8 -, 10 -, and 12- member oxygen ring systems, dual pore systems and mesoporous systems [92]. Their pore structures can be characterized by crystallography, adsorption, and measurements and/or through diagnostic reactions. One such diagnostic characterization test is the "constraint index" test. The concept of constraint index was defined as the ratio of the cracking rate constant of n-hexane to 3-methylpenthane. The constraint index of a typical medium-pore zeolite usually ranges from 3 to 12 and those of the large-pore zeolites are the range 1-3. For materials with an open porous structure, such as amorphous silica alumina, their constraint indices are normally less than 1. On the index for erionite are 38.

A comprehensive bibliography of zeolite structures has been published by the International Zeolite Association [98]. The structural characteristics of assorted zeolites are summarized in Table 3.2

Zeolite with 10-membered oxygen rings normally possesses a high siliceous framework structure. They are of special interest in industrial applications. In fact, they were the first family of zeolite that was synthesized with organic ammonium salts. With pore openings close to the dimensions of many organic molecules, they are particularly useful in shape selective catalysis. The 10-membered oxygen ring zeolites also possess other important characteristic properties including high activity, high tolerance to coking and high hydrothermal stability. Among the family of 10-membered oxygen ring zeolites, the MFI - type (ZSM-5) zeolite as presented in Figure 3.3 is probably the most useful one.ZSM-5 zeolite has two types of channel systems of similar sized, one with a straight channel of pore opening 5.3x5.6Å and the other with a tortuous channel of pore opening 5.1x5.5 Å. Those intersecting channels are perpendicular to each other, generating a three dimensional framework.ZSM-5 zeolites with a wide range of SiO_2/Al_2O_3 ratio can easily be synthesized. High

siliceous ZSM-5 zeolites are more hydrophobic and hydro thermally stable compared with many other zeolites. Although the first synthetic ZSM-5 zeolite was discovered more than two decades ago (1972) new interesting applications are still emerging to this day. For example, its recent application in NO_x reduction, especially in the exhaust of lean-burned engine, has drawn much attention. Among various zeolite catalysts, ZSM-5 zeolite has the greatest number of industrial applications, covering from petrochemical production and refinery processing to environmental treatment.

Table 3.2 Structural characteristics of selected zeolite [93]

Zeolite	Number of rings	Pore opening Å	Pore/Channel structure	Void volume (ml/g)	D_{Frame}[a] (g/ml)	CI[b]
8-membered oxygen ring						
Erionite	8	3.6x5.1	Intersecting	0.35	1.51	38
10-membered oxygen ring						
ZSM-5	10	5.3x5.6 5.1x5.5	Intersecting	0.29	1.79	8.3
ZSM-11	10	5.3x5.4	Intersecting	0.29	1.79	8.7
ZSM-23	10	4.5x5.2	One-dimensional	-	-	9.1
Dual pore system						
Ferrierite (ZSM-35, FU-9)	10,8	4.2x5.4 3.5x4.8	One-dimensional 10:8 intersecting	0.28	1.76	4.5
MCM-22	12 10	7.1 Elliptical	Capped by 6 rings	-	-	1-3
Mordenite	12 8	6.5x7.0 2.6x5.7	One-dimensional 12:8 intersecting	0.28	1.70	0.5
Omega (ZSM-4)	12 8	7.4 3.4x5.6	One-dimensional One-dimensional	- -	- -	2.3 0.6
12membered oxygen ring						
ZSM-12	12	5.5x5.9	One-dimensional	-	-	2.3
Beta	12	7.6x6.4 5.5x5.5	Intersecting	-	-	0.6
Faujasite (X,Y)	12 12	7.4 7.4x6.5	Intersecting 12:12 intersecting	0.48	1.27	0.4
Mesoporous system						
VPI-5	18	12.1	One-dimensional	-	-	-
MCM41-S	-	16-100	One-dimensional	-	-	-

[a]Framework density

[b]Constraint index

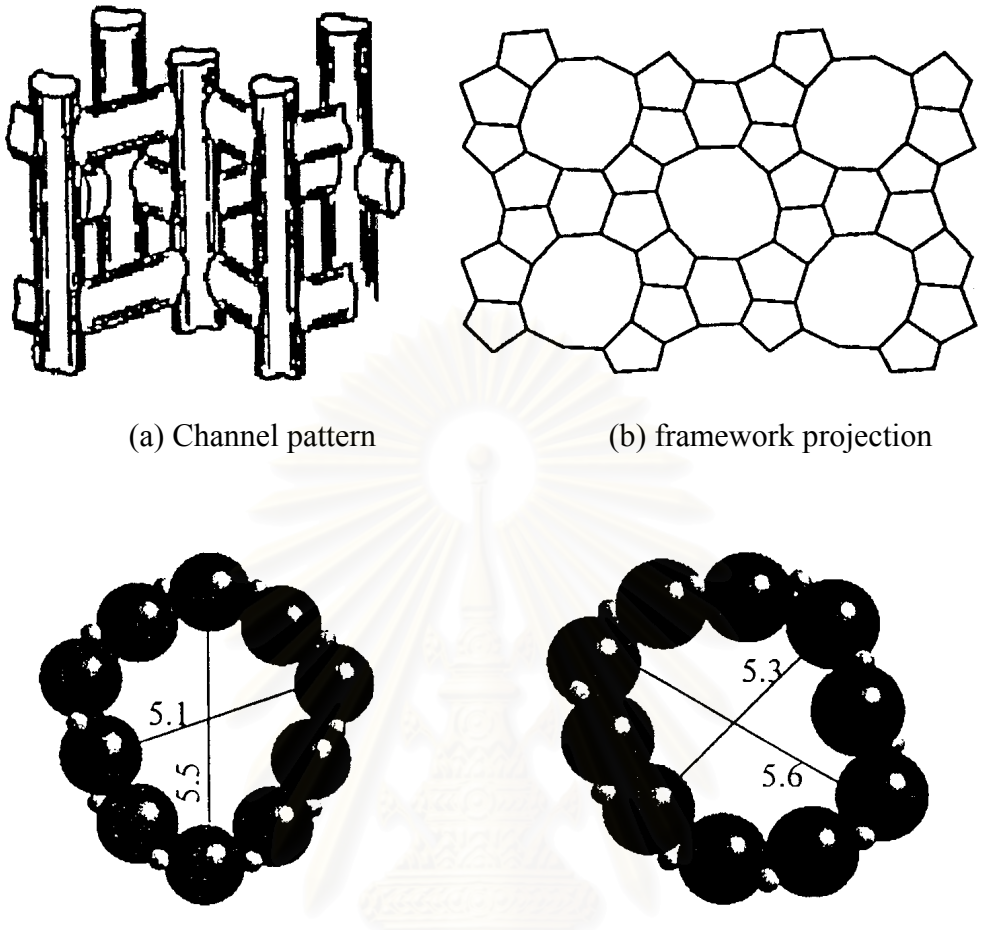

(a) Channel pattern (b) framework projection

(c) tortous channel (d) straight channel

Figure 3.3 Structure of ZSM-5 [91]

Although the 10-membered oxygen ring zeolite was found to possess remarkable shape selectivity, catalysis of large molecules may require a zeolite catalyst with a large-pored opening. Typical 12-membered oxygen ring zeolites, such as faujasite-type zeolites, normally have pore opening greater than 5.5 Å and hence are more useful in catalytic applications with large molecules, for example in trimethylbenzene (TMB) conversions. Faujasite (X or Y; Figure 3.4) zeolites can be synthesized using inorganic salts and have been widely used in catalytic cracking since 1960s. The framework structures of zeolite beta and ZSM-12 are shown in Figure 3.5 and 3.6, respectively.

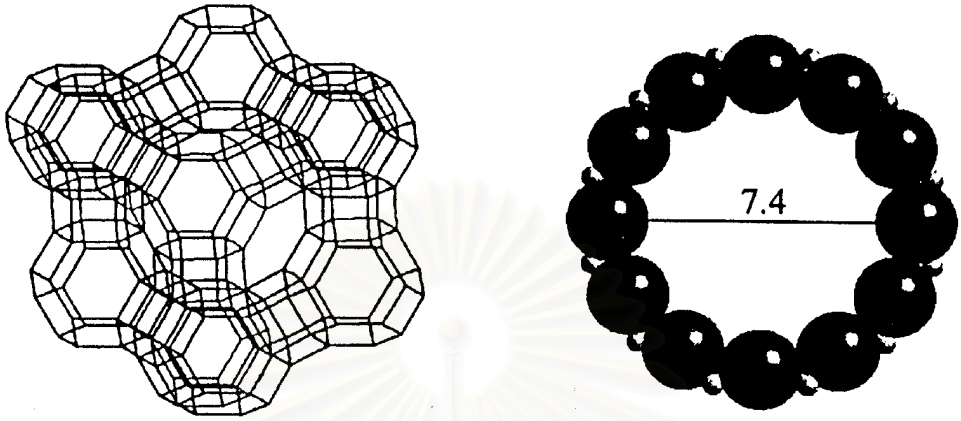

(a) framework structure (b) pore opening

Figure 3.4 Structure of Faujasite [91]

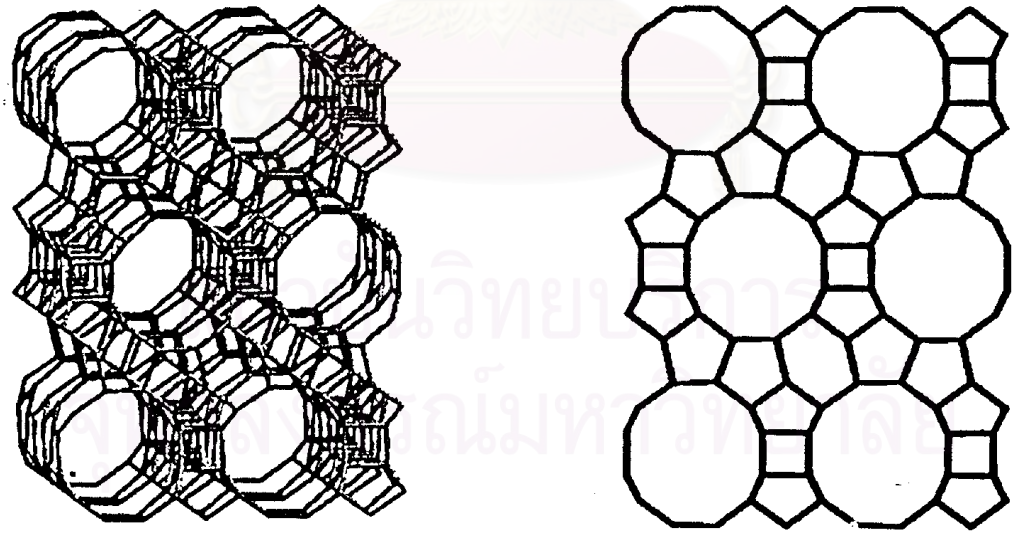

(a) framework structure (b) framework projection

Figure 3.5 Structure of zeolite beta [91]

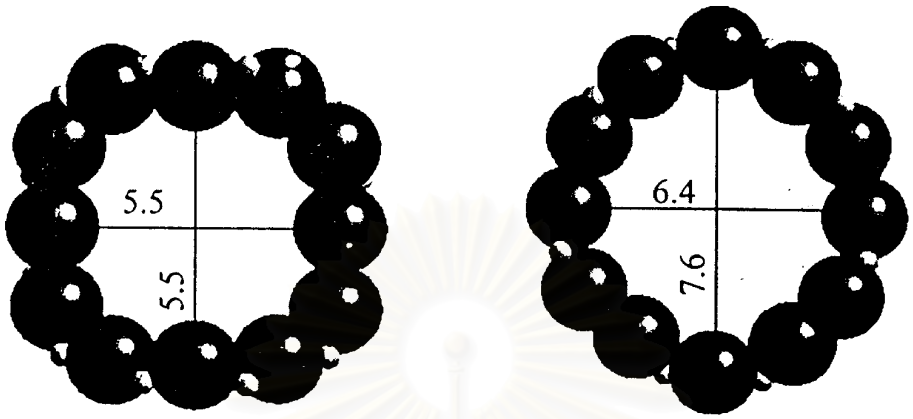

(c) tortous channel (d) straight channel

Figure 3.5 Structure of zeolite beta [91]

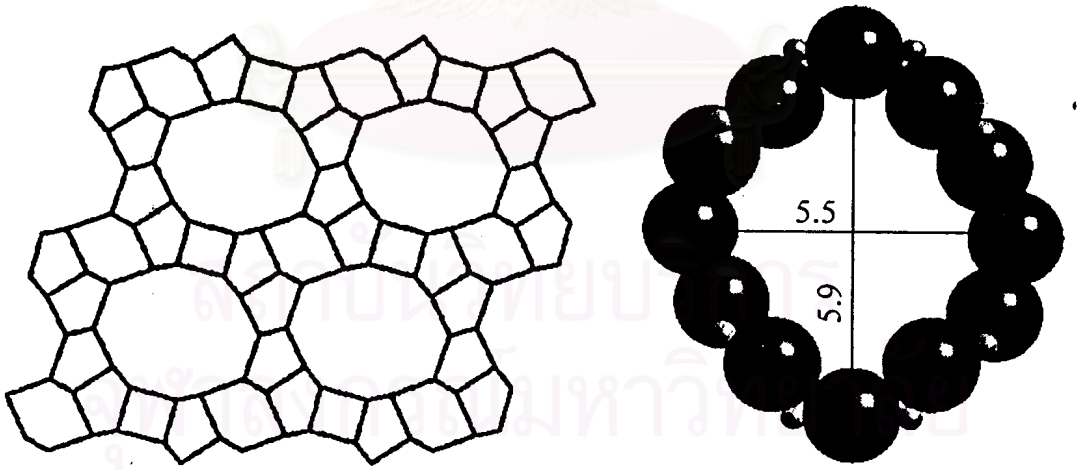

(a) framework projection (b) pore opening

Figure 3.6 Structure of zeolite ZSM-12 [91]

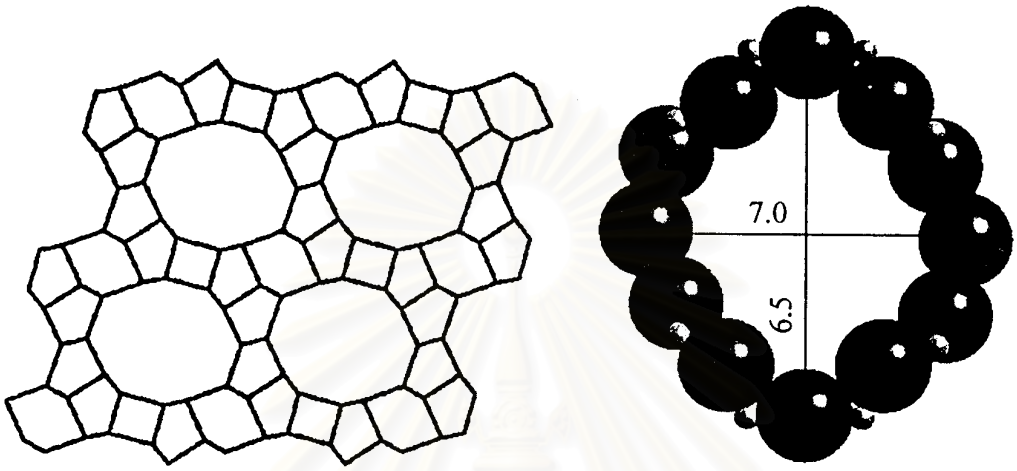

(a) framework projection (b) pore opening

Figure 3.7 Structure of Mordenite [91]

Zeolites with a dual pore system normally possess interconnecting pore channels with two different pore opening sizes. Mordenite is a well-known dual pore zeolite having a 12-membered oxygen ring channel with pore opening 6.5x6.7 Å which id interconnected to 8-membered oxygen ring channel with opening 2.6x5.7 Å (Figure 3.7 [91]). MCM -22, which was found more than 10 years, also possess a dual pore system. Unlike Mordenite, MCM-22 consists of 10- and 12-membered oxygen rings (Figure 3.8 [91]) and thus shows prominent potential in future applications.

In the past decade, many research efforts in synthetic chemistry have been invested in the discovery of large-pored zeolite with pore diameter greater than 12-membered oxygen rings. The recent discovery of mesoporous materials with controllable pore opening (from 12 to more than 100 Å) such as VPI-5, MCM-41S undoubted will shed new light on future catalyst applications.

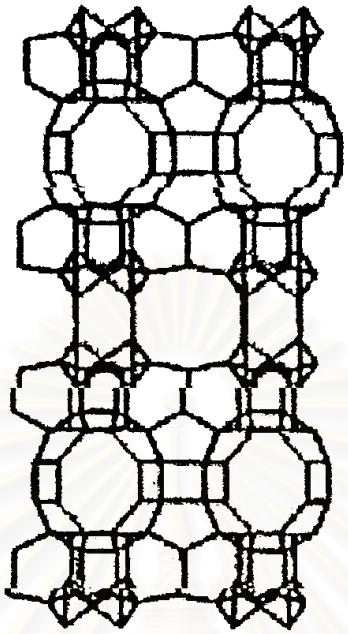

Figure 3.8 Framework structure of MCM-22 [91]

3.3 Shape Selective

Many reactions involving carbonium intermediates are catalyzed by acidic zeolite. With respects to a chemical standpoint the reaction mechanisms are nor fundamentally different with zeolites or with any the acidic oxides. What zeolite adds is shape selectivity effect. The shape selective characteristics of zeolites influence their catalytic phenomena by three modes: shape selectivity, reactants shape selectivity, products shape selectivity and transition states shape selectivity. These types of selectivity are illustrated in Figure 3.9.

Reactants of charge selectivity results from the limited diffusibility of some of the reactants, which cannot effectively enter and diffuse inside crystal pore structures of the zeolites. Product shape selectivity occurs as slowly diffusing product molecules cannot escape from the crystal and undergo secondary reaction. This reaction path is established by monitoring changes in product distribution as a function of varying contact time.

Restricted transition state shape selectivity is a kinetic effect from local environment around the active site, the rate constant for a certain reaction mechanism is reduced of the space required for formation of necessary transition state is restricted.

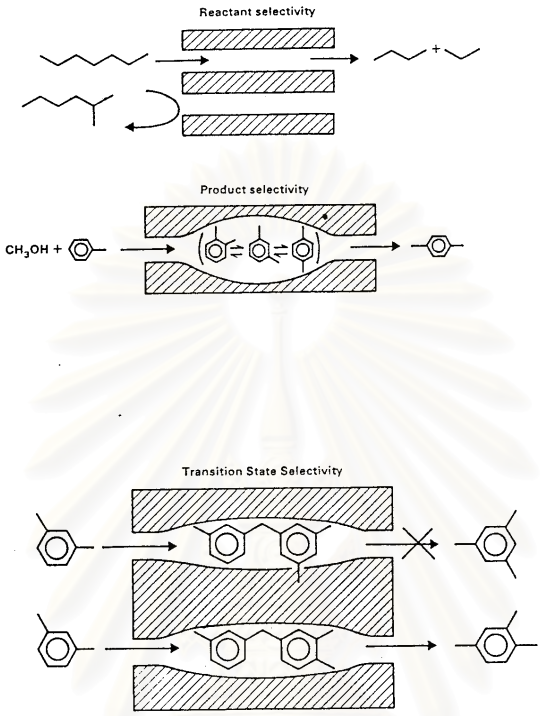

Figure 3.9 Diagram depicting the three type of selectivity [90]

The critical diameter (as opposed to the length) of the molecules and the pore channel diameter of zeolites are important in predicting shape selective effects. However, molecules are deformable and can pass through opening, which are smaller than their critical diameters. Hence, not only size but also the dynamics and structure of the molecules must be taken into account.

3.4 Zeolite Synthesis

Zeolites are generally synthesized by a hydrothermal process from a source of alumina (e.g., sodium aluminate or aluminium sulfate) and of silica (e.g., a silica sol, fumed silica, or sodium water glass) and an alkali such as NaOH, and/or a quaternary ammonium compound. An inhomogeneous gel is produced which gradually crystallizes, in some cases forming more than one type of zeolite in succession.

Nucleation effects can be important, and an initial induction period at near ambient temperature may be followed by crystallization temperature that may range up to 473 K or higher. The pressure is equal to the saturated vapor pressure of the water present.

The final product depends on a complex interplay between many variables including SiO_2/Al_2O_3 ratio in the starting medium, nucleating agents, temperature, pH, water content, aging, stirring, and the presence of various inorganic and organic cations. Much remains to be learned about how the initial reaction mixture forms the precursor species and how these arrange into the final crystalline products. A key concept is that the cations present give rise to a templating action, but clearly the process is more complex.

Bauer and coworkers in the early 1960s developed the use of reaction mixtures containing quaternary ammonium ions or other or other cations to direct the crystallization process. In their work and succeeding studies, a primary motivation was to attempt to synthesize zeolites with large apertures than X and Y. This did not occur, but instead organic species were found to modify the synthesis process in a variety of ways that led to the discovery of many new zeolites, and new methods of synthesizing zeolite with structures similar to previously know zeolite.

The mechanism of action of the organic species is still controversial. It was originally thought to be primarily a templating effect, but later it was found that at least some of zeolites could be synthesized without an organic template. Further, organic species other than quaternary ammonium compounds had directing effects not readily ascribed to their size or shape. However, an important result was the zeolites of higher SiO_2/Al_2O_3 ratio than before could be synthesized. Previously, only structures with SiO_2/Al_2O_3 ratios of about 10 or less could be directly forms, but with organic additives, zeolites with ratio of 20 to 100 or more can be directly prepared.

After synthesis the zeolite are washed, dried, heated to remove water of crystallization, and calcined in air, e.g., at about 823 K. Organic species are also thus

removed. For most catalytic purpose, the zeolite is converted into acidic form. For some zeolites this can be achieved by treatment with aqueous HCl without significantly altering the framework structure. For other zeolites Na^+ is replaced with NH_4^+ via an ammonium compound such as NH_4OH, NH_4Cl or NH_4NO_3.Upon heating NH_3 is driven off, leaving the zeolite in the acid form. For some reaction a hydrogenation component such as platinum or nickel is introduced by impregnation or ion exchange [5].

3.5 Y Zeolite

In Y zeolite structure, the diameter of the supercage is 12.5 Å while the diameters of the sodalite cage and the double 6-ring are 6.6 and 2.6 Å, respectively. Each supercage contains four windows of 12-membraned Al or Si rings with a diameter of 7.4 Å.

The cation sites of Y zeolite are illustrated in Figure 3.10. Type I sites are located at the centers of the hexagonal prisms, type I' sites are located in the sodalite cage across the hexagonal faces from type I sites, type II sites are located in the supercages near the unjoined hexagonal faces, and type II' sites are located in the sodalite across the type II sites. Type III sites are located in the supercage, further from the hexagonal faces than the type II sites.

For hydrated NaY with a Si/Al ratio of 2.3, the chemical formula for a unit cell will be $Na_{58}[(AlO_2)_{58}.(SiO_2)_{134}]_{.235}H_2O$. In dehydrated NaY (58 Na^+ ions), a cation distribution of 7.63 Na+ ions at site I, 19.84 Na+ ions at site I', and 30.53 Na+ ions at site II was reported. [94] There are 8 supercages per unit cell; therefore, 3.82 Na+ ions on average resided in the supercages. With four 6-rings per supercages, there is about 1 Na+ ion per 6-ring of the supercage.

Y zeolite can contain up to approximately 235 water molecules per unit cell which are distributed in both the large supercages and the small sodalite cages.

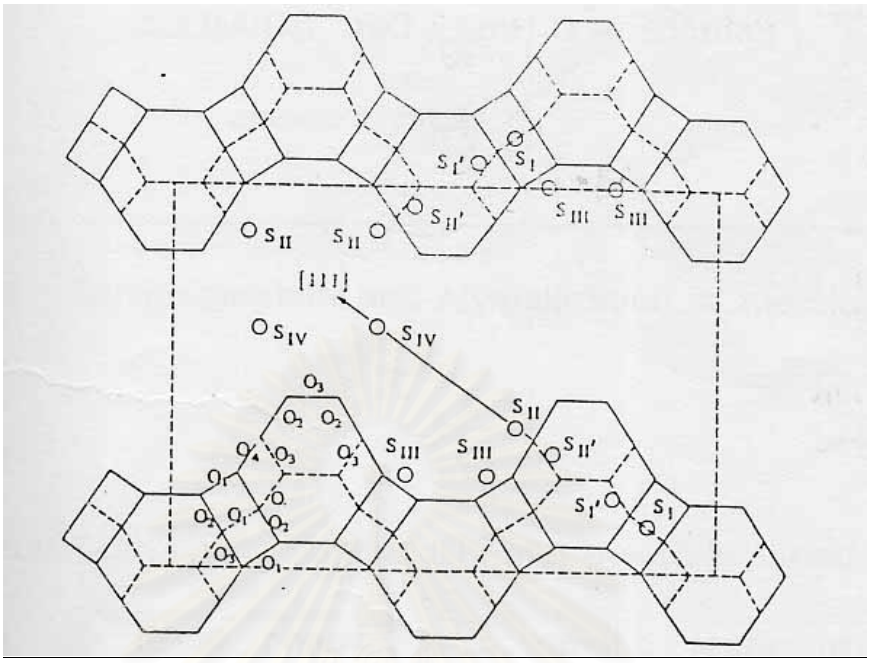

Figure 3.10 locations of cation sites in Y zeolite

3.6 Fluid Catalytic Cracking (FCC) process

3.6.1 Fluid Catalytic Cracking Unit (FCCU)

Since the start-up of the first commercial Houdry fixed-bed plant in 1936, the technology of catalytic cracking has been seen many innovations: from moving bed cracking, fluid-bed catalytic cracking (dense bed) to the present riser and residue FCC processes [95-96]. A typical FCC unit consists of a riser reactor, where catalytic cracking of hydrocarbon occurs, and a fluidized bed regenerator, where spent catalysts are regenerated.

A preheated vacuum distillate feed is in introduced to the unit at the bottom of the riser. Feed is contacted with the catalyst which is coming from the regenerator at high temperature (973 K), and immediately is vaporized and cracked. At the riser exit, catalyst is recovered in two cyclones connected in series and the hydrocarbon vapors are separated. At the lower part of the reactor is the stripper for spent catalyst. In the

regenerator, spent catalyst is fluidized by combustion air. High temperature combustion removes any coke deposited on the catalyst to carbon dioxide (CO_2).

3.6.2 FCC catalyst

FCC catalyst is a complex composite acid solid with two main components: zeolite, which is the main active acidic agent, and matrix. It is usually in the form of microspheres with 50-70 μm average diameters. The microstructure of FCC catalyst is shown in Figure 3.11

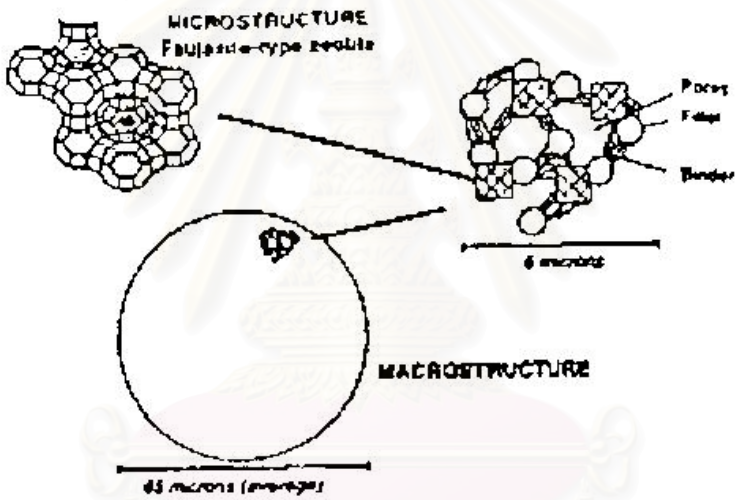

Figure 3.11 FCC catalyst components (Schematic) [97].

The matrix is composed of kaolin clay filler and silica or alumina binder. The major role of matrix is to bond the zeolite particles together and also to form a diffusion medium for the oil molecules. Another role is to act as a diluent media to moderate zeolite activity [98]. The zeolite content in FCC catalyst ranges between approximately 10-50% by weight.

According to the desired selectivity, the following forms of Y zeolites can be introduced into FCC catalyst [1]. Rare earth exchanged Y zeolite (REY) with high hydrogen transfer properties gives high yields of gasoline. The hydrogen form of

ultra-stable Y zeolite (H-USY) is a zeolite without any rare earth, with a low acid density that results in lower gasoline yield but with much better octane and lower coke yield. RE-H-Y and RE-H-USY zeolites have intermediate properties between the previous two zeolites.

3.7 Thermal stability

The thermal stability of zeolites increase with increasing silica content and by exchange with rare earth cations. Most sieves are uncharged by dehydrating to 673 K; high silica (ultrastabilized forms prepared by steam pre-treatment) and rare earth-exchanged sieves are stable to 973-1073 K. Generally, extensive dehydration causes loss of Brønsted acidity due to the removal of OH or silanol surface groups.

Thermal treatment of zeolites in the presence of water normally leads to dealumination. In fact, it is one of the recommended methods for preparing ultrastable zeolites. Moderate dealuminating generally increases catalytic activity or leaves it unchanged, whereas advanced dealumination leads to a decrease in activity due to a loss of active sites and ultimately collapse of the zeolite structure. For example, dealumination of mordenite significantly changes important chemical and physical properties such as crystal structure, thermal stability, sorption capacity and acidity, as well as catalytic properties. Maximum thermal stability is reached for a SiO_2:Al_2O_3 ratio of about 19. The sorption capacity towards water is highly reduced after dealumination because of the absence of strong polarizing cations which can dissociate water to strongly adsorbed hydroxyl groups; accordingly, the number of Brønsted acid sites also decrease. Nevertheless, the hydrocarbon cracking activity of mordenite increase with increasing Si:Al ratio. For further details on zeolite stability, the reader is referred to the comprehensive review of McDaniel and Maher [99].

CHAPTER IV

EXPERIMENTAL

In this chapter, experimental is divided into three sections. First, preparation of HY-type zeolite is presented in section 4.1. Second, hydrothermal treatment procedure is showed in section 4.2. Third, characterization of HY-type zeolite by using SEM, XRD, ^{27}Al MAS NMR, BET, NH_3TPD, and FTIR pyridine adsorption is presented in section 4.3.

4.1 Preparation of Y-Type Zeolite

The synthesis of Y zeolite was described in parent literature [26]. The stoichiometrical ratio between initial solution of aluminosilicate solution and sodium silicate solution is $Na_2O:Al_2O_3:SiO_2:H_2O$ = 3.68:1:12:148. The preparation procedure of Y zeolite is shown in Figure 4.1, while reagents used are shown in Table 4.1

4.1.1 Materials

Chemical used in this experiment have to be specified as follows:

1. Sodium Aluminate [$NaAlO_2$] manufactured by Wako Pure Chemical Industries CO.,Ltd., Japan.

2. Sodium Silicate solution [$Na_2Si_3O_7$] manufactured by Merck Ltd., Germany.

3. Sodium Hydroxide [NaOH] manufactured by Merck ltd., Germany.

4.1.2 Preparation of uniform slurry

Sodium aluminate and sodium silicate solution were used as Al and Si sources of Al and Si, respectively; while Na source was substantially obtained from sodium hydroxide. The uniform slurry was prepared by the two main steps as follows:

1. S_1 was slowly added into S_2 while vigorous stirring. The mixture was continuously stirred for 2 h. Then the mixture was heated to 333 K and maintained at that temperature for 1 h to form a gel. The gel mixture was separated from the supernatant solution by a centrifuge.

Table 4.1 Reagents used for the preparation of Y zeolite [100].

Reagents	Quantity
First step:	
Solution S_1	
$NaAlO_2$	32.81 g
Distilled water	158 ml
Solution S_2	
$Na_2Si_3O_7$	218.6 g
NaOH	95.91 g
Distilled water	534 ml
Second step:	
Solution S_3	
$Na_2Si_3O_7$	216.72 g
NaOH	95.91 g
Distilled water	534 ml

Then it was washed by water and separated from solution by repeating cycles of centrifugation and decantation until the pH of supernatant solution was about 13.5.

2. 181 g of obtained gel from the above step was poured into S_3. Subsequently, the resultant mixture was stirred to obtain uniform slurry.

4.1.3 Crystallization

1. The uniform slurry was charged into a closed glass vessel and placed at room temperature at different aging time of nucleation (0.5, 2, 4.5, 6.5 days).

2. The glass vessel charged with slurry was heated at various temperatures (363, 373, 383 K) and maintained at such temperature for 24 h.

3. The prepared Y zeolite was left to cool down to ambient temperature, then it was washed with distilled water until the pH of slurry became 7 by repeating cycles of centrifugation and decantation. The obtained crystals were dried overnight at 383 K.

4.1.4 Preparation of the Proton-Type Y (HY)

a) Ammonium Ion-Exchange of NaY Zeolite

1. 2 g portion of the NaY Zeolite was added by 80 ml of 1 N NH_4NO_3 aqueous solution, after that the mixture was heated at 353 K for 1 h.

2. The powder was washed twice by distilled water to remove nitrate ions. Then water was repeated by centrifugation.

3. Steps 1 and 2 were repeated for five times.

4. The sample was dried overnight in an oven at 383 K. The Na-form crystal was thus changed to NH_4-form catalyst.

b) HY-Type Zeolite

The NH_4Y zeolite was converted to HY Zeolite by removing NH_3 species from the catalyst surface. NH_3 can be removed by thermal treatment of the NH_4Y zeolite. This was done by heating a sample in an air stream at 773 K for 2 h; by heating them from room temperature to 773 K at a heating rate of 280.9 K/min. After the catalyst was cooled down, it was stored in a glass bottle in desiccators for further used.

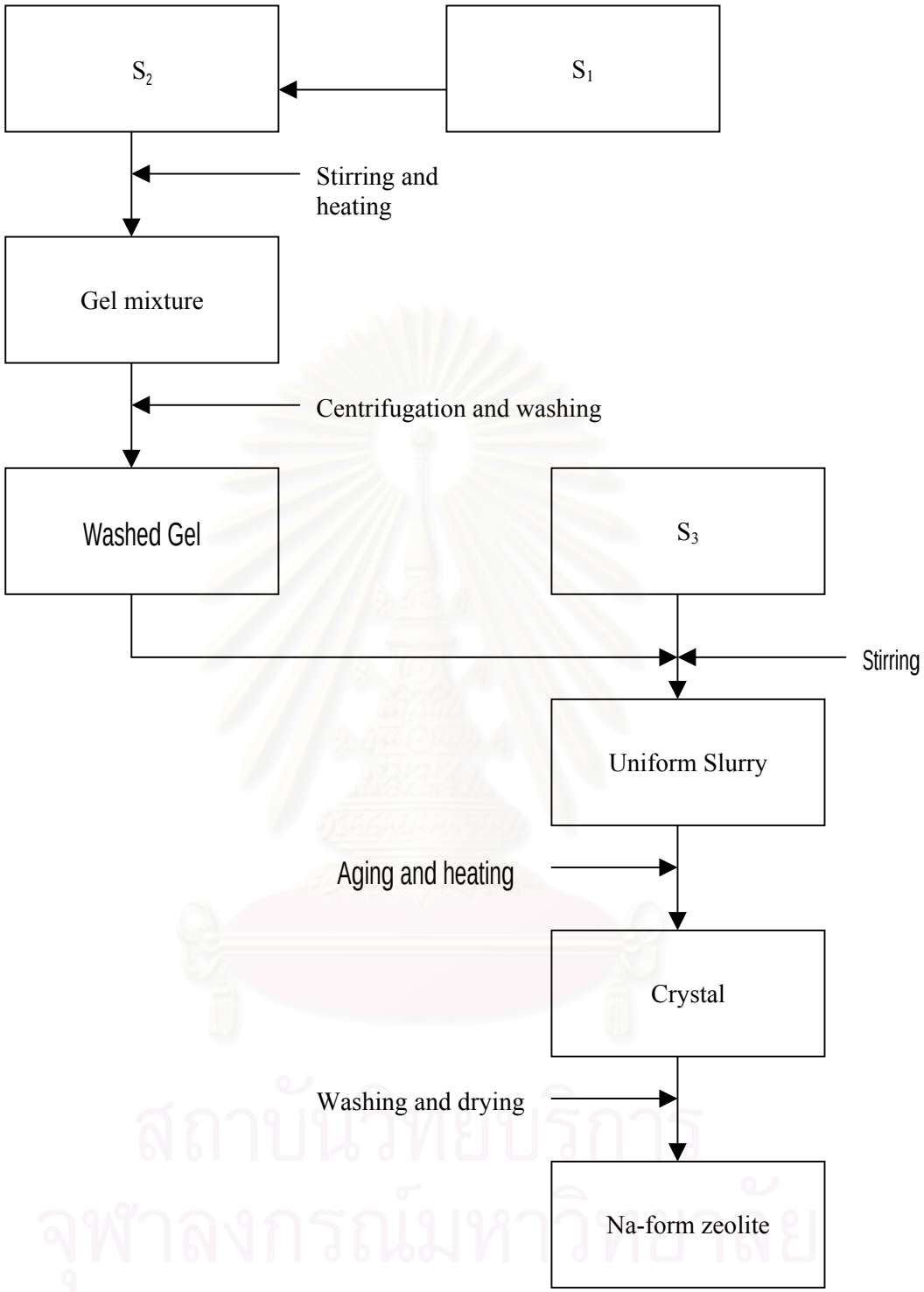

Figure 4.1 The preparation procedure of Na Y-zeolite catalyst. [100]

4.2 Hydrothermal Pretreatment

In order to investigate the effect of hydrothermal treatment on the stability of zeolite with different particle size, the hydrothermal treatment is carried out in an apparatus which is schematically represented in Figure 4.2. About 0.5 g of samples is introduced into the reactor at room temperature. Next, the catalyst is heated in a N_2 stream while elevating temperature from room temperature to desired temperature (873, 973, 1073, 1173 and 1273 K) with a constant heating rate of 283 K/min. The catalyst sample is then kept at the desired time (0.5, 1, 2, 3, and 5 h) while steam is added at different partial pressures (0.05, 0.1, 0.2, 0.5, and 1.0). Subsequently, the zeolite is cooled down to room temperature in N_2 stream.

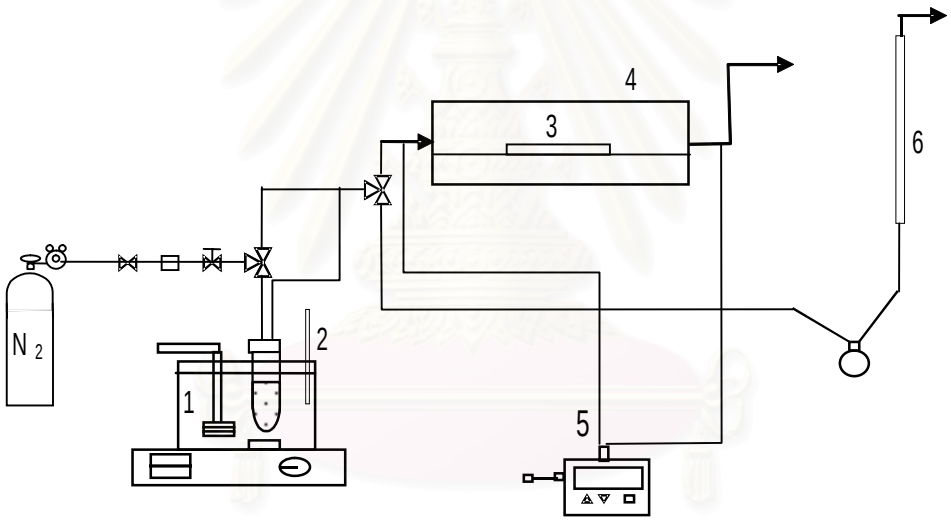

Figure 4.2 Scheme of the apparatus for hydrothermal treatment: 1, steam generating system; 2, thermocouple; 3, sample; 4, carbolite; 5, temperature control; 6, bubble flow meter.

4.3 Characterization

4.3.1 Scanning Electron Microscopy (SEM)

Scanning Electron Microscopy was employed for including the shape and size of the prepared zeolite crystal. The JEOL JSM-35 CF model at the Scientific and Technological Research Equipment Centre, Chulalongkorn University (STREC) was used for this purpose.

4.3.2 X- ray Diffraction Analysis (XRD)

The Crystallinity and X-ray diffraction (XRD) patterns of the catalysts were performed by an X-ray diffractometer SEIMENS D500 connected with a personal computer with Diffract AT version 3.3 programs for fully control of the XRD analyzer. The experiments was carried out by using CuK_{α} radiation with Ni filter and the operating condition of measurement are 4-40 degree 2θ, with a resolution of 0.04.

The functions of base line subtraction and smoothing were used in order to get the well formed XRD spectra.

4.3.3. ^{27}Al Magnetic Angle Spinning Nuclear Magnetic Resonance (^{27} Al MAS NMR)

Quantitative analysis of aluminum tetrahedral in zeolite was conformed by ^{27} Al-magnetic angles spinning nuclear magnetic resonance (^{27}Al MAS NMR, BRUKER DPX-300 spectroscopy operating at 78.2 MHz) at National Metal and Materials Technology Center (MTEC), Bangkok.

4.3.4 Surface area measurement

Physical adsorption isotherms are measured near the boiling point of a gas (e.g., nitrogen, at 77 K). From these isotherms the amount of gas needed to form a

monolayer can be determined. If the area occupied by each adsorbed gas molecule is known, the surface area can be determined for all finely divided solids, regardless of their chemical composition.

The specific surface area of samples was calculated using the Brunauer-Emmett-Teller (BET) single point method on the basis of nitrogen uptake measured at liquid-nitrogen boiling point temperature equipped with a gas chromatograph.

4.3.4.1 BET apparatus

The reaction apparatus of BET surface area measurement consisted of two feed lines of helium and nitrogen. The flow rate of the gases was adjusted by means of fine-metering valve on the gas chromatograph. The sample cell made from pyrex glass. The operation condition of gas chromatograph (GOW-MAC) is shown in Table 4.2.

Table 4.2 Operating condition of gas chromatograph (GOW-MAC)

Model	GOW-MAC
Detector	**TCD**
Helium flow rate	30 ml/min
Detector temperature	80^{o}C
Detector current	80 mA

4.3.4.2 Measurement

The mixture gas of helium and nitrogen was flown through the system at the nitrogen relative pressure of 0.3. The catalyst sample was placed in the sample cell, ca. 0.3-0.5 g, which was then heated up to 433 K and held at that temperature for 2 h. Then the catalyst sample was cooled down to room temperature and the specific surface area was measured. There were three steps to measure the specific surface area.

Adsorption step: The catalyst in the sample cell was dipped into the liquid nitrogen. Nitrogen gas that was introduced into the system was adsorbed on the surface of the catalyst sample until equilibrium was reached.

Desorption step: The sample cell with nitrogen gas-adsorbed catalyst sample was dipped into a water bath at room temperature. The adsorbed nitrogen gas was desorbed from the surface of the catalyst sample. This step was completed when the integrator line was back in the position of the base line.

Calibration step: 1 ml of nitrogen gas at atmospheric pressure was injected through the calibration port of the gas chromatograph and the area was measured. The area was the calibration peak. The calculation method is explained in Appendix A-5.

4.3.5 X-Ray Fluorescence analysis (XRF)

Quantities of Si and Al in the sample were determined by using XRF analyzer at the Science Service Department, Rama VI Road, Bangkok.

4.3.6 Temperature programmed desorption of adsorbed ammonia (NH_3TPD)

NH_3 TPD is carried out in an apparatus to measure the amount of acidic sites on the catalysts. About 250 mg of zeolites samples are put in a quartz cell with U shape and pretreated *in situ* during 1 h at 773 K in flow of nitrogen of 283 K/min. After cooling to 353 K, adsorption of ammonia (10%NH_3/He) is carried out with flow of 60 ml/min. After the catalyst surface became saturated for a certain period of time, excess ammonia is removed. The temperature-programmed desorption is performed with a linear heating rate of approximately 283 K/min from 363 K to 973 K. The NH_3 that desorbed is measured by a thermal conductivity detector and the electrical signals from the detector and the thermocouple are transmitted to a computer.

4.3.7 FT-IR pyridine Adsorption

4.3.7.1 Chemicals and reagents

Ultra high purity (99.99%) nitrogen supplies by TIG Ltd. and pyrindine, analytical grade supplied by Univax or Ajax chemical were used in these experiments.

4.3.7.2 Instruments and apparatus

Flow diagram

The schematic diagram of the *in situ* FT-IR apparatus is depicted in Figure 4.3. All gas lines, valves and fittings in this apparatus were made of pyrex glass except the IR gas cell and the sample disk holder, which were made of quartz glass in order to avoid the adsorption of any glass species which may remain on the inner surface of glass tube while the system was evacuated. Nitrogen was used for purging before starting the experiment. Pyrindine was added to a glass tube connected which a valve which can open to the glass line system. A home made electro-magnetic pump, fixed in the gas line, was used for circulating the gas (including the pyrindine vapour) through the sample in order to accomplish the adsorption of gas or pyrindine species on the sample surface. A Labconco 195-500 HP vacuum pump, which theoretically had capacity at 10^{-4} Torr, was used for system evacuation.

FT-IR

The FTIR spectrometer was used as a detector in the experiments. A Nicolet model Impact 400 FT-IR equipped with a deuterated triglycine sulfate (DTGS) detector and connected to a personal computer with Omnic version 1.2a on Windows software (to fully control the functions of the IR analyzer) were applied to this study. The analyzer was place on a moveable table for conveniently adjustment.

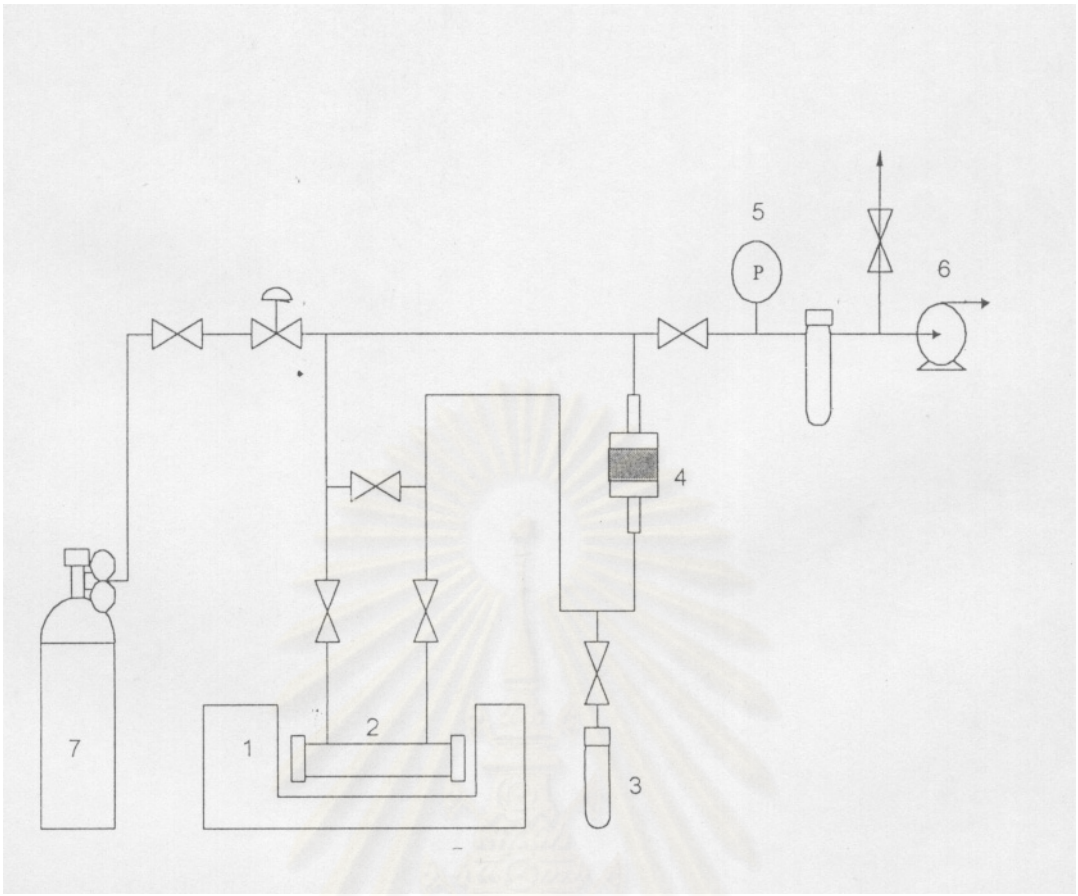

1. FT-IR Analyzer
2. IR quartz gas cell
3. Pyrindine tube
4. Electro magnetic circulating pump
5. Digital pressure indicator
6. Vacuum pump
7. Nitrogen gas cylinder

Figure 4.3 The schematic diagram of the *in situ* FT-IR apparatus [101]

IR gas cell

The IR gas cell used in this experiment, shown in Figure 4.4, was made of quartz and covered with 32×3 mm NaCl windows at each end of the cell. Each window was sealed with two O-rings and a stainless flange fastened by a set of screws.

The cell is roughly divided into two zones; heating and cooling with respect to their temperature. The quartz sample holder is arranged inside the IR cell to keep the sample disk perpendicular to the IR beam in the heating zone. A thermocouple is used to measure the sample disk temperature. The temperature is controlled by a variable voltage transformer and a temperature controller. Cooling water was connected to both ends of the IR cell to reduce the excessive heating, which may damage O-ring seals and the windows.

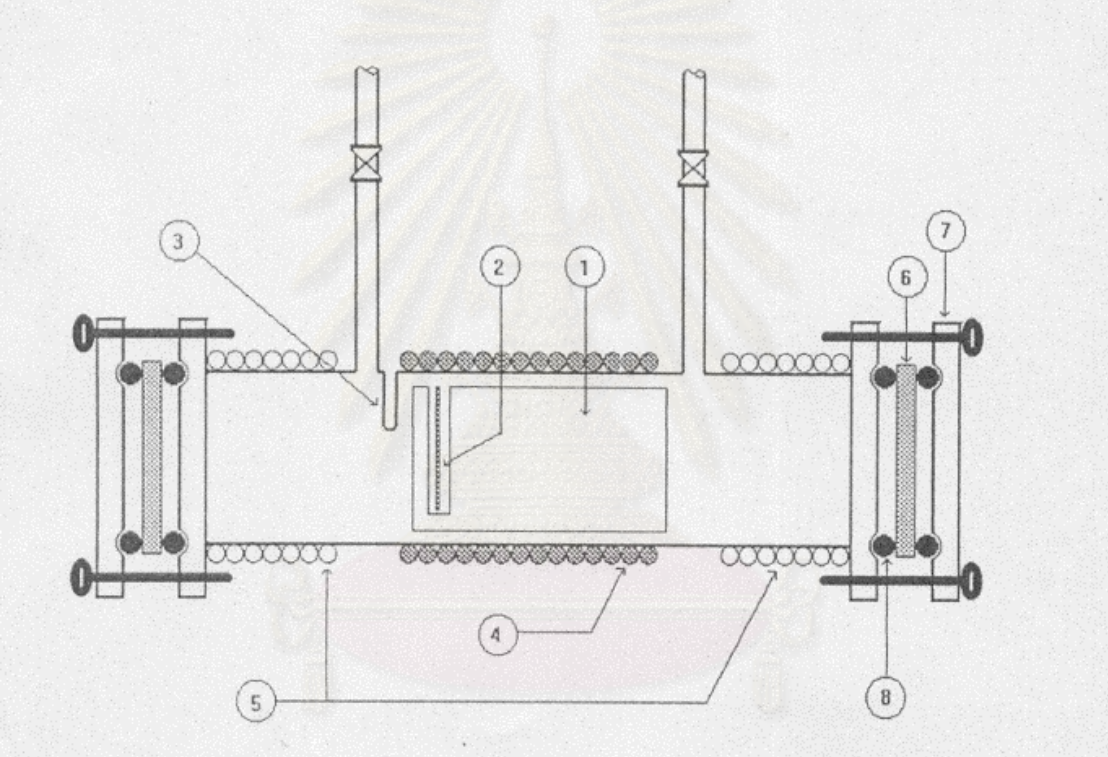

1. Sample Holder
2. Sample Disk
3. Thermocouple Position
4. heating rod
5. Water Cooling line
6. KBr Window
7. Flange
8. O-ring

Figure 4.4 The IR gas cell [101]

Sample disk preparation

To produce a self-supporting catalyst sample disk for an IR experiment the catalyst was milled thoroughly in a small quartz mortar to obtain a very fine powder. This minimized the scattering of infrared radiation and provided a high quality of spectrum.

The die used was made of stainless steel and is shown in figure 4.5. The most important part of this die, which contacts directly with the sample are the so-called the support disks. The support disks are composed of upper and lower disks, of which has a diameter of 20 mm. The support disks are highly polished to a mirror like finish in order to overcome the sticking of sample to the surface of the die, the main problem in pressing disks. About 0.006-0.065g of powder sample was spread to totally cover the surface of the lower support disk placed in the die to make approx 15-20 mg/cm^2 sample. All part of die was put together and was pressed by a manual hydraulic press at a pressure of 140-180 Kg/cm^2 for 5 minutes. The pressure should not be too low to form a self-supporting disk. After pressing, the well-formed disk was carefully removed from the die and mounted in the IR cell.

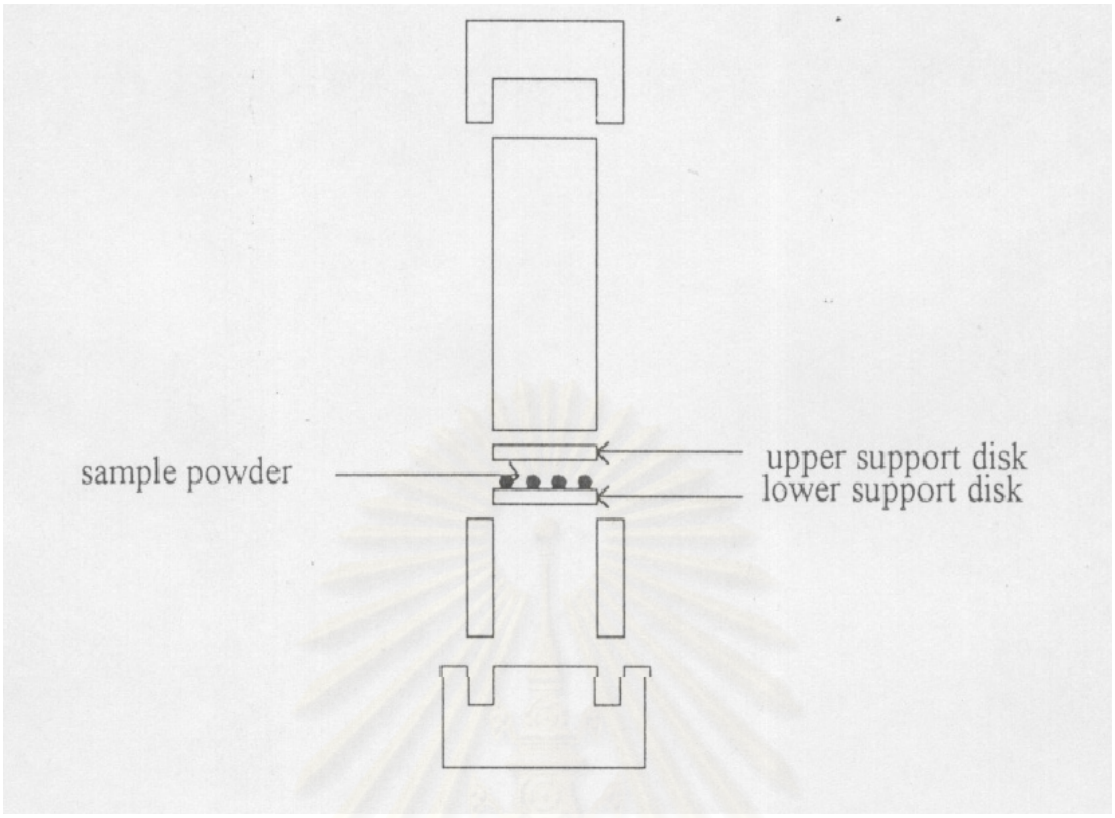

Figure 4.5 The support disks [101]

Experimental procedure

A well-formed disk sample was placed in the sample holder which was placed into the middle of the IR gas-cell. The sample disk is located as close to the thermocouple probe hole as possible. Once the KBr windows were sealed at both ends and there is no leakage, the IR gas cell was evacuated by a vacuum pump through the gas line for at least 30 min to place the system under vacuum. The sample disk was evacuated in vacuum for 1 hour at room temperature. However, since no change of the IR spectrum of the sample was found during the pre-treatment, this step sometimes was ignored. Pyrindine vapour was brought into contact with the disk at room temperature. Under vacuum, liquid pyrindine evaporates from the pyrindine tube in to the gas line leading to the IR gas cell. To achieve the maximum adsorption of pyrindine, pyrindine vapour was circulated through the system by the electro-magnetic pump for 1 h or until no change in IR spectra was observed. After that, the IR cell and gas line were evacuated to remove not only pyrindine vapour remaining in

the cell and gas line but also the physisorbed pyrindine from the catalyst surface. The vacuum pump was operated until the IR spectra peaks of pyrindine vapour and physisorbed pyrindine totally vanished and there was no change in any other peaks of the spectra. This normally took around 1.5 h, and then FT-IR measurement of the spectra of the pyrindine-adsorded sample was started at room temperature and was repeated at elevated temperature in 323 K steps.

The vacuum pump was kept running while the sample disk and the IR gas cell were heating to remove all species desorbed from the sample surface out of the system in order to avoid disturbing the result spectra by such species. On the other hand, since the vibration would occur and bring about bad scans, the vacuum was switched off while the temperature was held constant for IR detection. The measurement was completed when all peaks of adsorbed pyrindine disappeared so that the IR spectra of the sample was identical to the one before pyrindine dosing

CHAPTER V

RESULTS AND DISCUSSION

In this chapter, the results and discussion are classified into three parts. First, the effects on the synthesis of different Y zeolite are discussed in section 5.1. In addition, the effect of particle size on hydrothermal stability of Y zeolite is analyzed by SEM, XRD, ^{27}Al MAS-NMR, BET, NH_3TPD and pyridine adsorption measurement in section 5.2 and last, correlation between crystallinity with its particle size is illustrated in section 5.3.

5.1 Effect of Preparation Conditions on Particle Size of Y Zeolite

Synthesis of Y zeolite is a typical inorganic reaction procedure, the properties of the product being affected by temperature, stirring, mixing method, concentration, and time of aging. These effects are important in the synthesis of Y zeolite: with the same ratio of Na_2O:Al_2O_3:SiO_2:H_2O, a series of products with different average particle sizes is obtained for laboratory and industrial procedures.

A detailed investigation was carried out to determine effects of time and temperature of aging and crystallization on the synthesis of Y zeolite. Gels were prepared by adding a sodium silicate solution to an initial solution of aluminosilicate and strring until a clear mixture formed.

The first influencing parameter studied is Y zeolite formation at different particle size. Silica, alumina, sodium hydroxide and water are mixed together to form alumino-silicate nucleation centers as illustrated in table 5.1. Aging time of nucleation at room temperature is varied from 0.5 to 6.5 days and the reaction

temperatures for Si-Al gel is set between 363 to 383 K at which optimum production of Y zeolite was reported [102].

Table 5.1 Synthetic parameters of zeolite formation at different particle size

Aging Time (day)	Reaction Temperature (°C)	Average Particle Size (μm)[a]
	90	1.19
0.5	100	amorphous
	110	amorphous
	90	0.45
2	100	1.81
	110	2.01
	90	0.31
4.5	100	0.45
	110	0.4
	90	0.16
6.5	100	0.25
	110	0.45

[a]Average particle size was evaluated using SEM.

The different particle sizes of Y zeolites ranging from 0.16-0.21 μm used in this study were prepared by varying aging time of nucleation and gel reaction temperature. Average particle sizes of Y zeolites obtained from various synthesis conditions are reported in Table 5.1. The reaction temperature of 363-383K has been found to be the optimum temperature for producing Y zeolite [104]. The minimum time to obtain zeolite crystal structure was determined to be ca. 2 days otherwise amorphous materials were produced. It was found that lower reaction temperature (lower crystal growth rate) and longer aging time of nucleation resulted in smaller zeolite crystals. A similar result has been reported by Zhdanov *et al*. [8] for the synthesis of Na-A zeolite. Typically the particle size of zeolites depends on the relative rates of the two competing phenomena occurring during synthesis namely, nucleation and crystal growth. Both rates decreased with decreasing temperature [103], however, the impact was more pronounced on the crystal growth rate than on the nucleation rate resulting in smaller particle size at lower temperature [104]. Another factor influences the size of zeolite crystals is the aging time of nucleation.

The longer aging time of nucleation, the less uniformity of nuclei precursors in the reaction mixture, consequently smaller zeolite particles are formed [24].

5.2 Hydrothermal stability of Y zeolite for the different particle size

5.2.1 Morphology and Particle size of Y zeolite samples

Y zeolites synthesized by hydrothermal method have different particle size, average 0.16, 0.31, 0.45, 0.82, and 2.01 μm. Average particle size was calculated from

$$\text{Average particle size} = \frac{\sum [(\text{particle size was measured from SEM}) \times (N^*)]}{\sum N^*}$$

N = Number of sample

Shape and average size of the particle before hydrothermal treatment can be observed from scanning electron microscopy (SEM) picture as shown in Figures 5.1 (a), (c), (e), (g), (i), and (k), respectively. SEM micrographs of the particle after hydrothermal treatment are illustrated in Figure 5.1 (b), (d), (f), (h), (j), and (l), respectively. Y zeolites prepared with different preparation conditions resulted in spherical particles with average particle sizes varying from 0.16-2.01 μm. The particle sizes and shape remained unaltered after encountered the hydrothermal treatment at 1073 K for 1 hour.

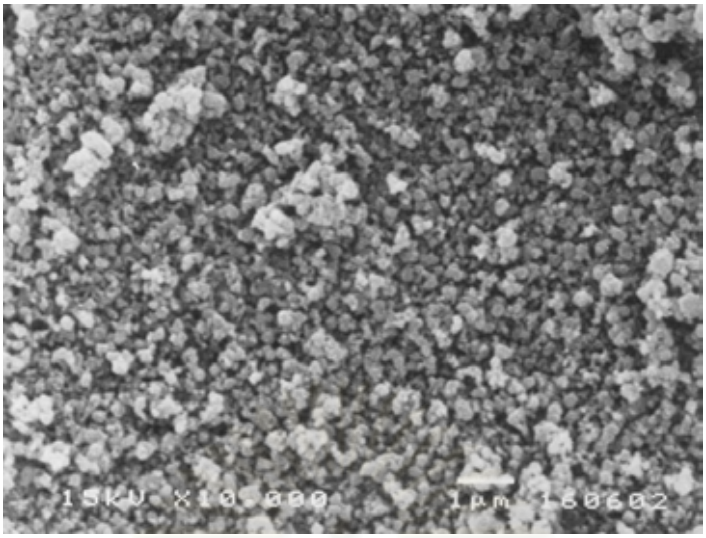

(a)

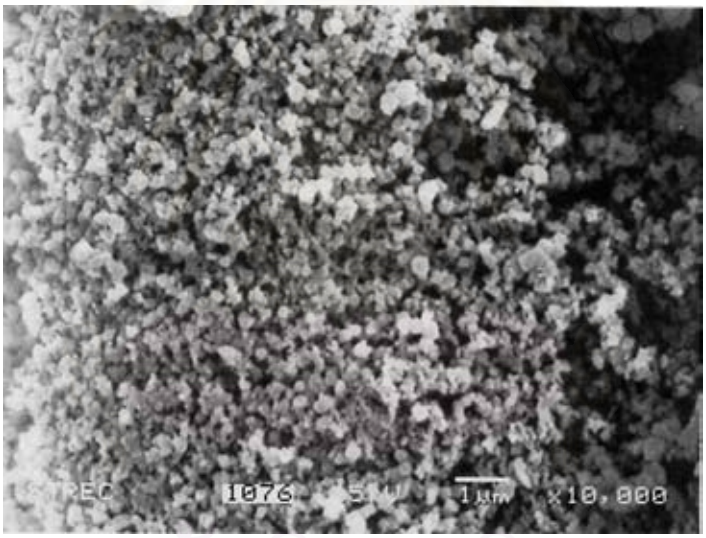

(b)

Figure 5.1 Scanning electron micrographs of Y zeolite particle size 0.16 μm (a) fresh (b) treated

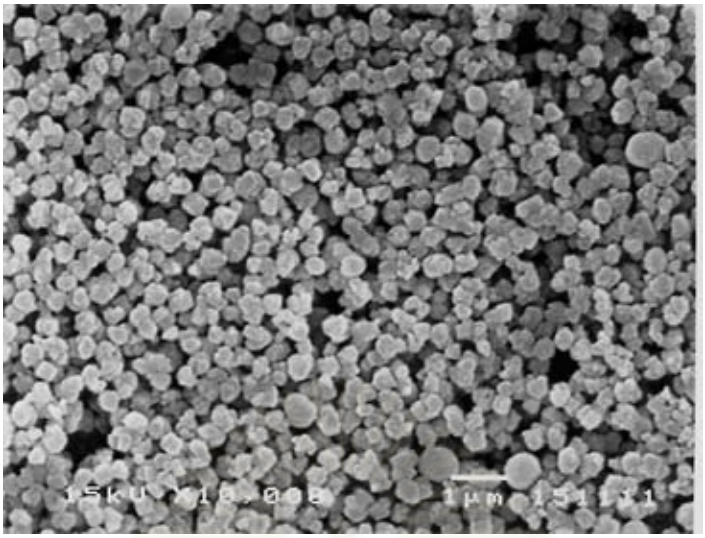

(c)

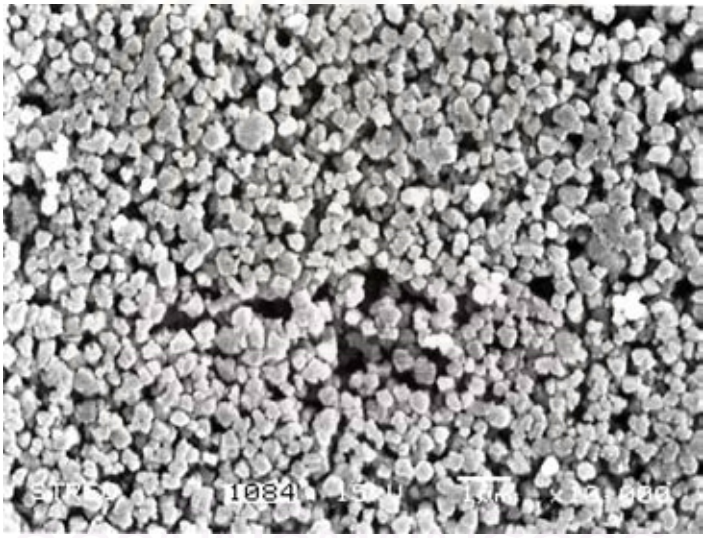

(d)

Figure 5.1 (Cont.) Scanning electron micrographs of zeolite particle size 0.31 μm (c) fresh (d) treated

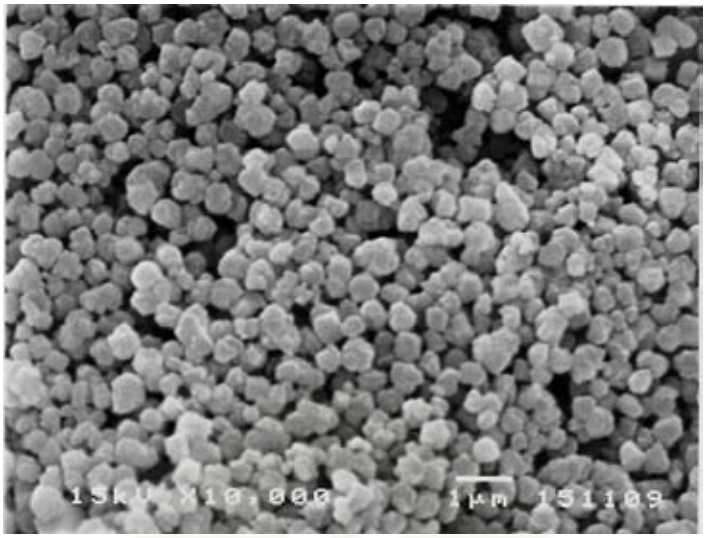

(e)

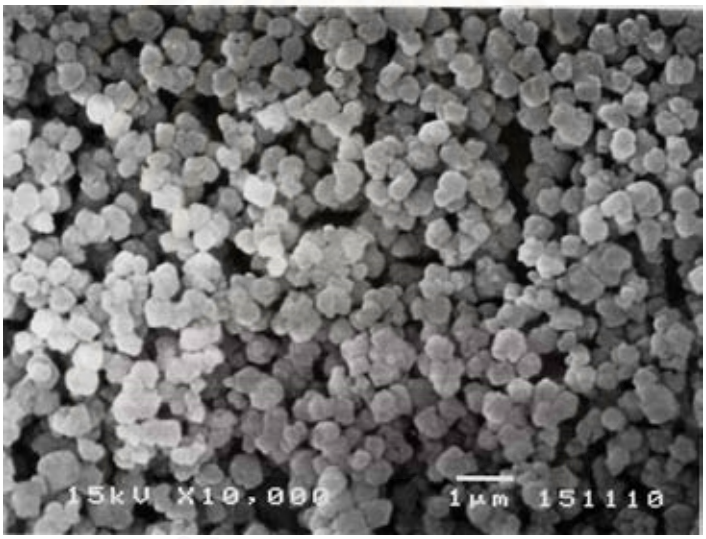

(f)

Figure 5.1 (Cont.) Scanning electron micrographs of zeolite particle size 0.45 μm (e) fresh (f) treated

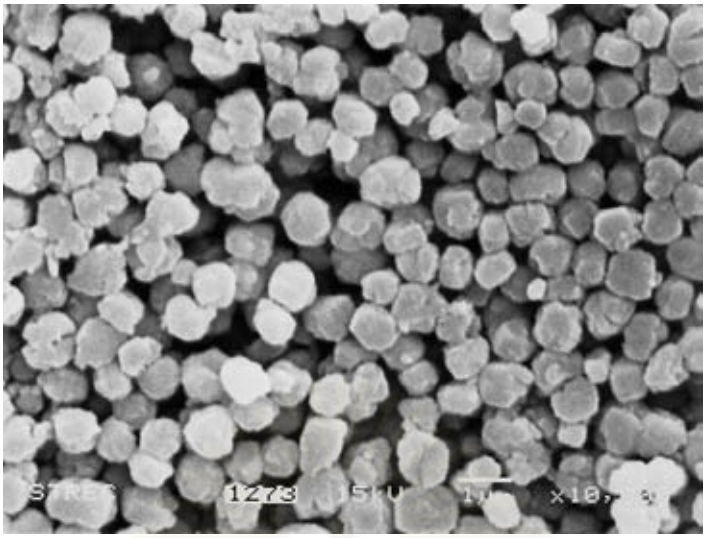

(g)

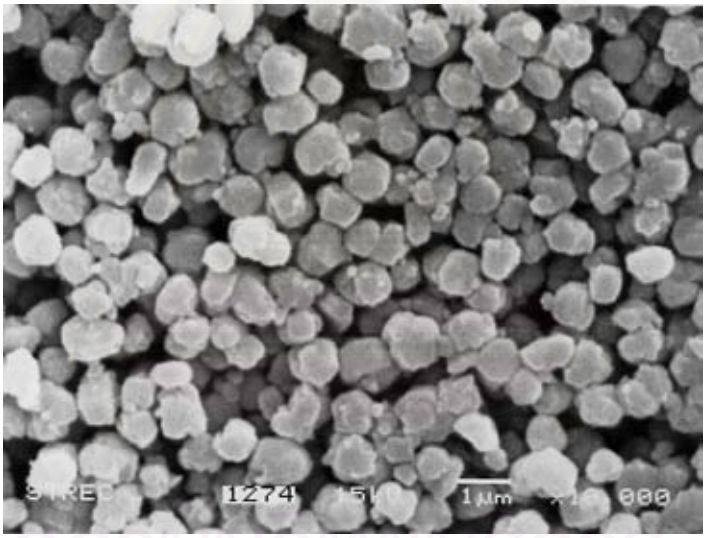

(h)

Figure 5.1 (Cont.) Scanning electron micrographs of zeolite particle size 0.82 μm (g) fresh (h) treated

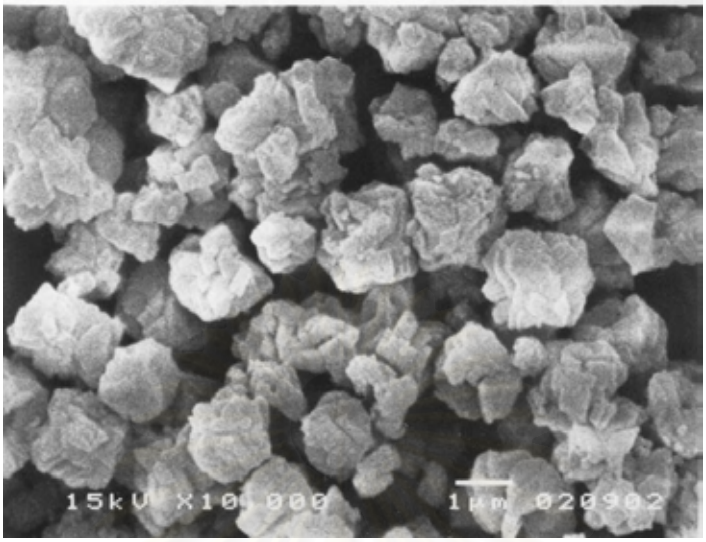

(i)

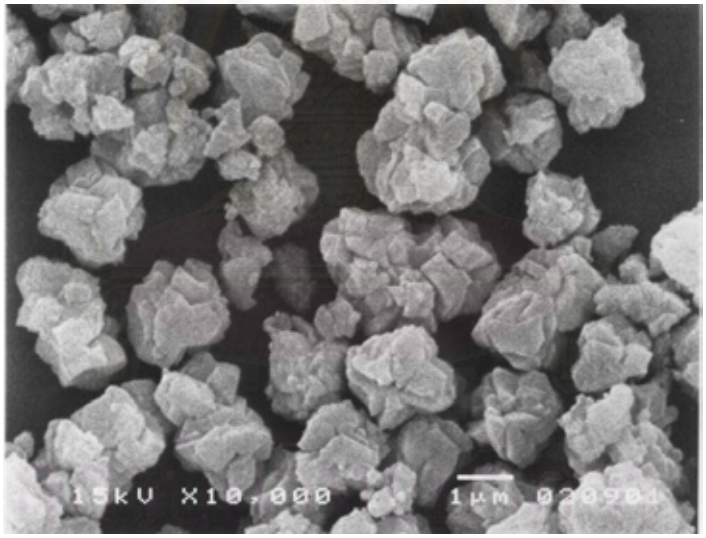

(j)

Figure 5.1 (Cont.) Scanning electron micrographs of zeolite particle size 1.81 μm (i) fresh (j) treated

5.2.2 Crystallinity

X-ray diffraction is a technique which can identify the crystal structure. Figure 5.2 shows the comparative XRD patterns of HY zeolite both before and after hydrothermal treatment for each crystallite sizes. The XRD patterns of commercially available Y zeolite "JRC-Z-Y" supplied by Tosoh Corporation were also showed for comparison. All the XRD patterns indicate similar eight main peaks at 2θ as 15.7, 18.7, 20.4, 23.7, 27.1, 30.8, 31.5 and 34.2 from literature [105]. In addition to identify a catalyst sample, the XRD pattern can indicate the crystallinity through the intensity values of the observed peak compared to that of the reference peak as the following equation:

$$\% \text{ crystallinity} = \frac{\text{Sum of integral peak intensities for the sample}}{\text{Sum of the integral peak intensities for the reference}} \times 100$$

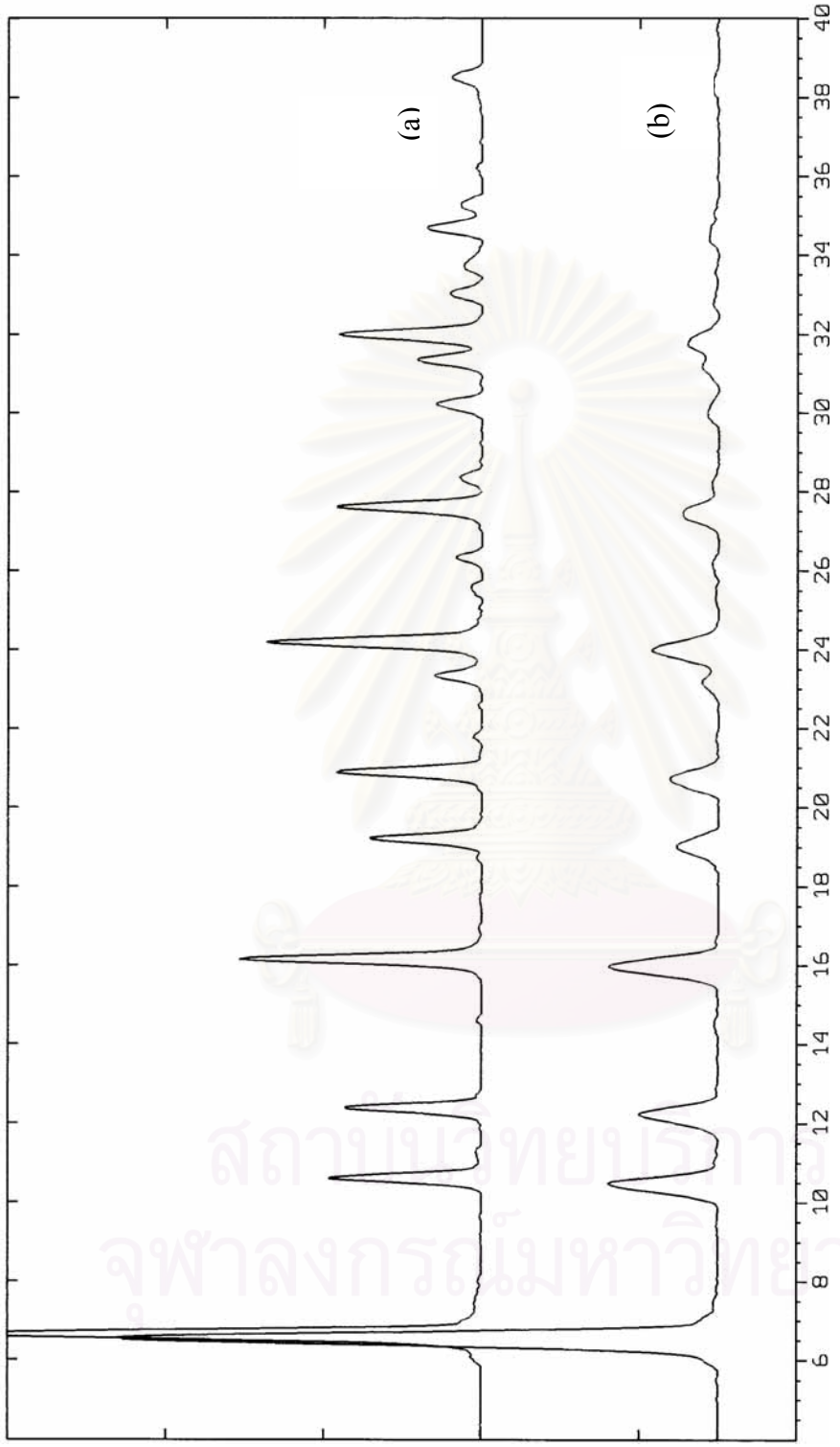

Figure 5.2 XRD spectra of Y zeolite particle size 0.16 μm (a) fresh (b) treated

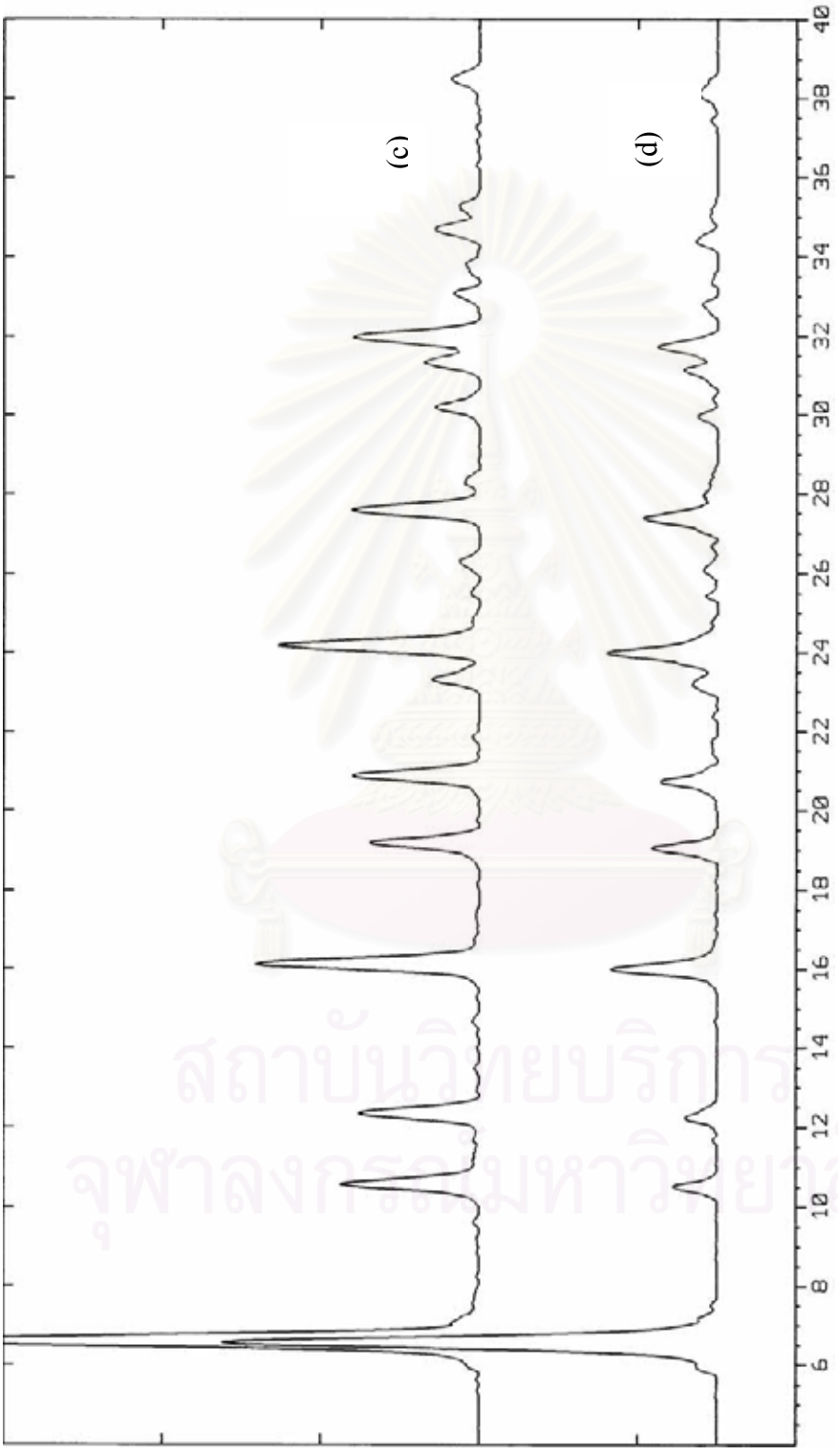

Figure 5.2 (Cont.) XRD spectra of Y zeolite particle size 0.25 μm (c) fresh (d) treated

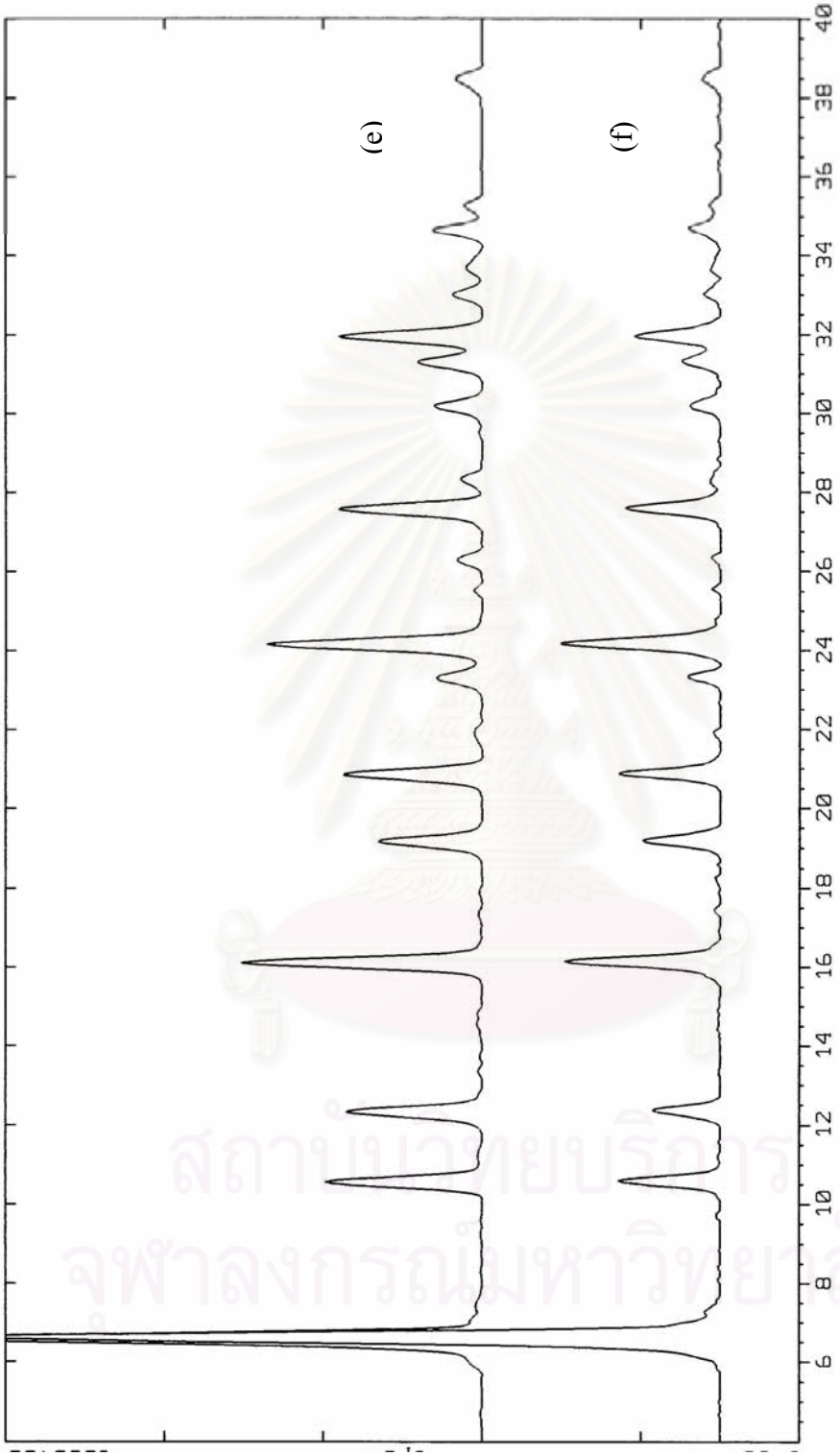

Figure 5.2 (Cont.) XRD spectra of Y zeolite particle size 0.31 μm (e) fresh (f) treated

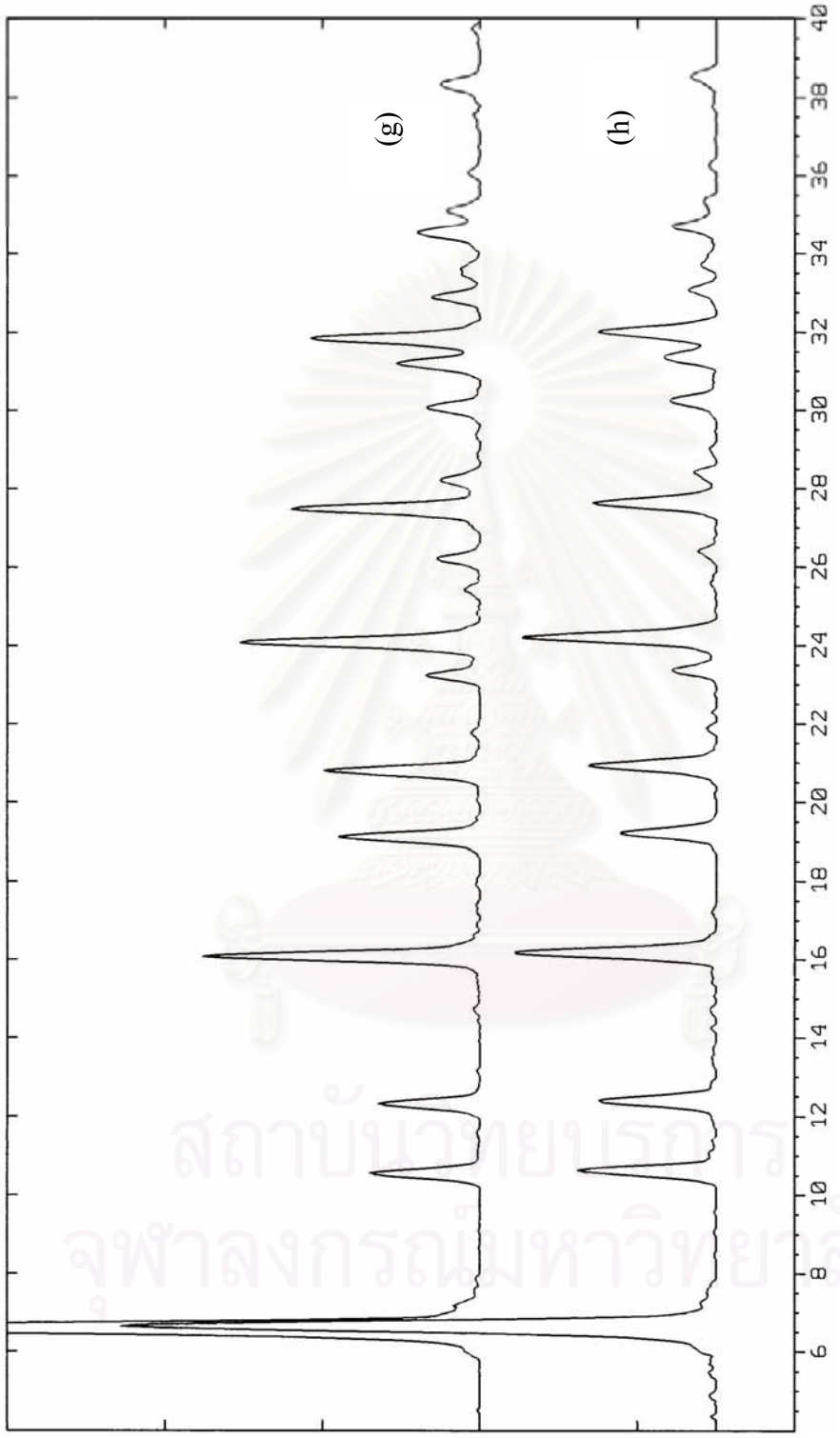

Figure 5.2 (Cont.) XRD spectra of Y zeolite particle size 0.40 μm (g) fresh (h) treated

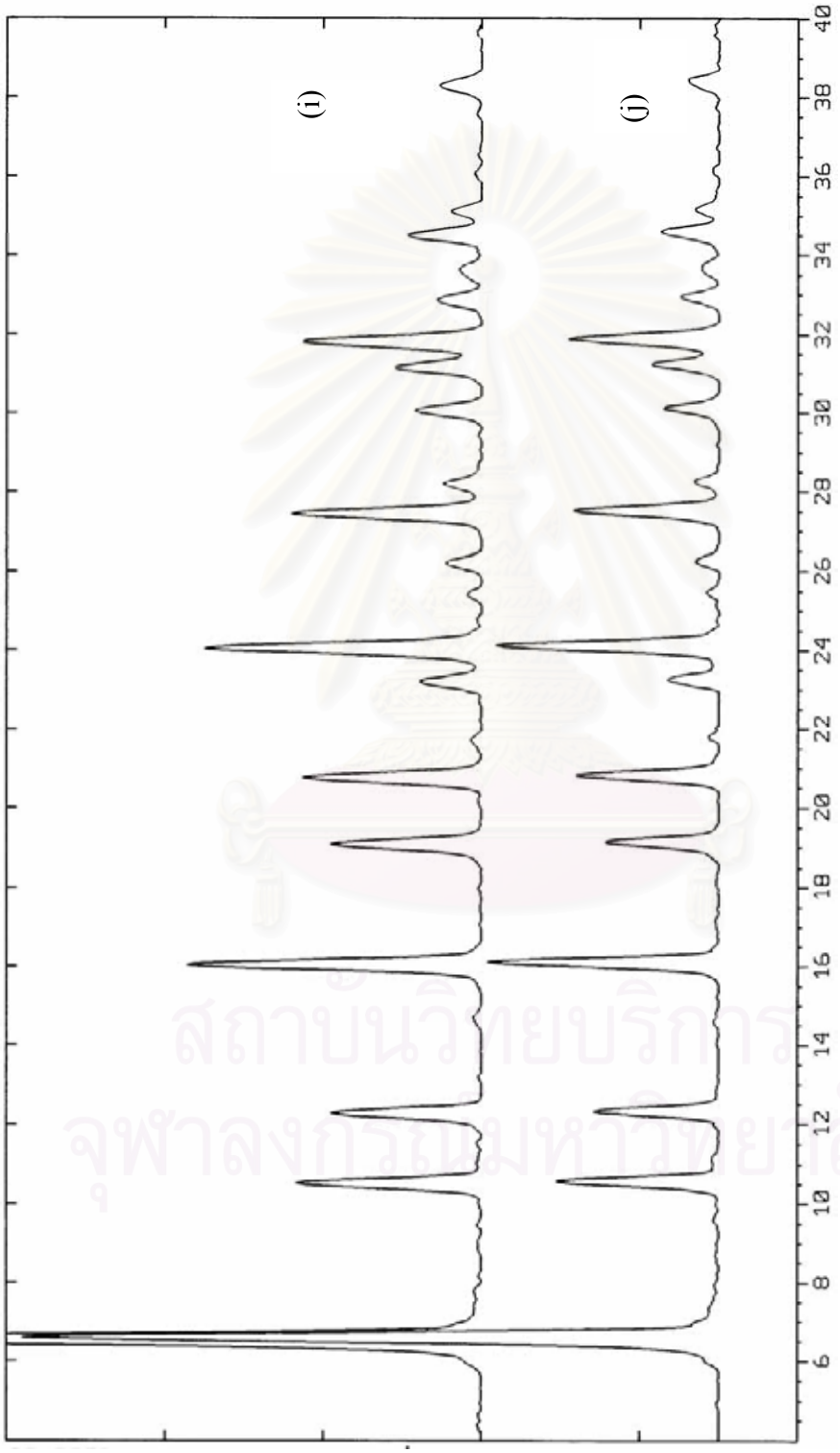

Figure 5.2 (Cont.) XRD spectra of Y zeolite particle size 0.45 μm (i) fresh (j) treated

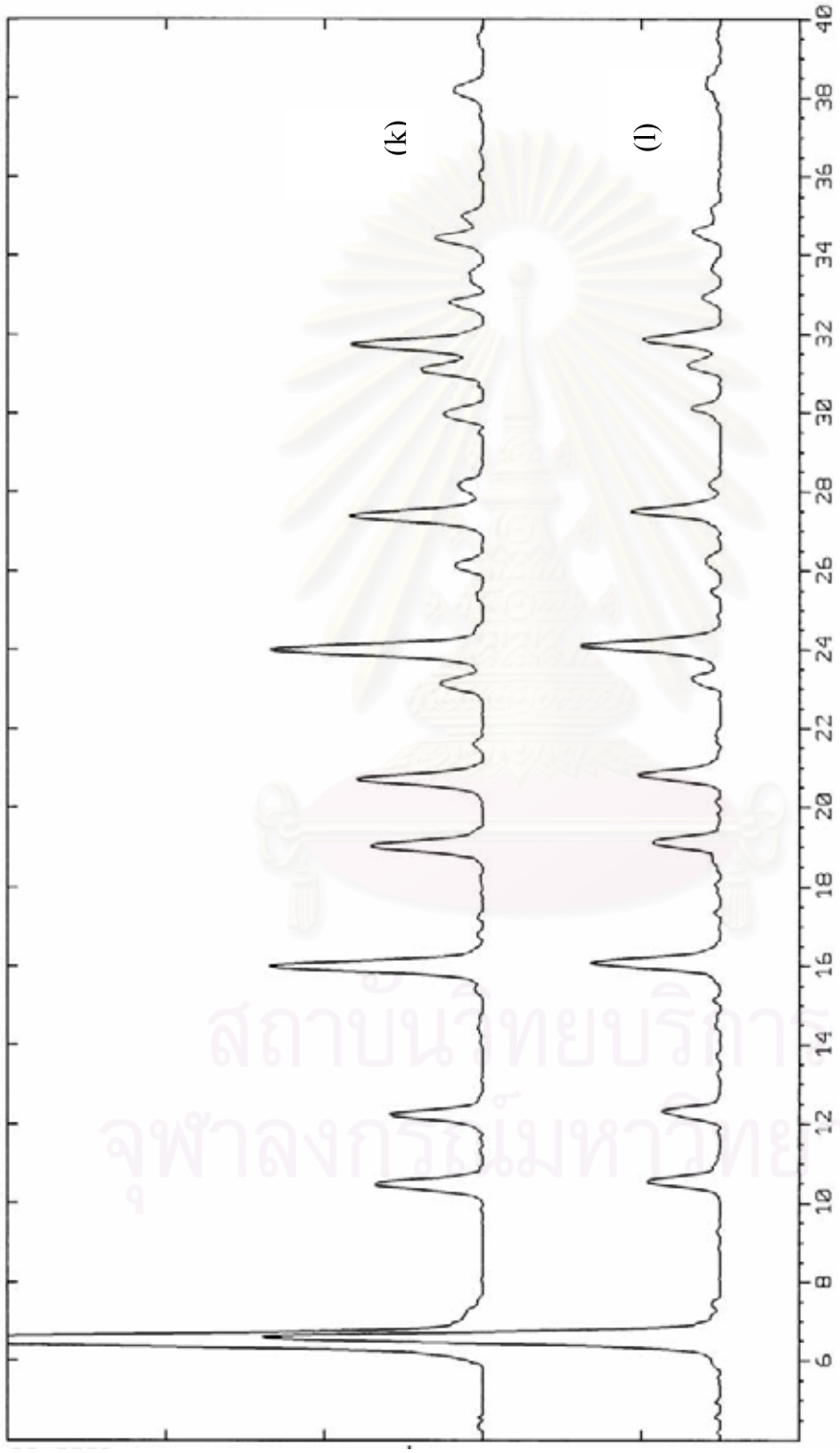

Figure 5.2 (Cont.) XRD spectra of Y zeolite particle size 0.82 μm (k) fresh (l) treated

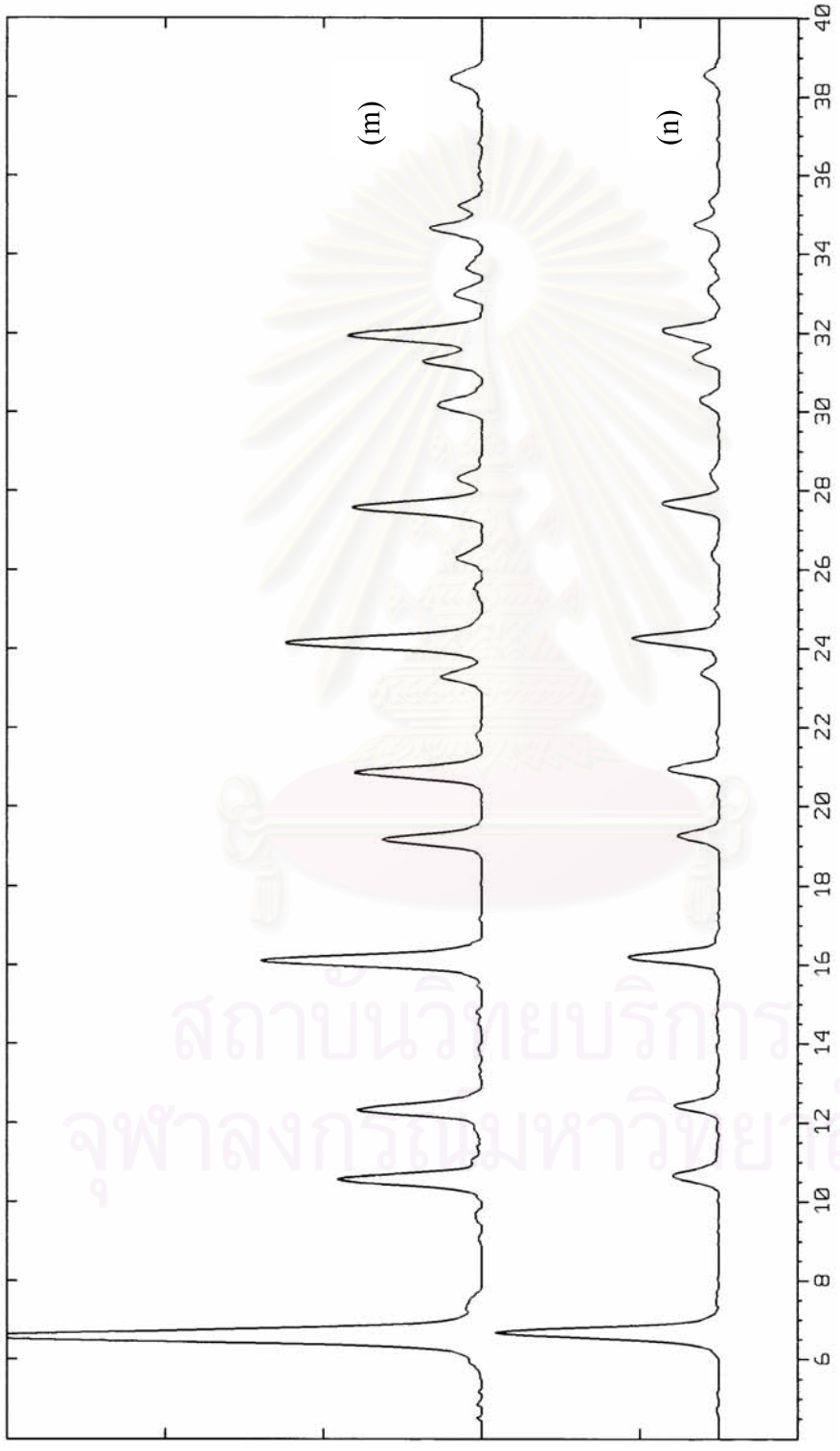

Figure 5.2 (Cont.) XRD spectra of Y zeolite particle size 1.19 μm (m) fresh (n) treated

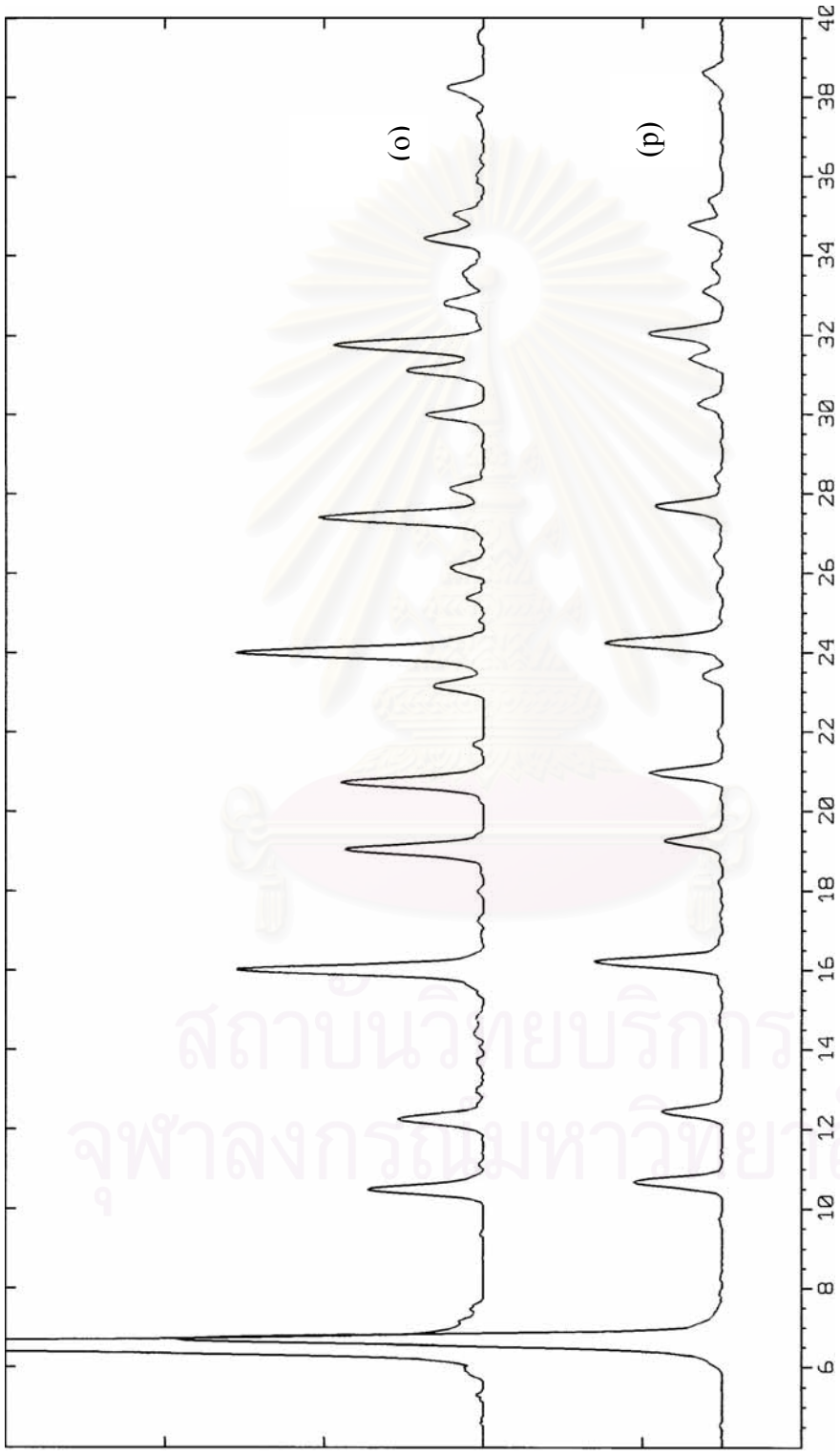

Figure 5.2 (Cont.) XRD spectra of Y zeolite particle size 1.81 μm (o) fresh (p) treated

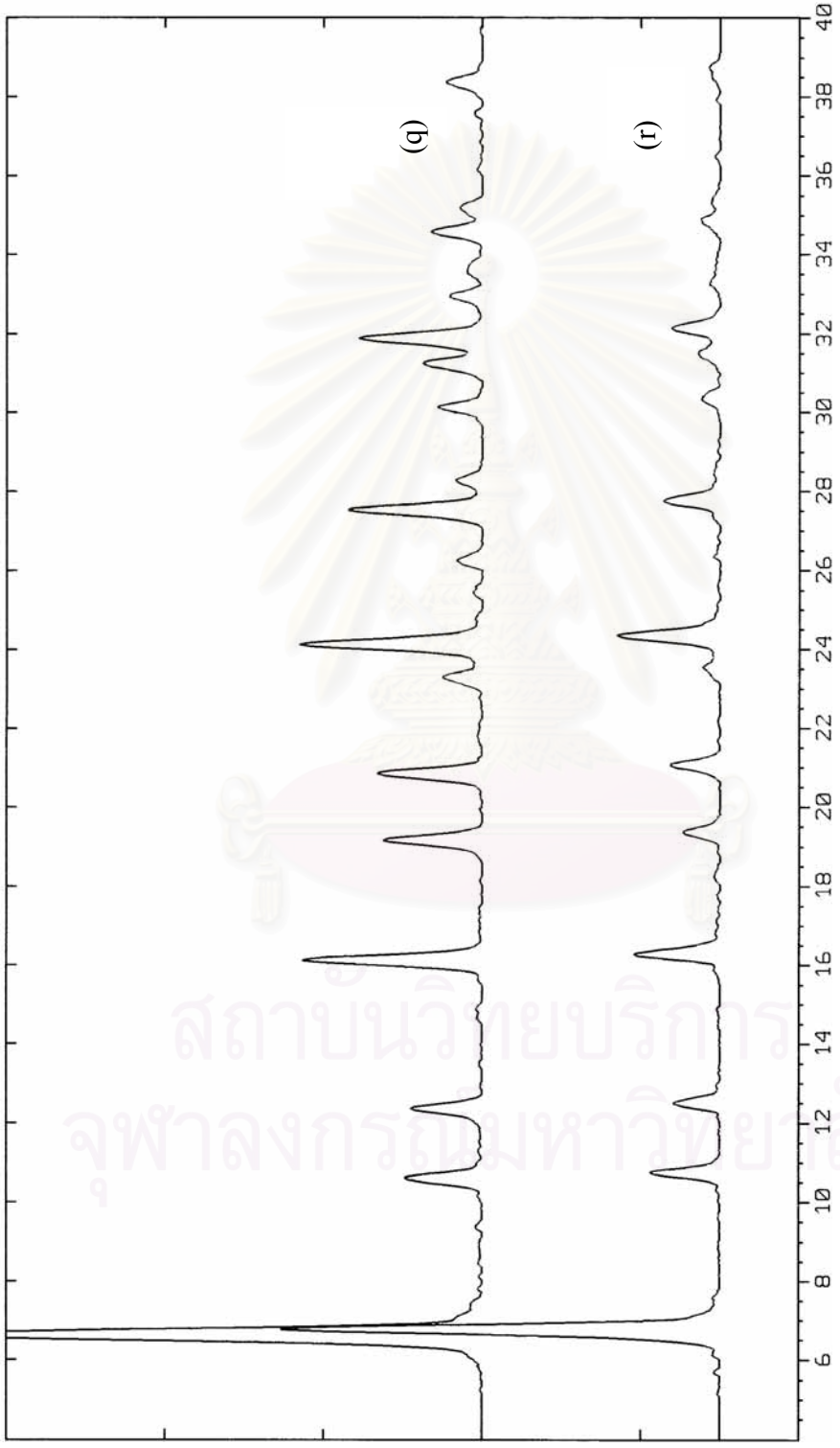

Figure 5.2 (Cont.) XRD spectra of Y zeolite particle size 2.01 μm (q) fresh (r) treated

However, it is known that the crystallinity of Y zeolite was affected during hydrothermal treatment due to aluminum extraction and dehydroxylation [106]. Its property is based on the crystallinity as the structure of the as-synthesized sample was investigated by XRD. Afterwards, effect of particle size between 0.16-2.01 μm on the crystallinity of Y zeolite at different treated parameters is demonstrated in Figure 5.3 show the effect of particle size on the crystallinity of Y zeolite when varying aging parameters is as follows: (a) temperature, (b) aging time, and (c) steam partial pressure, respectively. The relationships between crystallinity and the particle size of Y zeolite when varying aging parameters follow similar volcano trend. The percentages of crystallinity significantly decreased with increasing hydrothermal temperature, steam partial pressure, and aging time, which is typical hydrothermal behavior for zeolite in FCC catalysts [2]. In this study, the lowest crystallinity was observed for the most severe hydrothermal conditions (1273K, 100% steam partial pressure, and 300 min).

The hydrothermal stability of Y zeolites was also found to be strongly dependent on the particle size of Y zeolites. For the particle sizes ranging from 0.16-0.45 μm, crystallinity increased with increasing particle sizes and the maximum crystallinity of ca. 80-90% was observed for the particle size of 0.45 μm. This trend is in agreement with the literature that smaller crystallite zeolites are more active but less stable than larger ones [81,107]. The increase in crystallinity with increasing particle size in this range is probably due to a structural arrangement in the gel during crystal forming [24]. The crystallinity of Y zeolites, however, gradually decreased when particle sizes were larger than 0.45 μm. The hydrothermal behavior of larger particle Y zeolite is still unclear; however, the decrease in crystallinity is probably due to the large amount of acidic defects in larger particle size Y zeolite. In addition, there may be an influence from the average distance between acidic and metallic sites, [108] or the various pore sizes in large particle shape-selective zeolite. In a previous study, Praserthdam et al. [19] reported that the larger particle Co/HZSM-5 catalysts significantly lost crystallinity and tetrahedral aluminum upon hydrothermal treatment while those for the smaller particle ones remained unaffected.

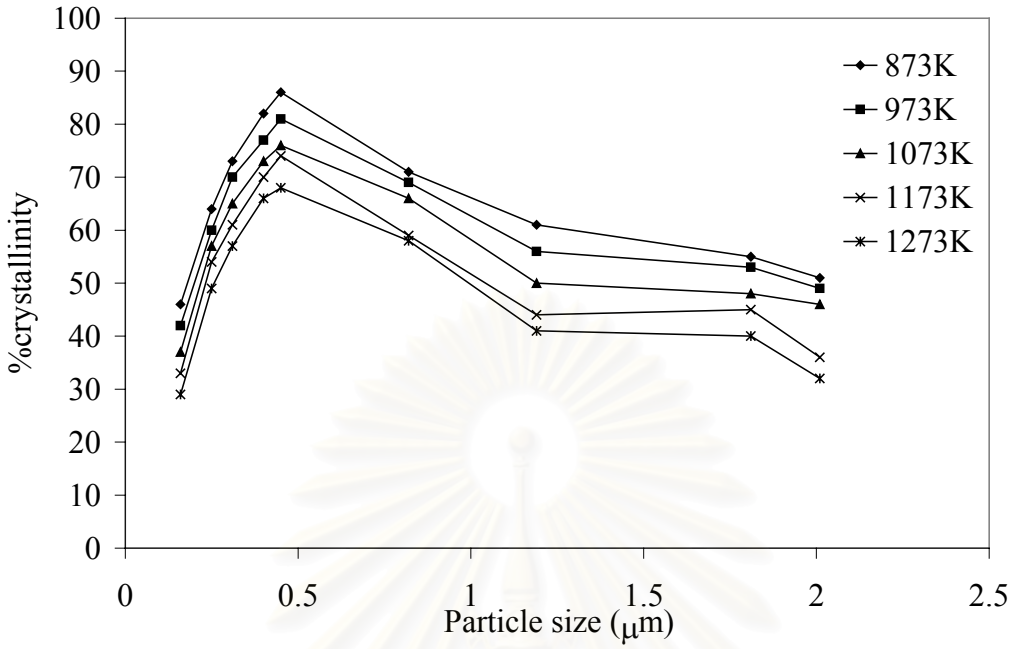

5.3 a

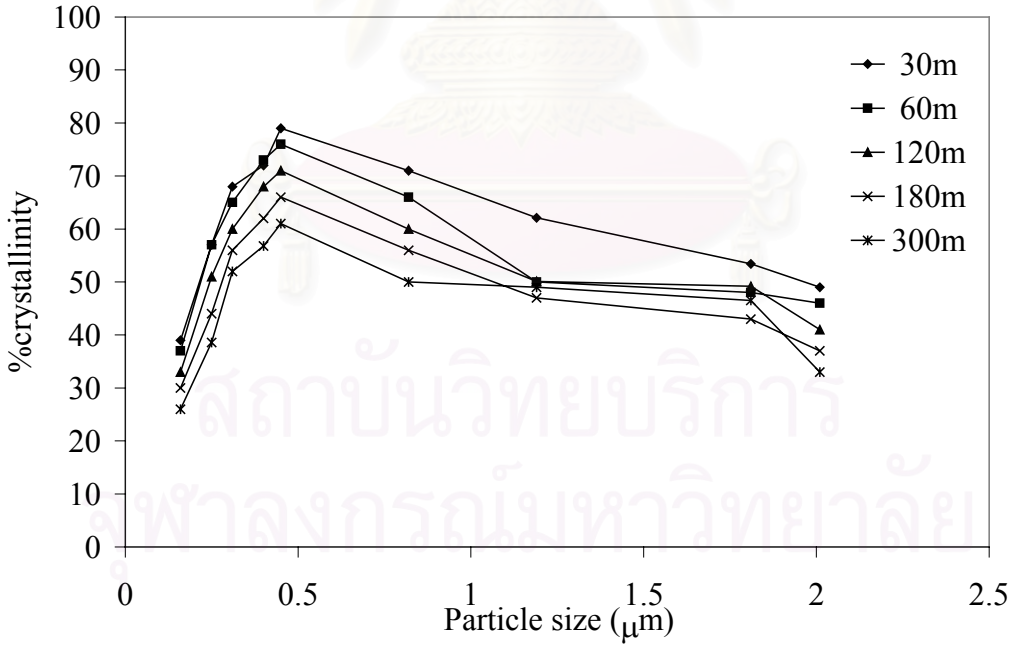

5.3 b

Fig.5.3. Relationship between crystallinity and particle size of Y zeolite after hydrothermal treatment at different treated parameters (a) 873-1273 K, 10% mol and 60 min (b) 30-300 min, 10%mol steam and 1073 K

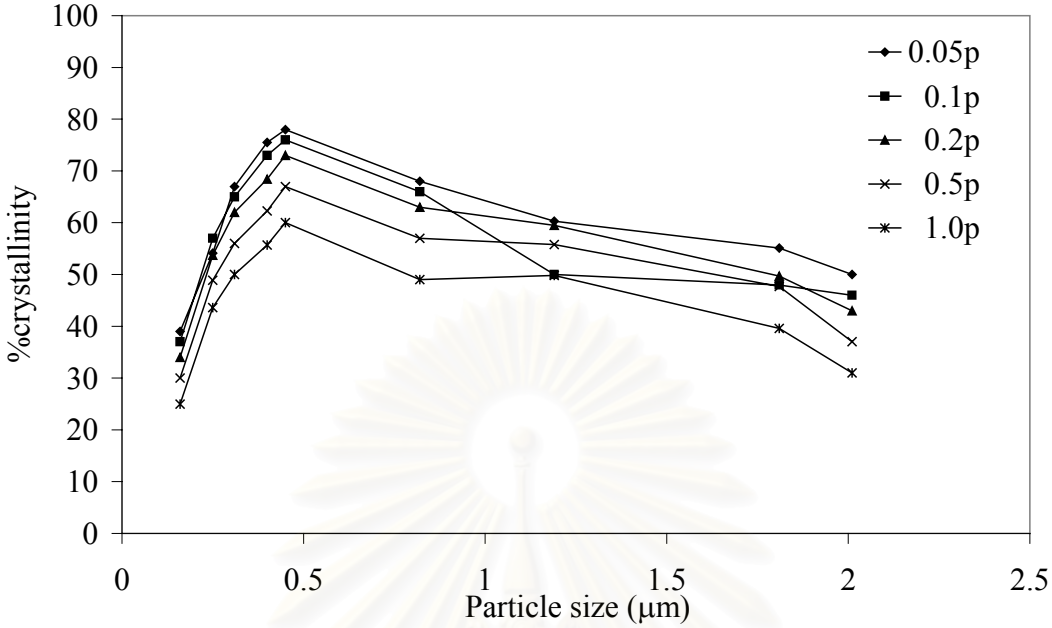

5.3 c

Fig.5.3. Relationship between crystallinity and particle size of Y zeolite after hydrothermal treatment at different treated parameters (a) 873-1273 K, 10%mol steam and 60s (b) 30-300 min, 10%mol steam and 1073K (c) 0.05-1 P/P_0, 60s and 1073K

5.2.3 Framework Al content, ^{27} Al MAS NMR Spectra

Measuring ^{27}Al MAS NMR spectra provides information about the environment of the aluminum atoms in the zeolite sample. Al-tetrahedral presented in the zeolite framework ($Al(OSi)_4$), displays an NMR feature at ~ 60 ppm. Next, Extra-framework aluminum (EFAl) species are usually octahedral coordinates which appear singnal at a chemical shift of ~ 0 ppm.

Figure 5.4 shows the ^{27}Al MAS NMR spectra of Y zeolites with different particle sizes before and after hydrothermal aging. In the fresh samples (Figure 5.4 (a), (c), (e), (g), and (j)), a strong signal at ca. 56 ppm and a weak signal at ca. 0 ppm were detected. These peaks correspond to tetrahedral coordinated Al species (Al^{IV}) in

the zeolitic framework and octahedral coordinated extra framework Al (Al^{VI}), respectively [109-110]. After hydrothermal aging at 1073 K for 1 h, a decrease in tetrahedral aluminum and an increase in octahedral aluminum were observed for Y zeolites in all particle sizes used in this study except for the medium size (0.45 μm). Loss in crystallinity is due to framework dealumination of the zeolite [19, 30]. For strongly dealuminated samples, another peak or a small shoulder is often visible between 30 and 50 ppm in the ^{27}Al MAS NMR spectra, which has been assigned to penta-coordinated aluminum atoms [111-112] or distorted tetrahedral coordinated aluminum atoms in extra-framework species [113-114].

Relative areas of tetrahedral ^{27}Al before and after hydrothermal treatment are reported in Table 5.2. They were found to be in accordance with the percentages of crystallinity. Medium particle size of Y zeolite (0.45 mm) exhibited the lowest amount of dealumination, subsequently the highest crystallinity was obtained.

Otherwise, metal and/or promoter loading may improve stability of catalysts and affect on catalytic performance, such as Praserthdam *et al* [11] reported that the dealumination at 10% steam and 1073 K of tetrahedral Al in Cu/H-MFI framework is completely prevented when loading Pd from 0.3 wt. % or higher, and Dangsawai *et al* [12] also supported that Pd-modification of Cu/HZSM-5 is an effective means of improving the stability of the NO conversion to N_2 under hydrothermal conditions at the same previous condition.

Table 5.2 Relative areas of tetrahedral ^{27}Al before and after hydrothermal treatment

Particle size (μm)	Relative area of tetrahedral ^{27}Al (%)*		
	fresh	treated	^{27}Al tetrahedral changed (%)
0.16	83.69	69.14	17.39
0.31	85.06	77.99	8.31
0.45	84.52	83.63	1.06
0.82	88.64	78.97	10.92
2.01	90.63	71.35	21.28

*The relative area of tetrahedral ^{27}Al was calculated from the area of tetrahedral aluminum per summation area of tetrahedral and octahedral aluminum.

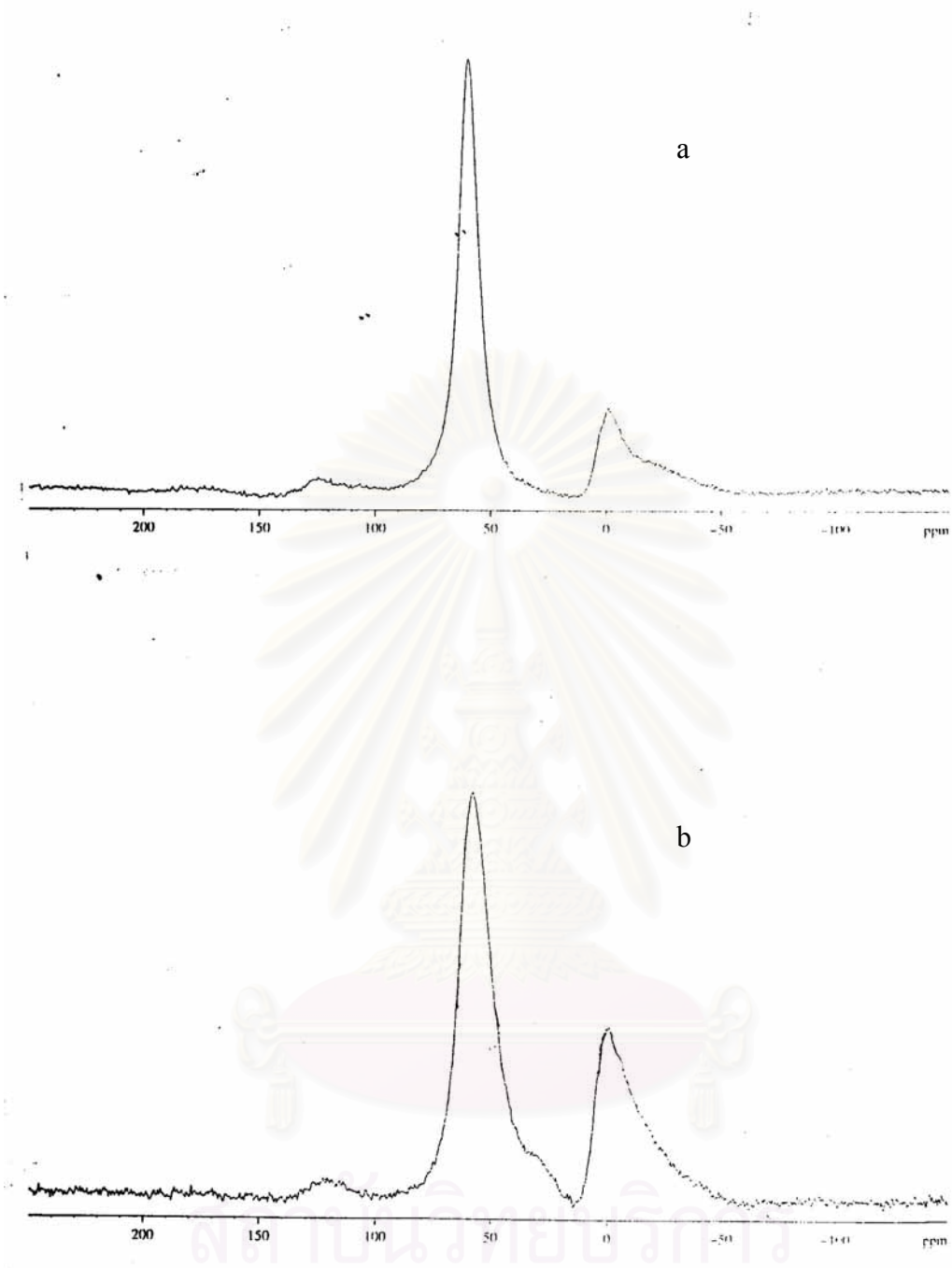

Figure 5.4 ^{27}Al MAS NMR spectra of Y zeolite particle size 0.16 μm (a) fresh (b) treated

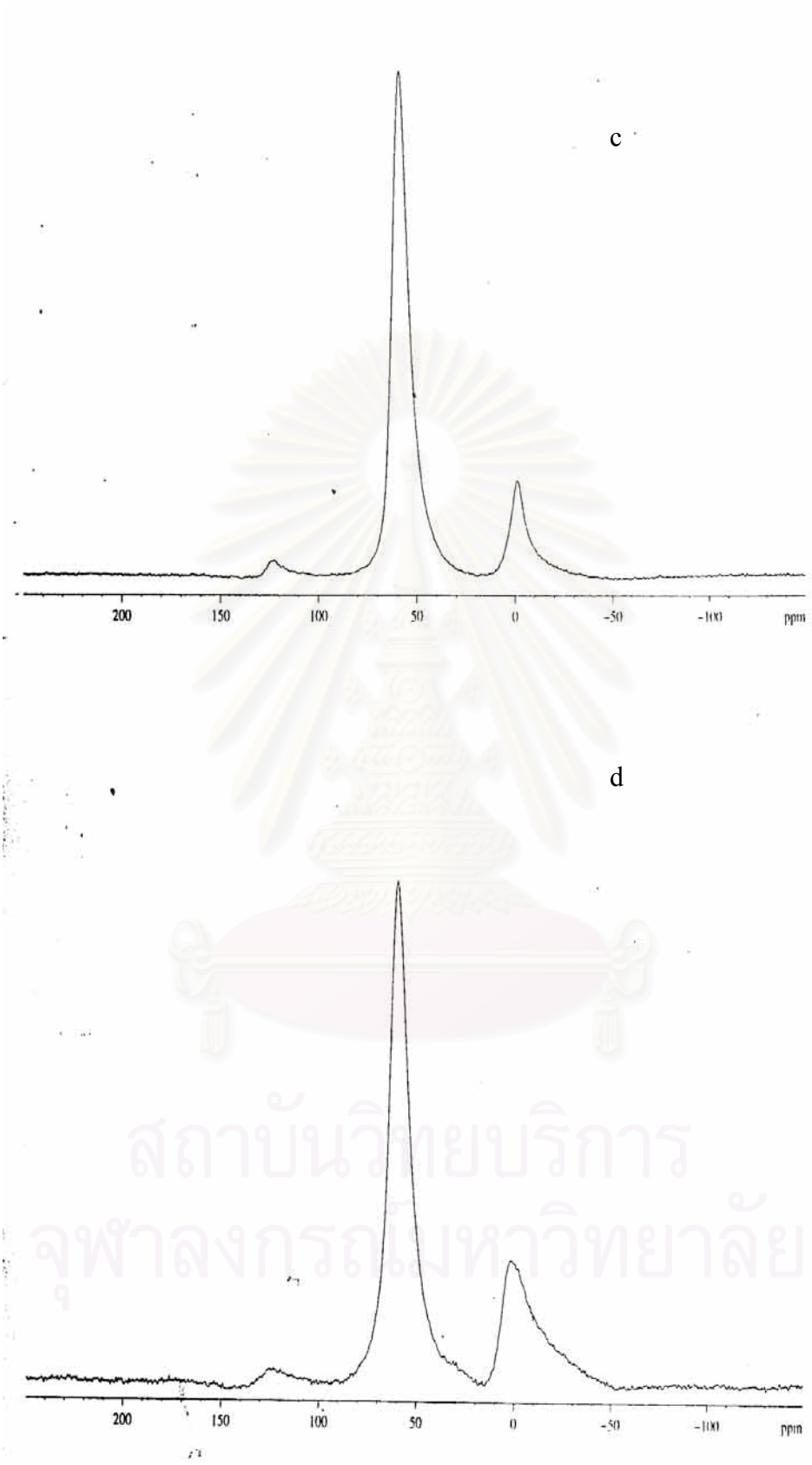

Figure 5.4 (Cont.) ^{27}Al MAS NMR spectra of Y zeolite particle size 0.31 μm (c) fresh (d) treated

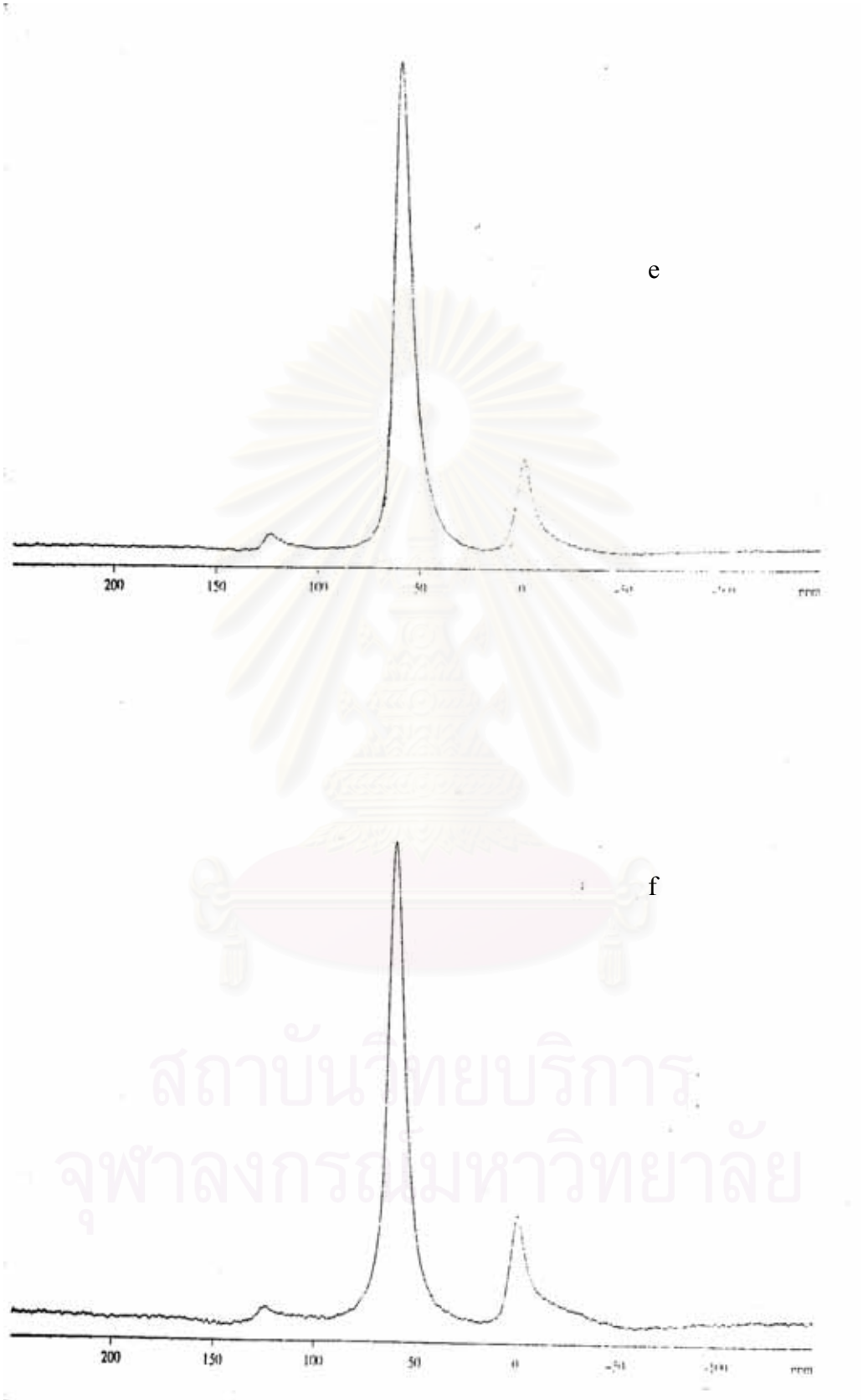

Figure 5.4 (Cont.) ^{27}Al MAS NMR spectra of Y zeolite particle size 0.45 μm (e) fresh (f) treated

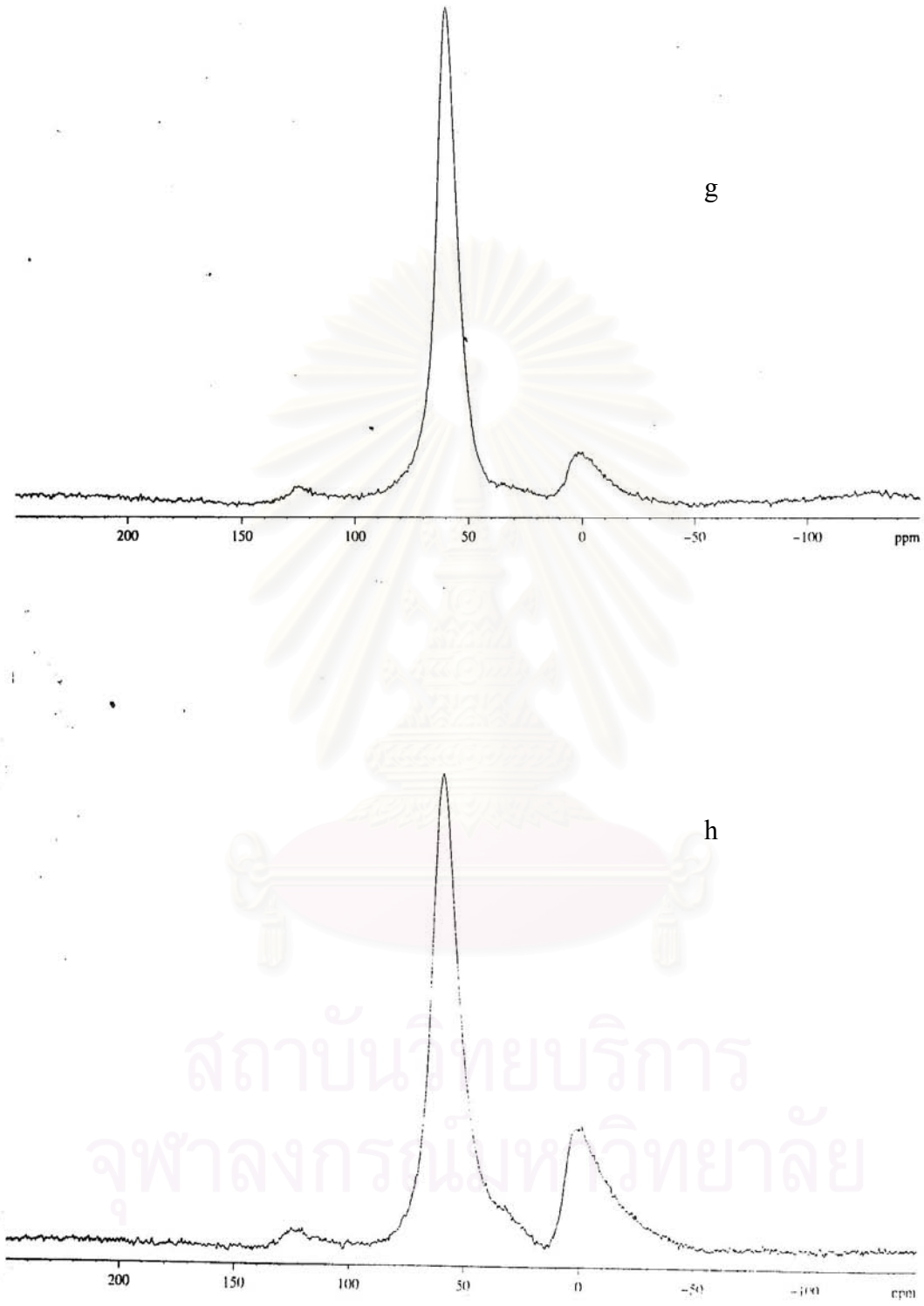

Figure 5.4 (Cont.) ^{27}Al MAS NMR spectra of Y zeolite particle size 0.82 μm (g) fresh (h) treated

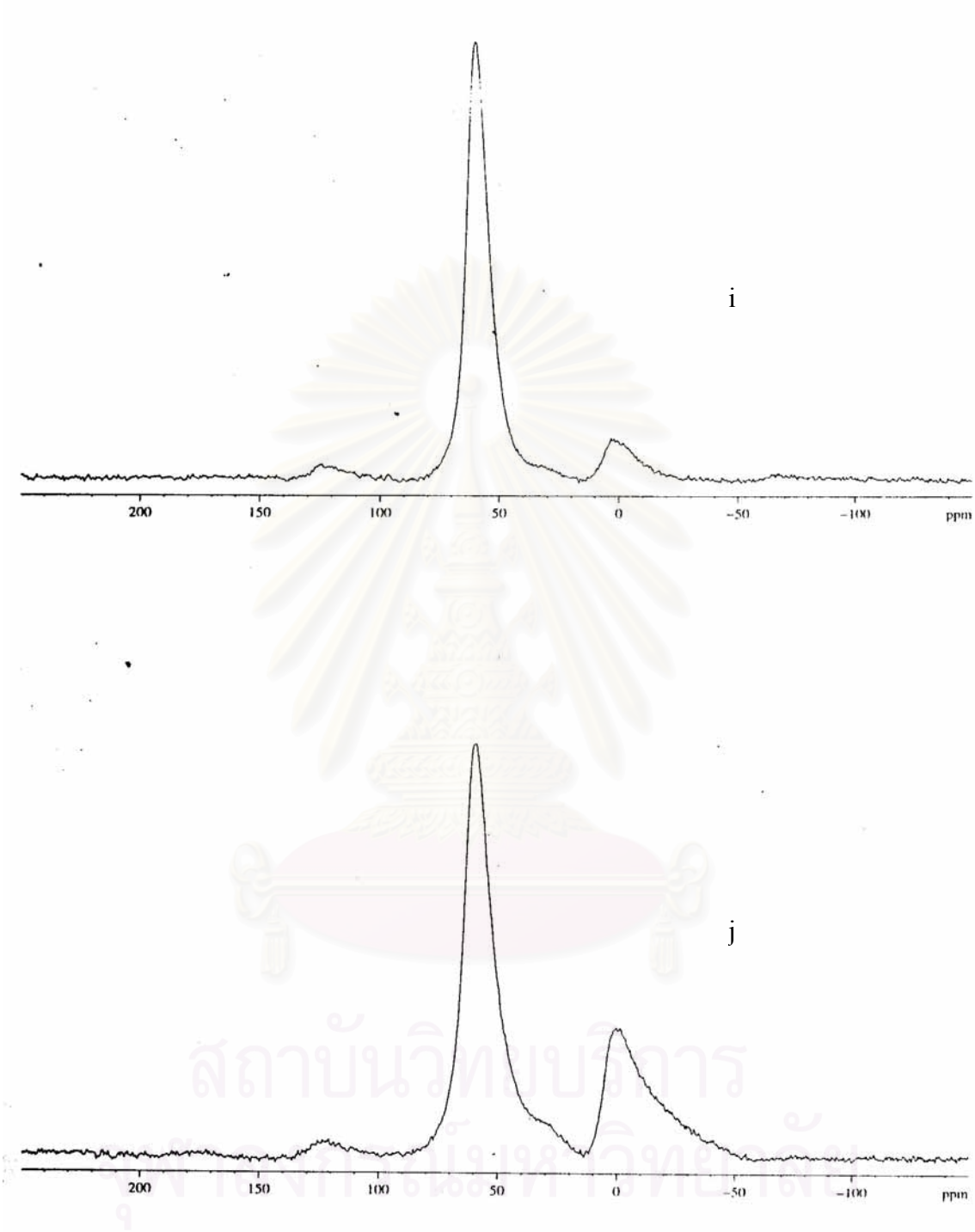

Figure 5.4 (Cont.) ^{27}Al MAS NMR spectra of Y zeolite particle size 2.01 μm (i) fresh (j) treated

5.2.4 Surface area

The single point BET surface area of Y zeolite, both fresh and treated with 10 mol % of water vapor, is shown in table 5.3. It is clear that the BET surface area for all Y zeolite decrease due to hydrothermal treatment corresponding to literature [115]. However, compared with a smaller and larger particle size, the BET surface area of a medium particle size decreases. This suggests that the structure of Y zeolite for small and large particle size may be easily changed. This is possible due to collapses at surface of zeolite framework [10]. These expectations are confirmed by the comparison of XRD patterns of these samples. The less BET surface area of small and large particle samples correspond to the lower intensity of XRD pattern which reflects the lower crystallinity of crystal.

Table 5.3 The single point BET surface area and the percent relative BET surface area of Y zeolite, fresh and treated samples

particle size (μm)	BET surface area (m^2/g)		
	fresh catalyst	treated catalyst	Relative BET surface area (%)
0.16	521	322	38
0.25	546	366	33
0.31	498	411	18
0.40	502	432	14
0.45	511	441	14
0.82	531	397	25
1.19	506	384	24
1.81	543	340	37
2.01	550	339	38

5.2.5 Characterization of Acidic Sites

NH_3 temperature programmed desorption (TPD) technique provides information on the amount and the strength of acidic sites. The peak area of a TPD profile represents the amount of desorbed NH_3 while the peak position corresponds to the strength of acidity. The NH_3 TPD profiles of Y zeolites with various particle sizes are shown in Figure 5.5. All catalyst samples exhibited similar TPD profiles. The first desorption peak at ca. 200°C is assigned to the sites of weak acid where the second peak at ca. 380°C correspond to strong acid sites [116]. The amount of weak acid sites was determined to be much higher than that of strong acid ones. Interestingly, higher amount of strong acid sites were detected on larger particle sizes of Y zeolite.

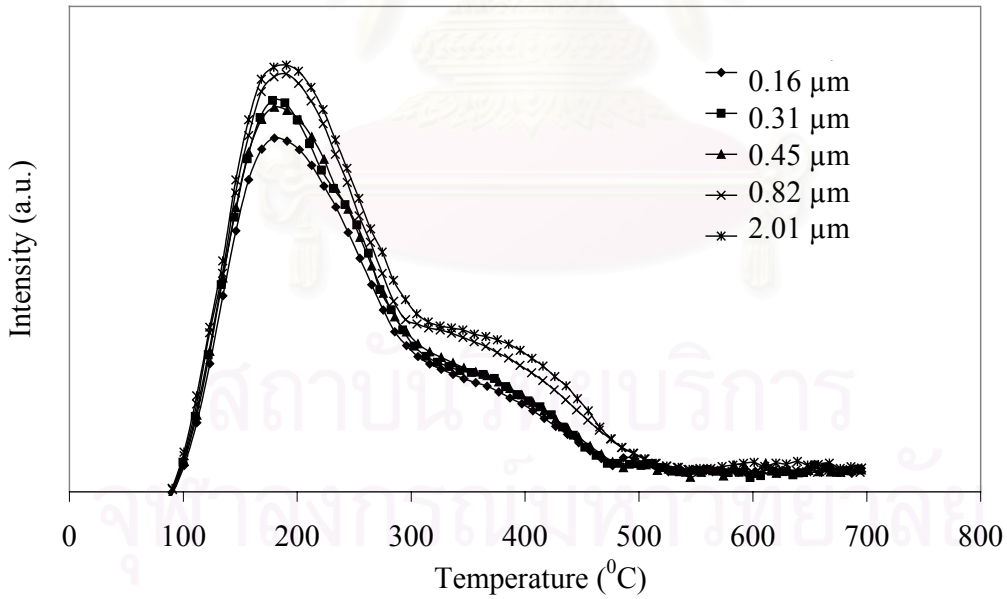

Figure 5.5 NH_3 TPD of fresh Y zeolite at various particle sizes

Pyridine adsorption IR spectroscopy is another powerful technique to measure and distinguish the acidic sites on zeolite surface. Figure 5.6 shows the pyridine

adsorption of fresh Y zeolites with different particle sizes. The two bands at ca. 1450 cm^{-1} and 1540 cm^{-1} are assigned to pyridine molecules adsorbed on Lewis acid and Brønsted acid, respectively. The integrated areas of the bands are proportional to the numbers of corresponding acid sites. The type of acid sites has been found to depend on the synthesis conditions. Kumar et al. [117] reported that fresh H-ZSM-5 catalysts synthesized at the longest aging time and largest particle size used in the study exhibited the highest number of Brønsted acid sites. The ratio of Brønsted acid and Lewis acid (B/L) as well as the relative area of ^{27}Al obtained from ^{27}Al MAS NMR as the function of particle size of Y zeolites were summarized in table 5.2. All Y zeolite catalyst samples contained both Lewis and Brønsted acid sites with the higher amount of Lewis acid sites than Brønsted ones. It was found that the larger particle sizes of Y zeolites exhibited higher Brønsted/Lewis acid sites (B/L) ratios than the smaller ones. The results from FTIR are in agreement with the NH_3 TPD results that higher amount of strong acid sites were detected on larger particle Y zeolites. This finding suggested that the acid defects in larger particle Y zeolites had an influence on the loss of crystallinity upon hydrothermal treatment due to larger particle sizes has been ascribed to the higher density of hydroxyl groups, which id parallel to that of Brønsted acid sites [23]. A shorter distance between hydroxyl groups increases the probability of dehydroxylation that dealumination is believed to occur during dehydroxylation consequently loss of crystallinity in large particle size.

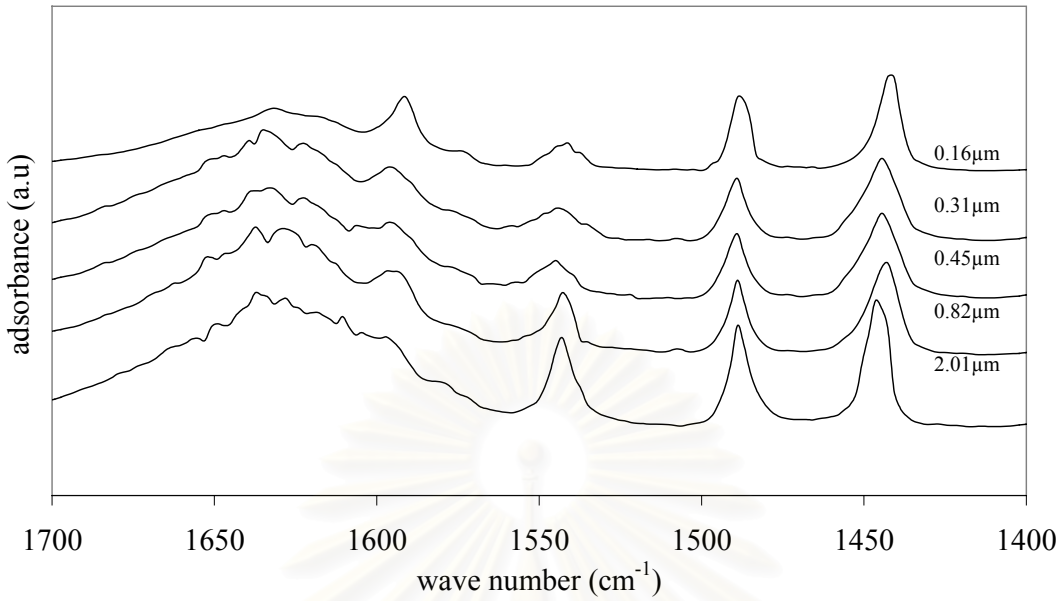

Figure 5.6 Pyridine adsorption of fresh Y zeolite at various particle sizes

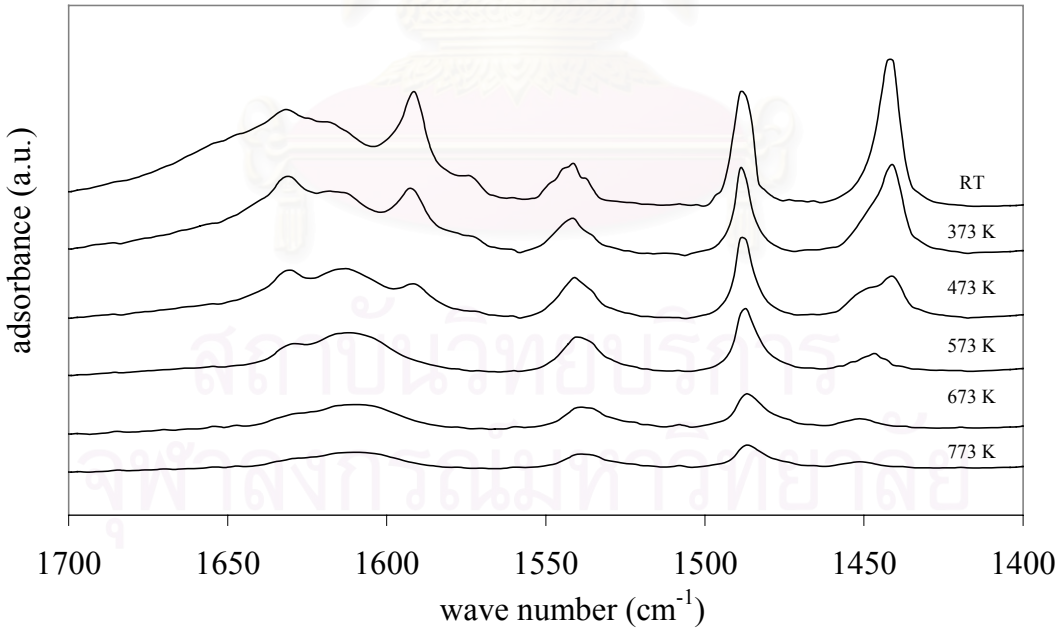

Figure 5.7 Pyridine adsorption of Y zeolite 0.16 μm at each temperature

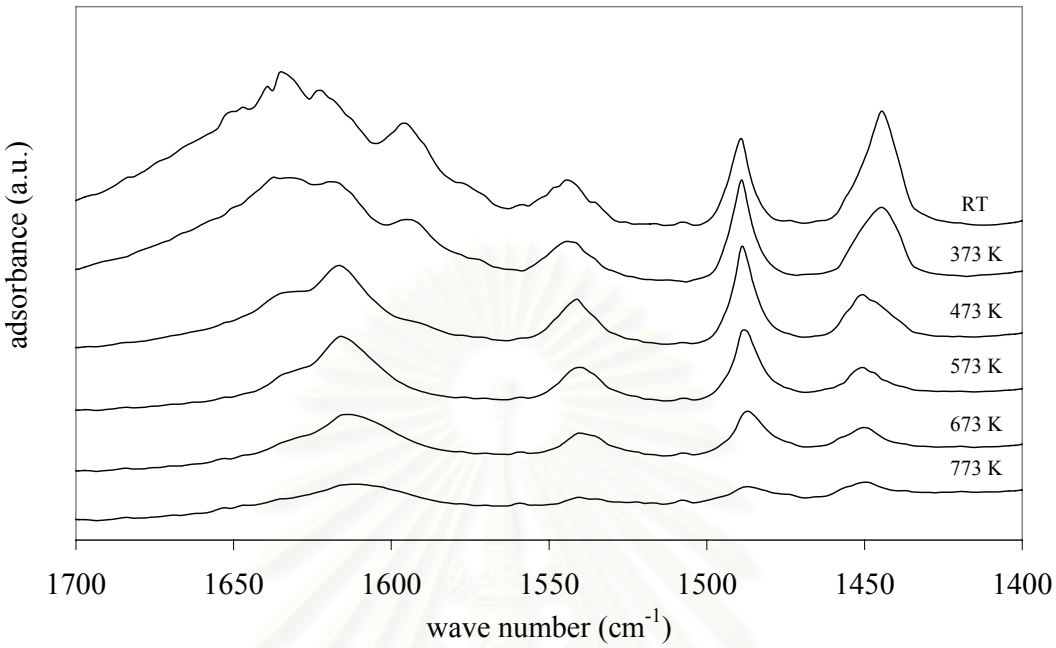

Figure 5.8 Pyridine adsorption of Y zeolite 0.31 μm at each temperature

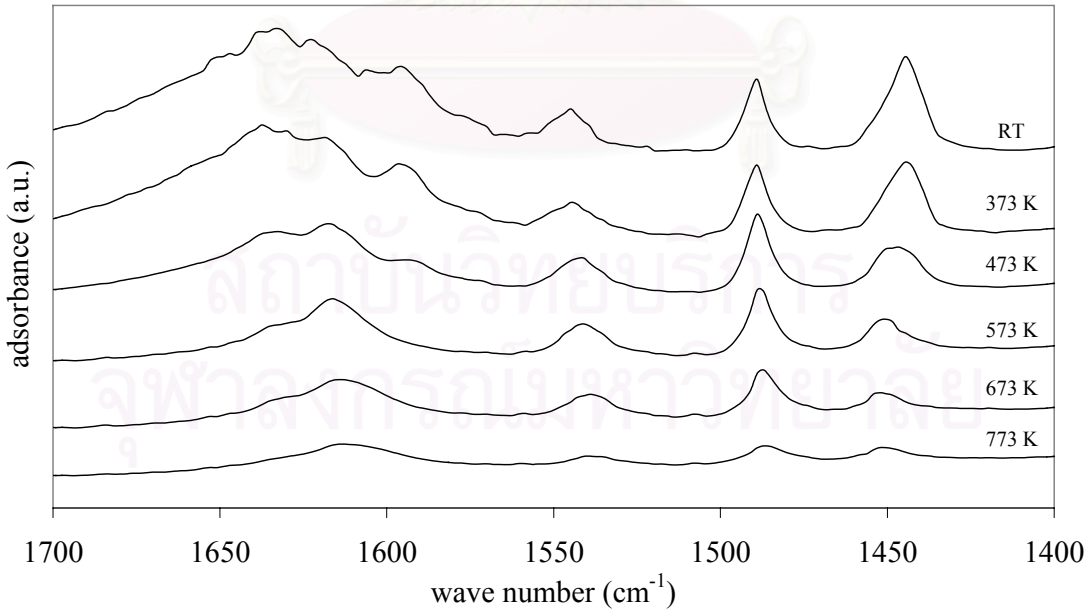

Figure 5.9 Pyridine adsorption of Y zeolite 0.45 μm at each temperature

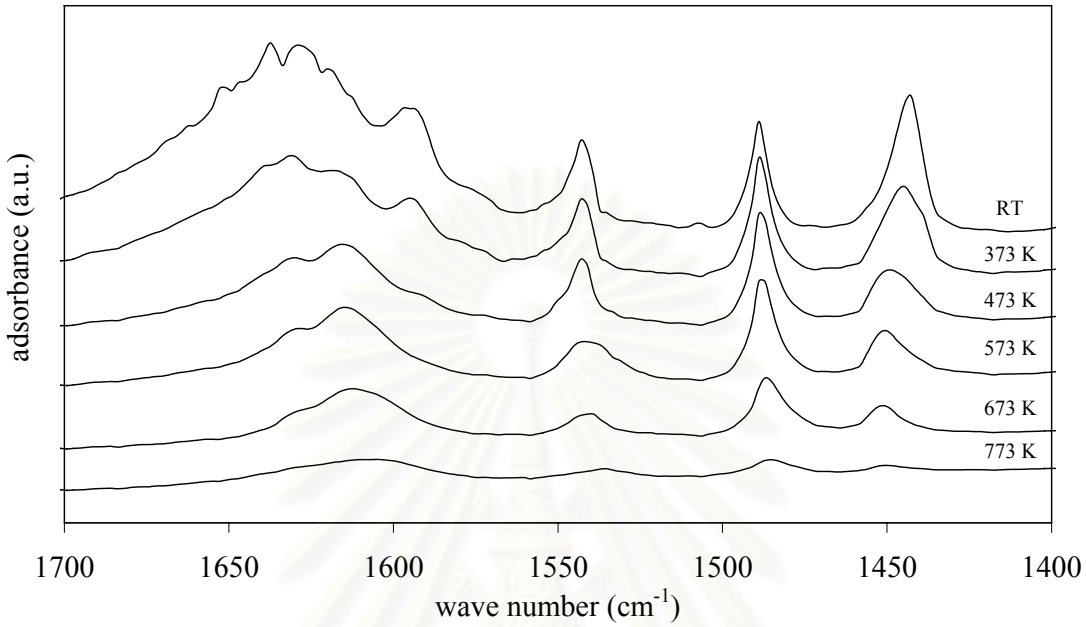

Figure 5.10 Pyridine adsorption of Y zeolite 0.82 μm at each temperature

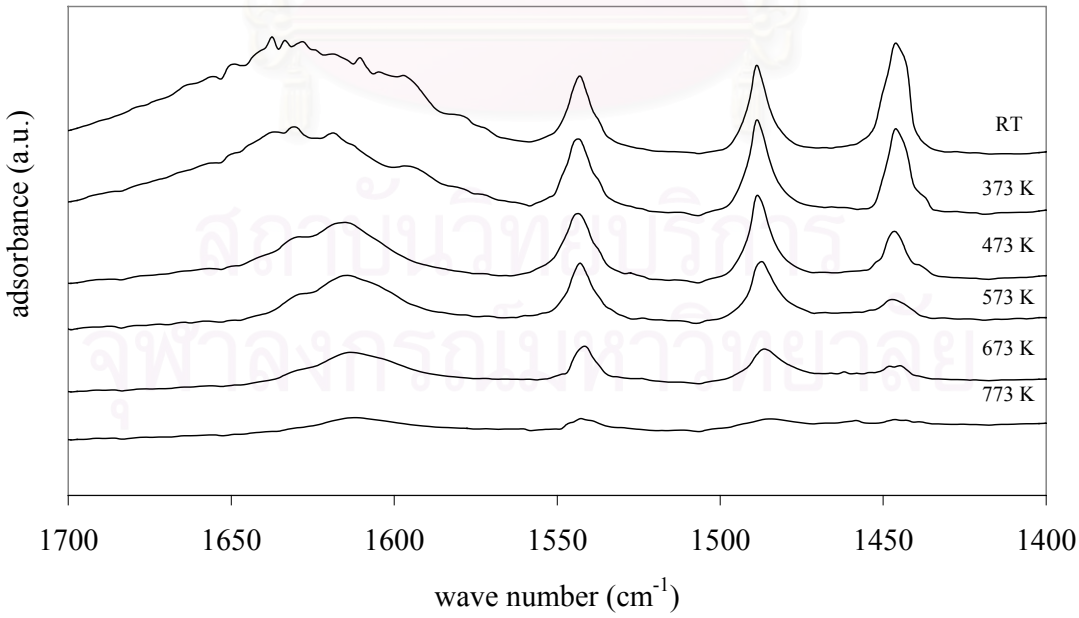

Figure 5.11 Pyridine adsorption of Y zeolite 2.01 μm at each temperature

The IR spectra of pyridine adsorption on 0.16, 0.31 and 0.45 μm of Y zeolite samples at various temperatures is shown in figure 5.7-5.9. Pyridine adsorbed on Lewis at low temperature dramatically decreases in the temperature ranges 323-473 K while at high temperature they continuously drop and hardly remained when temperature up to 773 K. On the other hand, pyridine adsorbed on Brønsted acid at low temperature seldom drop at room temperature up to 573 K. Three particle sizes at 573 K similarly have ratio of Lewis and Brønsted acid site whereas decreasing of Brø nsted acid is further illustrated after heating over 573 K. Generally, extensive dehydration causes loss of Brønsted acidity due to the removal of OH or silanol surface groups [108]. These results show that Brønsted acid site is the strong acid site, but Lewis acid is the weak acid site, which corresponding to NH_3 TPD results that three particle sizes similarly have acid content and acid strength.

Figures 5.10 and 5.11 show IR spectra obtained from pyridine adsorption on 0.81 and 2.01 μm of Y zeolite at different temperatures. The drop of pyridine adsorbed on Lewis acid site after heating up to 573 K can be elucidatory seen in each size, while that adsorbed on Brønsted acid site does not change significant at room temperature to 573 K. Thus, IR studies of pyridine desorption evidenced that, as well as strong Brönsted sites (Si-OH-Al), there were also weak Brönsted sites, not Si-OH-Al; their nature is not clear. When the desorption temperature is higher than 573 K, subsequently, the pyridine adsorbed on Brønsted acid site dramatically drop. These results suggest that large particle size of Y zeolite, Brønsted acid site are stronger than Lewis acid site. By comparing with small to medium particle size of Y zeolite, the substantially increase of the amount of pyridine desorbed from Brønsted acid sites can be observed at all temperature ranges. While the amount of pyridine desorbed from Lewis acid site is also the same in small size at all temperature ranges. It can be concluded that larger particle size not only increase the ratio of Brønsted per Lewis acid sites, but increase the acid strength of them as well.

5.3 Correlation between Particle Size and hydrothermal Stability of Y zeolite

The hydrothermal stability of Y zeolite was determined in terms of changes in crystallinity (C/C_0) where C_0 = the catalyst's initial crystallinity and C = the crystallinity observed after hydrothermal treatment. Figures 5.12a, 5.12b, and 5.12c show the plots between C/C_0 and $1/[(d_0)^{1/2}]$, where d_0 = particle size of Y zeolite, at different hydrothermal treatment conditions; (a) 0.1 steam partial pressure 60 sec, and 873-1273K, (b) 0.1 steam partial pressure, 1073 K, and 30-300 sec, and (c) 1073 K, 60 sec, and 0.1-1.0 steam partial pressure, respectively. It was found that all the plots have the same characteristic consisting of two parts. The first part representing the correlation between hydrothermal stability and particle size of larger particles show irregularly shapes while the second part representing the correlation for the smaller particles shows fairly the same linear trend. The irregular shape in the first part of each figure was probably caused by structure defects in solid such as acid defect as stated in the aforementioned paragraph.

However, the existence of the linear trend in the second part of Figure 5.12a gives new insight to the effect of the particle size on hydrothermal stability of Y zeolite. The high hydrothermal stability of Y zeolite can be predicted from particle size and operating temperature using this correlation. An empirical correlation of observed changes in zeolite crystallinity as a function of particle size and temperature is written as

$$\frac{C}{C_0} = m\left(\frac{1}{\sqrt{d_0}}\right) + A(T) \qquad (1)$$

$$\frac{C}{C_0} = -0.3937\left(\frac{1}{\sqrt{d_0}}\right) + \frac{498}{T} + 0.881 \qquad (2)$$

Where C_0 = the catalyst's initial crystallinity, C = the crystallinity observed after hydrothermal treatment, d_0 = the particle size before treatment (μm), m = the average slope of graph, A = arbitrary constant, and T = treated temperature (K).

This correlation was found to correctly predict the hydrothermal stability of small to medium particle size (0.1-0.45 μm) Y zeolites. The square root of particle size of Y zeolite prior to hydrothermal treatment in the correlation probably include the effects of nuclei density in amorphous gel at the reaction temperature and/or initial pseudo-cell concentration in gel phase since these two factors have been determined to be proportional to the gel reaction temperature and the particle size during crystallization of zeolites [118].

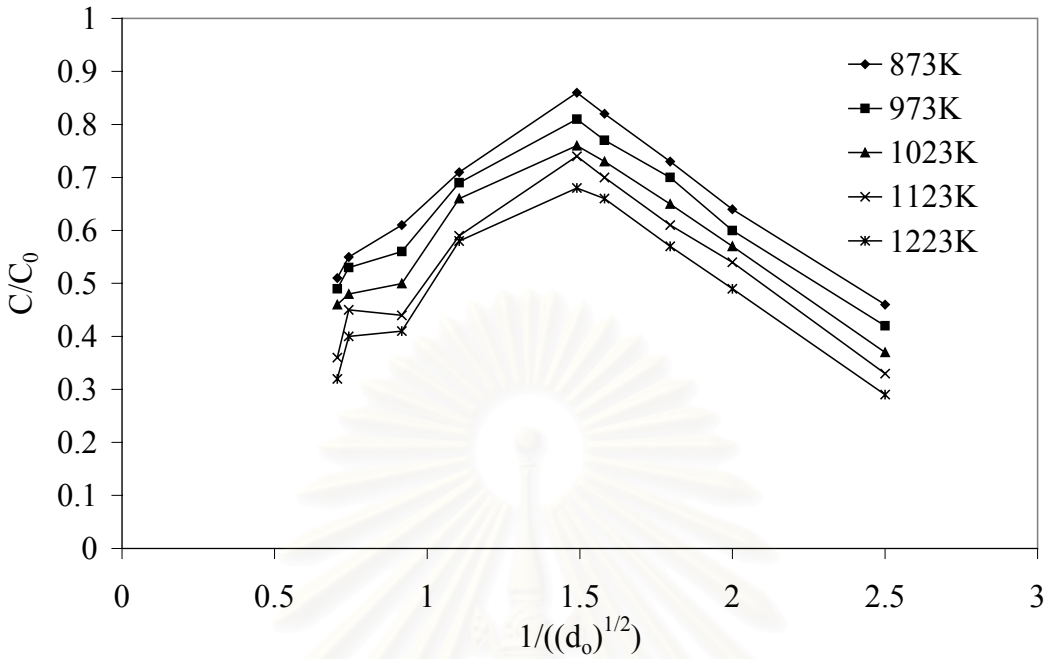

5.12a

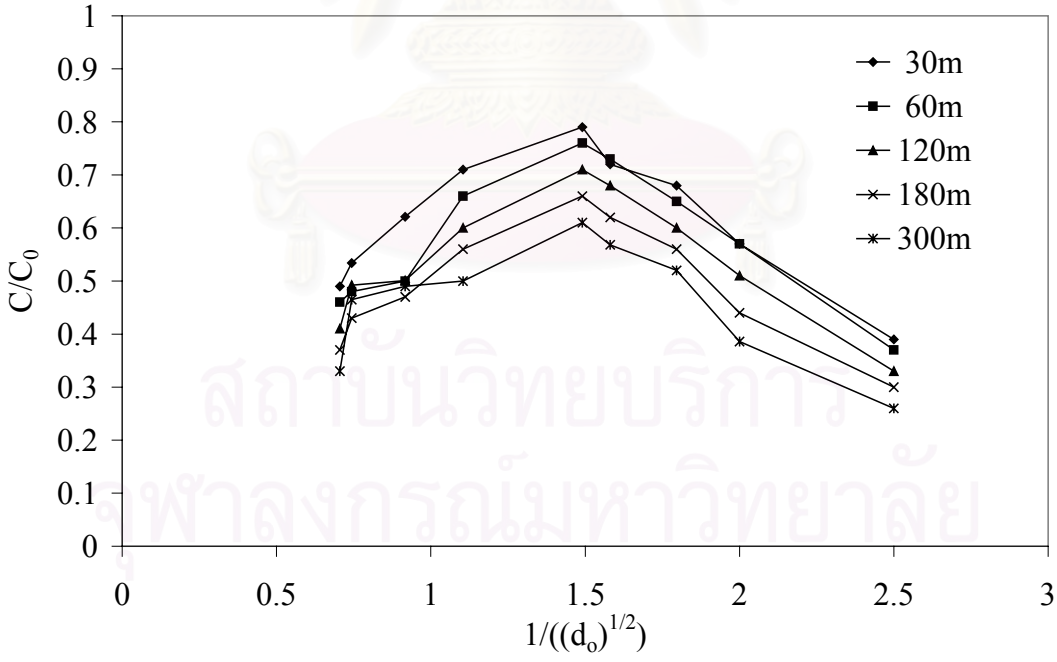

5.12 b

Figure 5.12 Correlation between C/C_0 and $1/((d_0)^{1/2})$ at different treated parameters (a) 873-1273 K, 10%mol steam and 60 min (b) 30-300 min, 10%mol steam and 1073K

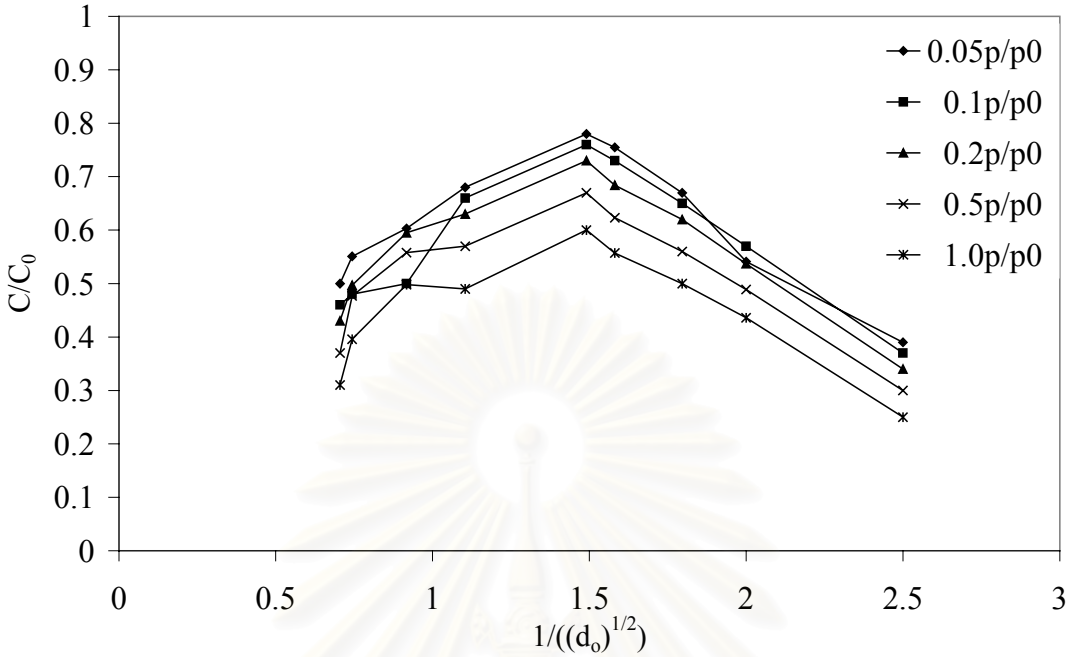

5.12c

Figure 5.12 (Cont.) Correlation between C/C_0 and $1/((d_0)^{1/2})$ at each steam partial pressure, 60 min and 1073 K

CHAPTER VI

CONCLUSION AND RECOMMENDATION

This thesis has described the effect of particle size on the hydrothermal stability of Y zeolite. The conclusions of this research can be summarized as follows:

1. The hydrothermal stability of Y zeolite was found to strongly depend on the particle size. The maximum crystallinity after hydrothermal treatment was obtained for the Y zeolite with particle size 0.45 μm.
2. By plotting the relative crystallinity (C/C_o) versus the particle size of Y zeolite (d_0) in the form of $1/\sqrt{d_0}$ for a given treated temperature (T), a new correlation can be written as $\frac{C}{C_0} = -0.3937\left(\frac{1}{\sqrt{d_0}}\right) + \frac{498}{T} + 0.881$

   The correlation can be applied for the small to medium particle sizes ranging from 0.1-0.45 μm.
3. For the larger particle sizes, the defects in Y zeolite structure were probably responsible for a decrease in crystal stability upon hydrothermal treatment.

From this research, the recommendations for further study are as follows:

1. Further studies of the effect of particle size on the hydrothermal stability should be investigated.
2. To test reaction at high temperature and in the presence of water.
3. To study effect and behavior of particle size on the hydrothermal stability at high Si/Al ratio.

REFERENCES

1 Dashiti, H., and Albazaz, H. *Fuel Science& Technology International*. 1995, *13*, 451.

2 Halász, I., Horváth, J., Mándy, T., Schmidt, L., and Tasnádi, E. *Elsevier Science Publishers*; Amsterdam;. 1985, 393.

3 Triantafillidis, C.S., Vlessidis, A.G., and Evmiridis, N.P. *Ind. Eng. Chem. Res.* 2000, *39*, 307.

4 Niu, G., Huang, Y., Chen, X., He, J., Liu, Y., and He, A. *Appl. Catal. B.* 1999, *21*, 63.

5 Gola, A., Rebours, B., Milazzo, E., Lynch, J., Benazzi, E., Lacombe, S., Delevoye, L., and Fernandez, C. *Micropor. Mesopor*. 2000, *40*, 73.

6 Zi, G., Yi, T., and Yugin, Z. *Appl. Catal*. 1989, *56*, 83.

7 Kugler E. L., Gardner T. H., and Panpranot, J. Hydrothermal Deactivation Kinetics of FCC Catalysts Containing USY Zeolite, Abstr. Pap. Am. Chem. Soc. 1999, *218*, 34.

8 Zhdanov, S.P., Feoktistova, N.N., and Vtjurina, L.M. *Catalysis and Adsorption by zeolites*; Elsevier Science Publishers B.V.; Amsterdam; 1991, 287.

9 Tian, H.P., Huang, C.J., and Fan, Z.B. *Catalyst Deactivation 2001*, Proceedings Studies in Surface Science and Catalysis. 2001, *139*, 351.

10 Gutierrez, L.; Boix, A.; Petunchi, J. *J. Catal*. 1998, *179*, 179.

11 Praserthdam. P., Phatanasri. S., Rungsimanop. J., and Kanchanawanichkun. P. *J. Mol. Catal. A-Chem*. 2001, *169*, 113.

12 Dangsawai. T., Praserthdam. P., Kim. J.B., and Inui. T. *Adv Environ Res*. 2000, *3*, 450.

13 Yang, G., Wang, Y., Zhou, J.Q., Liu, X.C., Han, X.W., and Bao, X.H. *J. Chem.Phys*. 2003, *18*, 9765.

14 Rajagopalan, K., Peters, A.W., and Edwards, G.C. *Appl. Catal*. 1986, *23*, 69.

15 Gianetto, A., Farag, H.I., Alberto, P.B., and de Lasa, H.I. *Ind. Eng. Chem. Res.* 1994, *33*, 3053.

16 Al-Khattaf, S., and de Lasa, H. *Appl. Catal. A*. 2002, *226*, 139.

17 Tatlier, M., and Erdem-Senatalar, A. *Microporous Mesoporous Mater*. 2000, *34*, 23.

18 Bonetto, L. Clamblor, M.A. Corma, A. and Perez-Pariente, J. *Appl. Catal. A.* 1992, *82*, 37.

19 Praserthdam, P., Mongkolsiri, N., and Kanchanawanichkun, P. *Catal Commun*. 2002, *3*, 191.

20 Mier, W.M., and Olson, D.H. *Altas of Zeolite Structure Types*, Butterworth-Heinemann, London, 1992.

21 Breck, D.W. *Zeolite Molecular Sieves: Structure*, Chemistry and Use, Robert E. Krieger Publishing, FL, 1984.

22 Pires, J., Brotas de Caralho, M., Ramoa Riberio F., and Derouane, E.G. *Zeolites*, 1991, *11*, 345.

23 Satterfield, C.N. *Heterogeneous Ctalysis in Industrial Practice*, 2 nd ed., New York: McGraw-Hill, 1991, *259*, 226

24 Köroğlu, H.J., Sarıoğlan, A., Tather, M., Şenatalar, A.E., and Savaşç, Ö.T. *J. Crystal Growth*. 2002, *241*, 481.

25 Prasad, V., Shertukde, W., Keith H., Jean-Marie D., and George M. *J. Catal*. 1993, *139*, 468.

26 Miyanohara, I., and Miyazaki, H. *U.S. Pat*. 4,376,106. 1983.

27 Zhdanov, S.P., and Samulevich, in N.N.: L.V.C. Rees (Ed.), *Proceedings of the Fifth International Zeolite Conference*, 1980, 75.

28 Cook J.D., and Thompson R.W. *Zeolites*. **1988, *8***, 322.

29 Bo W., and Hongzhu M. *Microporous Mesoporous Mater*. **1998, *25,*** 131.

30 Shah, N., and Ottino, J.M. *Chem. Eng. Sci*. 1987, *42*, 73.

31 Szostak, R., Van Bekkum, in H., Flanigen, E.M., and Jansen, J.C.(Eds.) *Introduction to Zeolite Science and Practice*, Elsevier, New York, 1991, 153.

32 Halász, I., Horváth, J., Mándy, T., Schmidt, L., and Tasnádi, E. *Zeolites*. Elsevier Science Publishers B.V.; Amsterdam; 1985, 393.

33 McElhiney, G. *Oil and Gas J*. Feb. 1988, *8*, 35.

34 ASTM D4463-91 *Standard Guide For Steam Deactivation of Fresh Fluid Cracking Catalyst*.

35 Moorehead, L., Margolis, J., and Mclean B. *Characterization and Catalyst Development*: An Interactive Approach A., Gattuso J. and Beertolacini, J. ACS Symposium Series. 1989, *411*, 120.

36 Campbell, S.M., Bibby, D.M., Coddington, J.M., Howe, R.F., and Meinhold, R.H. *J. Catal*. 1996, *161*, 383.

37 Scherzer, J., and Bass, L. *J. Catal*. 1973, *28*,101.

38 Kerr, G.T. *J. Catal*. 1969, *15*, 200.

39 Basacek, V., and Patzelova, V. *Catalysis on zeolites*, Kallo D., and Minachev, M. Ed.: Stillman. 1988, 169.

40 Zhang, W., Han, X., Lin. X., and Bao, X. *Microporous Mesoporous Mater*. 2001, *50*, 13.

41 Muller, M., and Harvey, G. *Microporous Mesoporous Mater*. 2000, *34*, 35.

42 Apelian, M.R., and Fung, A.S. *J. Phys. Chem.* 1996, *100*, 16577.

43 Zi, G., Yi, T., and Yugin, Z. *Appl. Catal*. 1989, *56*, 83.

44 Pellet, R., Blackwell, S., and Rabo A. *J. Catal*. 1998, *114*, 71.

45 Chang, C.D., and Chu, C.T. *European Patent*. 1984, 123449.

46 Persson, A.E., Schoeman, B.J., and Otterstedt, J.E. *Zeolites.* 1994, *14*, 557.

47 Muller, M., and Harvey, G. *Microporous Mesoporous Mater*. 2000, *34*, 135.

48 Reschetilowski, W., and Einicke, W.D., *Appl. Catal A*. 1989, *56*, L15.

49 Guisnet, M., and Ayrault, P.J. *Chem. Soc. Faraday Trans*. 1997, *93(8)*, 1661.

50 Kerr, G.T. *J. Phy.Chem*. 1968, *72*, 2594.

51 Gallezot, P., Beaumont, R., and Barthomeuf, D. *J. Phy. Chem*. 1974, *78*, 1550.

52 Sulikowski, B., Borbely, G., and Beyer, K., *J. Phy. Chem*. 1989, *93*, 3240.

53 Lombardo, E.A., Sill, G.A., and Hall, W.K. *J. Catal*. 1989, *119*, 426.

54 Aronson, M.T., Gorte, R.J., and Farneth, W.E. *J.Catal*. 1986, *98*, 434.

55 Uytterhoven, J.B., Christ, L.G., and Hall. W.K. *J.Phys.Chem*. 1965, *69*, 2117.

56 Ashton, A.G., Batamanian. S., and Dwyer, J. *Catalysis by Acid-Bases,* Amsterdam: Elesvir, 1985.

57 Barthoment, D. *Zeolites Science and Techonology* (Rebeira, F.H. et al.), Matinus Nijhoff Publishers, The Hange, 1984.

58 Tanake, K., Misona, M., Ona, Y., and Hattori, H. *Stud. Surf. Sci. Catal*. Tokyo: Elsevier. 1989, 51.

59 Sano. T., Fujisawa, K., and Higiwara, H, *Stud. Surf. Sci. Catal.* Amsterdam: Elsevier.1987, 34.

60 Boréave, A., Auroux, A., and Guimon, C. *Microporous Mater*. 1997, *11*, 275.

61 Cvetanovic, R.J., and Amenomiya, Y. *Adv. Catal*. 1967, *17*, 103.

62 Sawa, M., Niwa, M., Murakami, Y. *Zeolites* 1990, *10*, 307.

63 Richards, R.E., Rees, L.V.C. *Zeolites* 1987, *7*, 219.

64 Abello, M.C., Velasco, A.P., Gomez, M.F., and Rivarola, J.B. *Langmuir*, 1997, *13*, 2596.

65 Venuto, P.B., and Habib, E.T. *Fluid Catalytic Cracking with Zeolite Catalysts*, Marcel Dekker, New York, 1979.

66 Karger, J., and Ruthven, D.M. *Diffusion in Zeolites and other Microporous Solids,* Wiley, New York, 1992.

67 Humphries, A., and Wilcox, J. *Oil & Gas J.* 1989, *6*, 45.

68 Tsikoyiannis J., and Wei, J. *Chem. Eng. Sci.* 1991, *46(1)*, 233.

69 Biswas, J., and Maxwell, I.E. *Appl. Catal*. 1990, *63*, 197.

70 Wellenstein, D., and Alkemade, U. *Appl. Catal. A*. 1996, *137*, 37.

71 di Renzo, F. *Catal. Today***.**1998, *41*, 37.

72 Jansen, J.C., and Coker, E.N. *Curr. Opin. Solid State Mater. Sci.* 1996, 1, 65.

73 Zhang, L., Li, Z., and Xu, Y. *Petroleum Processing and Petrochemicals*. 1995, ***26****(10)*, 38.

74 Yang, S., Evmiridis, N.P., Weitamp, J., Karge, H.G., Pfeifer, H., and Holderich, W. *Stud. Surf. Sci. Catal*. Elsevier, Amsterdam, 1994, *84*, 155.

75 Camblor, M.A., and Corma, A. *Appl. Catal.* 1989, *55*, 65.

76 Breck, D.W. *US Patent 3130007*, 1964.

77 Climent, M.J., Corma, A., Garcia, H., Iborra, S., and Primo, J. *Appl. Catal. A*. 1995, *130*, 5.

78 Aguilar, J., Melo, F. V., and Sastre, E. *Catal Today*. 2000, *55*, 225.

79 Aguiar, E.F.S., Murta Valle, M.L., Silva, M.P., and Débora, F.S. *Zeolites*. 1995, *15*, 620.

80 Maselli, J., and Peters, A. *Catal. Rev. Sci. Eng.* 1984, *26*, 525.

81 Camblor, M., A. and Corma, A. *Stud. Surf. Sci. Catal*. 1997, *105*, 341.

82 Warzywoda, J. N., and Sacco A. *J. Crystal Growth*. 1999, *204*, 539.

83 Lepage, L.F., Ertl, G., Knozinger, H., and Weitkamp, J. *Preparation of solid Catalysts*, Wiley-VCH, Weinheim 1999, 4.

84 Vandry, F., Renzo, F.D., Fajula, F., and Schulz, P. *J. Chem. Soc., Faraday Trans*. 1998, *94(4)*, 617.

85 Bonetto,L., Camblor, M.A., and Corma, A. *Appl. Catal A*. 1992, *82*, 37.

86 Toophorm, U. *Effect of Particle Size and Silicon to Alumina Ratio on the hydrothermal stability of polycrystalline zeolite beta*, A Thesis Submitted in P artial Fulfillment of The Requirements for the Degree of Master of Engineering, Department of Chemical Engineering, Chulalongkorn University, 2002.

87 King, R.B. *Encyclopedia of Inorganic Chemistry*. Wiley & Sons, 1994, *7*, 4365.

88 Barrer, R.M. *Hydrothermal Chemistry of Zeolites*, London: Acedamic Press, 1982.

89 Bekkum, H.V., Flanigen. E.M., and Jansen, J.C. *Stud. Surf. Sci. Catal*. 1991, 578.

90 Szoztak, R. *Molecular Sieve Principles of Synthesis and Identification*, New York: Van Nostrand Reingold, 1989, 1.

91 Meier, W.M., and Olson, D.H. *Atlas of Zeolite Structure Types*, 3 rd revised ed.,int. Zeolite Asooc., Boston: Butterworth-Heiemann, 1992.

92 Wedlinger, R.L., Kerr, G.T., and Rosinski, E. *US Pat*. 3,308,069, 1967

93 Tsai, T., Lui, S., and Wang, I. *Appl. Catal*. A 1991, *181*, 355.

94 Dyer, A. *An Introduction to Zeolite Molecular Sieves*, Singapore: John Wiley & Sons, 1988.

95 Jansen J.C. *Stud. Surf. Sci. Catal*. 1994, *85*, 587.

96 Theologos, K.N., Nikou, I.D., Lygeros, A.I., and Markatos, N.C. *AIChE J*. 1997 ,43, 486.

97 Marcilly, C. *The Arabian J. for Sci. and eng*. 1996, *21*, 298.

98 Bhatia, S., *Zeolite catalysis: Principles and Applications*, CRC Press: Boca raton, 1990, 209.

99 McDaniel, C.V., and Maher, P.K. *American Chemical Society*, ACS Monograph. 1976, *171*, 285.

100 Jiratthitikan, P. *Catalytic Cracking of n-Octane Over Y Type Zeolite Catalyst*, A Thesis Submitted in P artial Fulfillment of The Requirements for the Degree of Master of Engineering, Department of Chemical Engineering, Chulalongkorn University, 1997.

101 Makpoon, V. *Metane Couping Over Y Zeolite*, A Thesis Submitted in P artial Fulfillment of The Requirements for the Degree of Master of Engineering, Department of Chemical Engineering, Chulalongkorn University, 2000.

102 Valtchev, V., Mintova, S., Dimov, V., Toneva, A., and Radev, D. *Zeolites*. 1995, *15*, 193.

103 Mintova, S., Valtchev, V., Vultcheva, E., and Veleva, S. *Zeolites*, 1992, *12*, 210.

104 Cundy, C.S., Lowe, B.M., and Sinclair, D.M.J. *Chem. Faraday Discuss*. 1993, *95*, 235.

105 ASTM D3906, Standard Test Method for Determination of Relative X-ray Diffraction Intensities of Faujasite-Type Zeolite.

106 Kubelkova, L., Beran, S., Malecka, A., and Mastikhin, V.M. *Zeolites*, 1989, 12.

107 Jacobs, P.A. Metal-zeolites: transetters in selective Fischer-Tropsch chemistry. *Catalysis by zeolites*; Elsevier Science Publishers B.V.; Amsterdam; 1980, 293.

108 Di Renzo, F. *Catal Today*. 1998, *41*, 37.

109 Thomas, J.M., and Klinowski, J. *Adv. Catal*. 1985, *33*, 199.

110 Budi, P., and Howe, R.F. *Catal. Today.* 1997, *38*, 175.

111 Sanz, J., Fornés, V., and Corma, A., *J. Chem, Soc., Faraday Trans*. 1988, *84*, 3113.

112 Jilson. J.P., Edwards. G.C., Peters, A.W., Rajagopalan, K., Wormsbecher, R.F., Roberie. T.G., and Shatlock, M.P. *J. Chem. Soc., Chem. Commun*. 1987, 91.

113 Samoson, A., Lippmaa, E., Engelhardt, G., Lohse, U., and Jerschkewitz, H.G. *Chem. Phys. Lett*. 1987, *134*, 589.

114 Omegna, A., Haouas, M., Kogelbauer, A., Prins, R. *Micropor. Mesopor*. 2001, *46*, 177.

115 Occelli L., Aurox A., baldirghi F., and Leoncini S. *The use of Microcalorimetry and Porosimetry to Investigate the effects of aging on the Acidity of Fluid Cracking Catalysts (FCC)* Fluid Cracking Catalysts Occeeli. and Connor, P., ed. Marcel Dekker: New York, 1997, 203.

116 Karge, H.G., Dondur, V., and Weitkamp, J. *J. Phys.Chem*. 1991, *95*, 283.

117 Kumar, N., Nieminen, V., Dermirkan, K., Salmi, T., Murzin, D.Y., and Laine, E. *Appl. Catal. A*. 2002, *235*, 113.

118 Falamaki, C., Edrissi, M., Sohrabi, M. *Zeolites*. 1997, *19*, 362.

APPENDICES

APPENDIX A

SAMPLE OF CALCULATIONS

A-1 Calculation of vapor pressure of water

Set the partial vapor pressure of water to the requirement by adjusting the temperature of saturator according to the antoine equation

$$\log P = A - \frac{B}{(T + C)}$$

When P = vapor pressure of water, mbar

T = temperature, ^{o}C

A, B and C is constants

Range of temperature that applied ability –20 –126 ^{o}C

The values of constants.

Reactant	A	B	C
Water	8.19625	1730.630	233.426

A-2 Calculation of % crystallinity

$$\% \text{ Crystallinity} = \frac{\text{Area under XRD pattern}(2\theta=22.4)\text{of sample} \times 100}{\text{Area under XRD pattern}(2\theta=22.4)\text{of reference}}$$

Reference is the fresh zeolite beta for the same size.

For example:

Area under XRD pattern of treated = 1132

Area under XRD pattern of fresh = 1175

$$\% \text{ Crystallinity} = \frac{1132 \times 100}{1175} = 96$$

A-3 Calculation of the relative area of tetrahedral aluminum(%)

$$\text{The relative area of tetrahedral aluminum (\%)} = \frac{\text{Area of tetrahedra } 1\text{Alx}100}{\text{Total Area}}$$

Area of tetrahedral Aluminum is a peak at a chemical shift of around 54 ppm. Total area is the total summation area of tetrahedral and octahedral aluminum(0 ppm).

For example:

Area of tetrahedral Al =weight of paper under peak area at 54 ppm = 0.0867
Area of octahedral Al = weight of paper under peak area at 0 ppm = 0.0225

$$\text{The relative area of tetrahedral aluminum (\%)} = \frac{0.0867 \times 100}{(0.0867+0.0225)} = 84$$

A-4 Calculation of the specific surface area

From Brunauer-Emmett-Teller (BET) equation

$$\frac{p}{n(1-p)} = \frac{1}{n_m C} + \frac{(C-1)p}{n_m C} \qquad \text{(A-5-1)}$$

Where, p = Relative partial pressure of adsorbed gas , P/Po

Po = Saturated vapor pressure of adsorbed gas in the condensed state at the experimental temperature, atm

P = Equilibrium vapor pressure of adsorbed gas, atm

n = Gas adsorbed at pressure P, ml. At the NTP/g of sample

n = Gas adsorbed at monolayer, ml. At the NTP/g of sample

$C = \text{Exp}[(H_c - H_l)/RT]$

H_c= Heat of condensation of adsorbed gas on all other layers

H_l = Heat of adsorption into the first layer

Assume $C \rightarrow \infty$, then

$$\frac{p}{n(1-p)} = \frac{p}{n_m}$$

$$n_m = n(1-p) \qquad \text{(A-5-2)}$$

The surface area, S, of the catalyst is given by

$$S = S_b \times n_m \qquad \text{(A-5-3)}$$

From the gas law

$$\frac{P_b V}{T_b} = \frac{P_t V}{T_t} \qquad \text{(A-5-4)}$$

Where, P_b = Pressure at 0 ^oC

P_t = Pressure at t ^oC

T_b = Temperature at 0 ^oC = 273.15 K

T_t = Temperature at t ^oC= 273.15 + t K

V = Constant volume

Then, $P_b = (273.15/T_t)\ P_t = 1$ atm

Partial pressure

$$P = \frac{[\text{Flow of } (He + N_2) - \text{Flow of } He]}{\text{Flow of } (He + N_2)}$$

= 0.3 atm

For nitrogen gas , the saturated vapor pressure equals to

P_o = 1.1 atm

Then, $p = P/P_o = 0.3 / 1.1 = 0.2727$

To measure the volume of nitrogen adsorbed, n

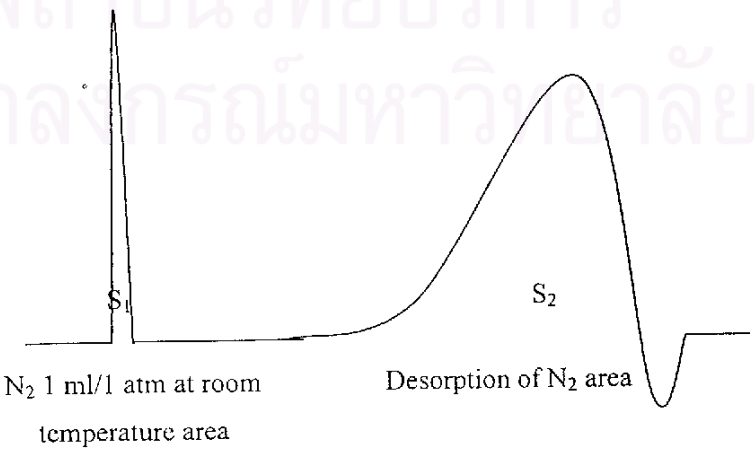

$$n = \frac{S_2}{S_1} \times \frac{1}{W} \times \frac{273.15}{T} \text{ ml. / g of catalyst} \qquad \text{(A-5-5)}$$

Where, S_1 = N_2 1 ml/ 1 atm at room temperature area

S_2 = Desorption of N_2 area

W = Sample weight, g

T = Room temperature, K

Therefore,

$$n_m = \frac{S_2}{S_1} \times \frac{1}{W} \times \frac{273.15}{T} \times (1 - p)$$

$$n_m = \frac{S_2}{S_1} \times \frac{1}{W} \times \frac{273.15}{T} \times 0.7273 \qquad \text{(A-5-6)}$$

Whereas, the surface area of nitrogen gas from literature equal to

S_b = 4.373 m^2 / ml of nitrogen gas

Then,

$$S = n_m = \frac{S_2}{S_1} \times \frac{1}{W} \times \frac{273.15}{T} \times 0.7273 \times 4.343$$

$$S = n_m = \frac{S_2}{S_1} \times \frac{1}{W} \times \frac{273.15}{T} \times 3.1582 \text{ } m^2 / g \qquad \text{(A-5-7)}$$

APPENDIX B

B-1 The Particle size and the percent crystallinity of Y zeolite at various operating temperatures

Particle Size (μm)	%Crystallinity at Various Temperature (°C)				
	600	700	800	900	1000
0.16	46	42	37	33	29
0.25	64	60	57	54	49
0.31	73	70	65	61	57
0.4	82	77	73	70	66
0.45	86	81	76	74	68
0.82	71	69	66	59	58
1.19	61	56	50	44	41
1.81	55	53	48	45	40
2.01	51	49	46	36	32

B-2 The Particle size and the percent crystallinity of Y zeolite at various operating times

Particle Size (μm)	%Crystallinity at Various Time (s)				
	30	60	120	180	300
0.16	39	37	33	30	26
0.25	57	57	51	44	39
0.31	68	65	60	56	52
0.4	72	73	68	62	57
0.45	79	76	71	66	61
0.82	71	66	60	56	50
1.19	62	50	50	47	49
1.81	53	48	49	43	47
2.01	49	46	41	37	33

B-3 The Particle size and the percent crystallinity of Y zeolite at various operating partial pressures

Particle Size (μm)	%Crystallinity at Various Partial Pressure (P/P_0)				
	0.05	0.1	0.2	0.5	1
0.16	39	37	34	30	25
0.25	54	57	54	49	44
0.31	67	65	62	56	50
0.4	76	73	68	62	56
0.45	78	76	73	67	60
0.82	68	66	63	57	49
1.19	60	50	60	56	50
1.81	55	48	50	48	40
2.01	50	46	43	37	31

B-4 Relative area of ^{27}Al NMR and acid properties of HY zeolite at various particle sizes

Particle size(μm)	The relative area of tetrahedral ^{27}Al[b]		Acid site[c]		Ratio of B/L[d]
	before	After	Brønsted	Lewis	
0.16	83.69	69.14	62	201	0.31
0.31	85.06	77.99	86	245	0.35
0.45	84.52	83.63	79	243	0.33
0.82	88.64	78.97	120	259	0.46
2.01	90.63	71.35	189	284	0.67

B-5 The single point BET surface area and the percent relative BET surface area of Y zeolite , fresh and treated samples

particle size (μm)	BET surface area (m^2/g)		
	fresh catalyst	treated catalyst	%relative BET surface
0.16	521	322	38
0.25	546	366	33
0.31	498	411	18
0.40	502	432	14
0.45	511	441	14
0.82	531	397	25
1.19	506	384	24
1.81	543	340	37
2.01	550	339	38

APPENDIX C

LIST OF PUBLICATION

1. Somyod Sombatchaisak and Piyasan Praserthdam, “Effects of crystallite size and Si/Al ratio on the hydrothermal stability of Y zeolite”, *IPCAT-3 & TSCRE-2003*. 2003, *1*, P-II-23.

P-II-23

Effects of crystallite size and Si/Al ratio on the hydrothermal stability of Y zeolite

Somyod Sombatchaisak and Piyasan Praserthdam*

Center of Excellence on Catalysis and Catalytic Reaction Engineering,
Department of Chemical Engineering,Chulalongkorn University, Bangkok, 10330, Thailand
E-mail:somyod24@hotmail.com
FAX number: 662-2186769

Introduction

Zeolite Y has been an important component in many catalytic processes, e.g., fluid catalytic cracking (FCC) [1], hydrocracking [2], Fischer-Tropsh synthesis [3] and oxidation [4]. One significant disadvantage of Y zeolite is its low hydrothermal stability, which results in a sharp dealumination of the framework ultimately leading to the collapse of the structure [5].

In this approach, we have studied influencing factors on Y zeolite, i.e., crystallite size, Si/Al ratio, aging time of nucleation and temperature of reaction Si-Al gel. Relationship between the crystallite size and hydrothermal stability of Y is particularly focused using X-Ray Diffraction (XRD), Scanning electron microscopy (SEM), and Aluminium Nuclear Magnetic Resonance (^{27}Al NMR) spectroscopy.

Experimental

Y zeolite was prepared by mixing of $NaAlO_2$ and $Na_2Si_3O_7$ solution at various Si/Al ratios (3.5, 4.5, 5.5 and 6.5). The mixture was continuously stirred for 2 h, then heated to 60^{o}C and maintained at this temperature for 1 h to form a gel. The gel mixture was separated from the supernatant solution by centrifugation. The process of centrifugation and washing by water was repeated until the pH of supernatant solution was 13.5. $Na_2Si_3O_7$ solution was added to the gel and the mixture was stirred to obtain a uniform slurry. The slurry was kept in a closed glass vessel and placed at room temperature at different aging of nucleation (0.5, 2, 4.5, 6.5 day). After aging, the slurry was heated at 95 or 110^{o}C in an oven and maintained at such temperature for 24 h. The prepared sample was left to cool down to ambient temperature, then it was washed with the distilled water until the pH of slurry became 7. The obtained as-synthesized sample was dried at 110^{o}C overnight and calcined in air at 500^{o}C for 2 h.

Hydrothermal treatment of Y zeolite was performed at 800^{o}C in 10% mol H_2O for 1 h. Structural stability was studied by XRD. Average crystallite size and crystal distribution were evaluated by SEM. ^{27}Al MAS NMR was used to investigate the framework Si and Al species of octahedral and tetrahedral coordination.

Results and Discussion

The first influencing parameter studied was aging time on Y zeolite formation. Silica, alumina, sodium hydroxide and water were mixed together to form alumino-silicate nucleation centers. Aging time of nucleation at room temperature was varied from 0.5 to 6.5 days and the structure of the as-synthesized sample was investigated by XRD. The structure of Y zeolite was built after at least 4.5 days of nucleation.

The reaction temperatures for Si-Al gel (Si/Al = 4.5) were set at 95 or 110 ^{o}C for 6.5 days of aging time. From XRD results, the solid phase of Y prepared at 110 ^{o}C tends to be amorphous rather than Y zeolite.

Hydrothermal stability of the Y zeolite was further studied based on the crystallinity, which is defined as:

$$\% \text{ Crystallinity} = (S_x/S_R) \times 100$$

where S_x and S_R are sum of integral peak intensities for the sample and for the reference, respectively.

SEM results showed that Y zeolite remained unaltered in shape and crystallite size after hydrothermal treatment. Then, effect of crystallite size between 0.16-2.01 μm on the crystallinity of Y zeolite was studied

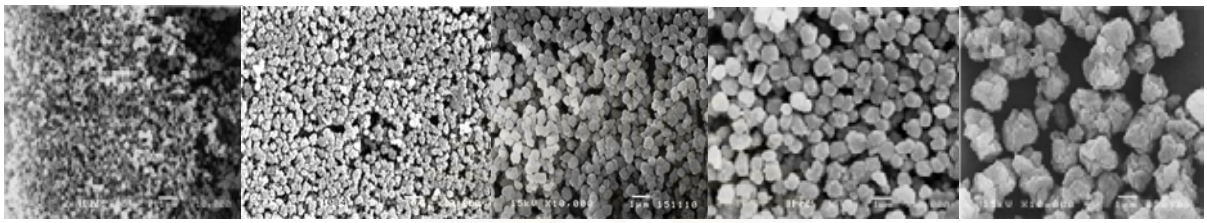

1a 1b 1c 1d 1e

Figure1. SEM images of Y zeolite after hydrothermal treatment at 800°C for 1 h at different average crystal size: (1a) 0.16 μm (1b) 0.38 μm (1c) 0.49 μm (1d) 0.82 μm (1e) 2.01 μm

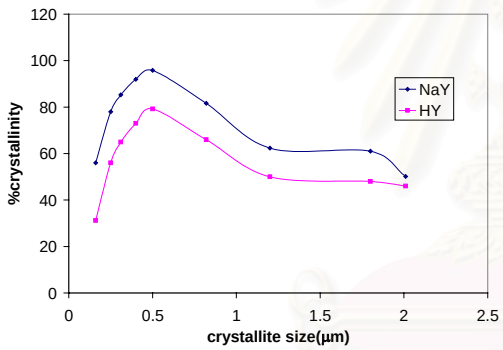

Figure 2. Relationship between %crystallinity and size of NaY and HY

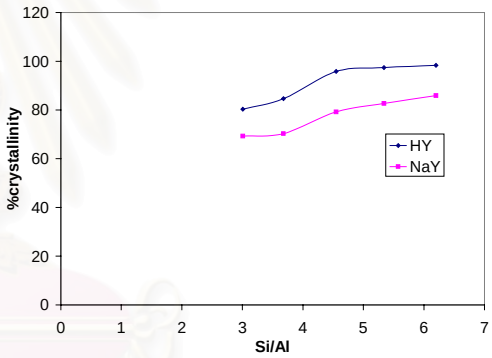

Figure 3. Relationship between % crystallite crystallinity and Si//Al ratio of NaY and HY.

The relationship between % crystallinity and the crystallite size show a volcano behaviour. Maximum hydrothermal stability was 95.8 and 79.21 for NaY and HY zeolite, respectively. Effect of Si/Al ratio with stability shows that hydrothermal stability increases relatively with Si/Al ratio as seen in figure 3. This could possibly be due to the high stability in a high Si/Al Y zeolite in the presence of Si in tetrahedral framework.

Investigation by ^{27}Al MAS NMR demonstrated that dealumination was consistent with crystallinity and crystallite size. Medium crystallite size was dealuminated less than Small crystallite size and large crystallite size.

Acknowledgements

The project was financially supported by the Thailand Research Fund (TRF) and TJTTP-J.

References

[1] Al-Khattaf, S., De Lasa, H., Appl. Catal. A., 226 (2002) 139.
[2] Li, D., Xu, H.F., Guthrie, G.D., J. Catal., 89 (2000) 281.
[3] Guczi, L., Bazin, D., Appl. Catal. A.,188 (199) 163.

[4] Park, C., Keane. M.A., Langmuir., 17 (2001) 8386.
[5] Niu, G.X., Huang, Y., Chen, X.Y., He, J.M., Liu, Y., He, A., Appl. Catal. B., 21 (1999) 63.

VITA

Mr Somyod Sombatchaisak was born on August 22, 1981 in Bangkok, Thailand. He received the Bachelor Degree of Chemical Technology from Faculty of Science, Chulalongkorn University in 2001.